Programmed DNA Self-Assembly and Logic Circuits

by

Wei Li

A Dissertation Presented in Partial Fulfillment
of the Requirements for the Degree
Doctor of Philosophy

Approved April 2014 by the
Graduate Supervisory Committee:

Hao Yan, Co-Chair
Yan Liu, Co-Chair
Julian Chen
Ian Gould

ARIZONA STATE UNIVERSITY

May 2014

ABSTRACT

DNA is a unique, highly programmable and addressable biomolecule. Due to its reliable and predictable base recognition behavior, uniform structural properties, and extraordinary stability, DNA molecules are desirable substrates for biological computation and nanotechnology. The field of DNA computation has gained considerable attention due to the possibility of exploiting the massive parallelism that is inherent in natural systems to solve computational problems. This dissertation focuses on building novel types of computational DNA systems based on both DNA reaction networks and DNA nanotechnology.

A series of related research projects are presented here. First, a novel, three-input majority logic gate based on DNA strand displacement reactions was constructed. Here, the three inputs in the majority gate have equal priority, and the output will be true if any two of the inputs are true**.** We subsequently designed and realized a complex, 5-input majority logic gate. By controlling two of the five inputs, the complex gate is capable of realizing every combination of OR and AND gates of the other 3 inputs. Next, we constructed a half adder, which is a basic arithmetic unit, from DNA strand operated XOR and AND gates. The aim of these two projects was to develop novel types of DNA logic gates to enrich the DNA computation toolbox, and to examine plausible ways to implement large scale DNA logic circuits. The third project utilized a two dimensional DNA origami frame shaped structure with a hollow interior where DNA hybridization seeds were selectively positioned to control the assembly of small DNA tile building blocks. The small DNA tiles were directed to fill the hollow interior of

the DNA origami frame, guided through sticky end interactions at prescribed positions. This research shed light on the fundamental behavior of DNA based self-assembling systems, and provided the information necessary to build programmed nanodisplays based on the self-assembly of DNA.

ACKNOWLEDGEMENTS

First and foremost, I would like to thank my wife Yu Liu, without whom I would not have accomplished all that I have. I am enormously grateful for her love, support, and encouragement. I would also like to thank my parents. They were very supportive during my five year PhD study.

I want to acknowledge my advisors, Dr. Hao Yan and Dr. Yan Liu. They brought me into the world of DNA nanotechnology. Their broad knowledge and earnest attitude about science guided me through my research. I am also grateful to the members of my committee, Dr. Julian Chen and Dr. Ian Gould, for their time and guidance.

Finally, I want to thank all the past and present graduate students, postdoctoral researchers, and lab members who I have interacted with along the way. Their advice and support have been greatly helpful. I give my special thanks to Dr. Yang Yang. He inspired me with many research ideas and provided extensive experimental support. I would also acknowledge Dr. Zhao Zhao and Dr. Minghui Liu for training me in sound lab techniques. I also want to thank Dr. Jeanette Nangreave for helping edit official documents.

TABLE OF CONTENTS

CHAPTER Page

CHAPTER Page

APPENDIX

LIST OF TABLES

LIST OF FIGURES

Figure Page

Figure Page

Chapter 1

DNA Computation and DNA Nanotechnology

1.1 Abstract

In this chapter, I will introduce and summarize the development of research in DNA Computation and DNA Nanotechnology. DNA (deoxyribonucleic acid) is the genetic carrier in biological systems. Studying the information encoded in DNA molecules is essential for understanding the secrets of life. Recently, DNA has been explored as a structural material in both computation and nanotechnology, apart from its biological function. DNA computation is an interdisciplinary area of research that bridges chemistry, biology, and computer science. It focuses on discovering, programming, and operating DNA reaction networks to achieve mathematical functions. It has demonstrated great potential application in regulating biochemical systems by executing logic computations. DNA nanotechnology utilizes DNA as a building material to construct well defined nanostructures. Scientists have developed a wide range of one-dimensional (1D), two-dimensional (2D), and three dimensional (3D) DNA structures. These structures can be divided into two categories: (1) 2D arrays or 3D crystals composed of branched DNA tiles as repeating units, and (2) DNA origami with precise shapes and sizes normally formed from a single, long scaffold strand and numerous unique short staples strands. These biocompatible and programmable templates have been used for the study of DNA properties, protein science, drug delivery, energy transfer, and many other areas. Both DNA computation and DNA nanotechnology are very important modern research areas, and the two research areas benefit from each other in terms of design principles and manipulation techniques.

1.2 Introduction

1.2.1 DNA. DNA is a biological macromolecule used by all known living organisms and many viruses to store genetic information.[1] The genetic information encoded in DNA molecules specifies the sequence and function of all of the proteins that are synthesized in a cell and carries the instructions for the behaviors of the cell and the development of entire organisms.

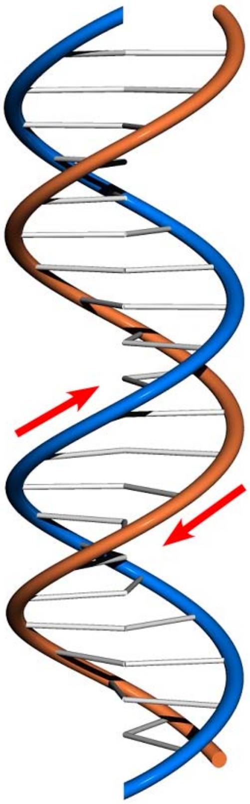

Figure 1.1. The double helical DNA structure proposed by Watson and Crick in 1953.[1] A double helix is composed of two single stranded DNA molecules. Each strand and the overall double helix follow a right-handed spiral pattern. The orange and blue spirals represent the sugar-phosphate backbone, and the grey rods represent the base pairs. The red arrows indicate the direction of each single strand from 5’ to 3’.

DNA was first extracted and identified by Johannes Friedrich Miescher in 1869.[2] Since the discovery of DNA, scientists have been endeavoring to study the structure, property, function, and synthesis of DNA and other nucleic acids, and their relation to the natural world. The iconic double helical structure of DNA molecules was first proposed by J. D. Watson and F. H. C. Crick in 1953.[1] (Figure 1.1) Over six decades after revealing the right handed double helical DNA structure, scientists have made tremendous progresses in research areas related to DNA, e.g. bioinformatics, genetic engineering and whole genome sequencing. Even today, DNA is one of the most important and interesting research areas of chemists, biologists, and even computer scientists.

1.2.2 Structural Properties of DNA. DNA is a biopolymer composed of repeating units called nucleotides. The structure of DNA can be described by three levels of structure: primary, secondary, and tertiary.[3]

The primary structure of a DNA molecule is the linkage between each individual nucleotide and the sequence of the different nucleotides in a DNA molecule.[4] In DNA molecules, a nucleotide contains three groups: a phosphate group, a 2'-deoxy-D-ribose sugar group, and a nucleobase.[3] (Figure 1.2) The nucleobase connects to the 1' carbon of the 2'-deoxyribose, and the phosphate forms a phosphate ester with the 5'-hydroxyl group of the 2'-deoxyribose in each nucleotide. In DNA polymers, the 5'-phosphate of a nucleotide also connects to the 3'-hydroxy group of the 2'-deoxyribose in another nucleotide, thus forms a phosphate di-ester. The phosphate-sugar-phosphate linkage forms the backbone of a DNA molecule.[3] There are four types of nucleobases in natural DNA, which are adenine, thymine, cytosine, and guanine. Thymine and cytosine are derivatives of purine, and adenine and guanine are derivatives of pyrimidine. The structures of the four bases are shown in Figure 1.2. Adenine, thymine, cytosine, and guanine are usually abbreviated as A, T, C, and G, respectively. The sequence of a DNA molecule is defined as the sequence of the bases from the 5' end to the 3' end of a single strand. The direction of single-stranded DNA (ssDNA) is also the direction from the 5' end to the 3' end. The 5' end is defined as the end that does not have any nucleotide linked to the 5' carbon of the 2'-deoxyribose, and the 3' end is defined as the end that does not have any nucleotide linked to the 3' carbon of the 2'-deoxyribose.[4] (Figure 1.2)

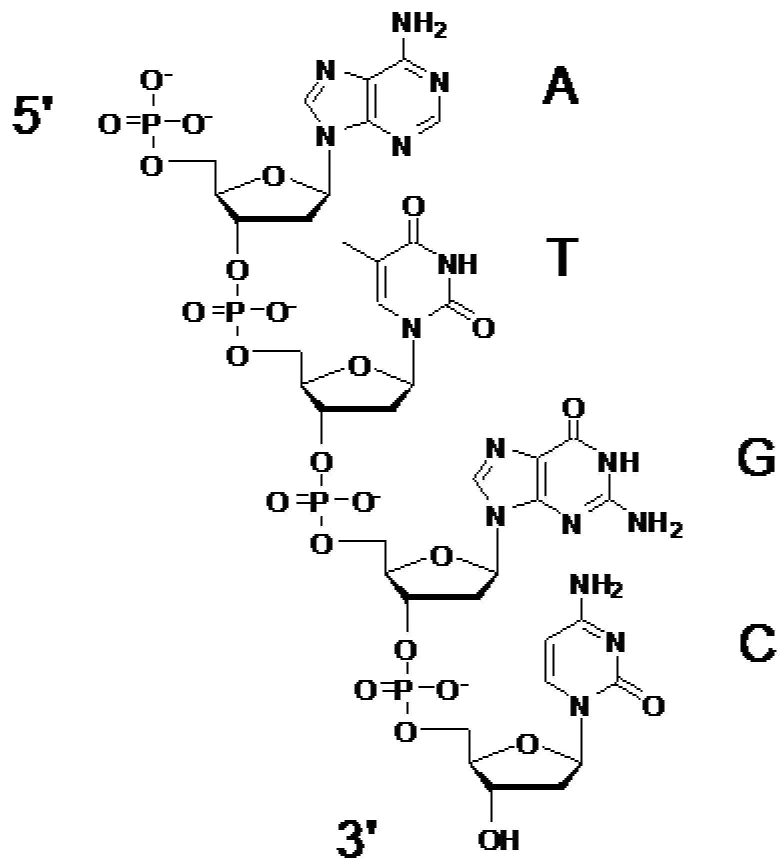

Figure 1.2. The primary structure of DNA. Each individual unit in the polymer is a nucleotide. The phosphate-sugar-phosphate linkage forms the backbone of the molecule. The structure of the four nucleobases adenine (A), thymine (T), guanine (G), and

Cytosine (C) are shown from top to bottom. The 5' end of the molecule is at the top, and the 3' end is at the bottom. The sequence of the DNA molecule shown in the figure is ATGC.

The secondary structure is any stable structure adopted by a nucleic acid by all or some of its nucleotides.[4] The foundation of the secondary structure of DNA is based on the Watson-Crick base pairing rule.[1] Two bases, one each from complementary single strands, pair with each other through hydrogen bonds. Specifically, adenine pairs with thymine through two hydrogen bonds, and guanine pairs with cytosine through three hydrogen bonds. (Figure 1.3)

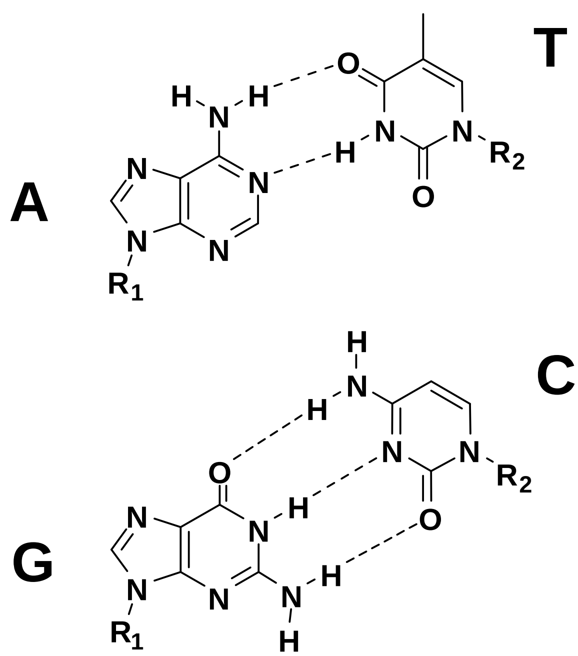

Figure 1.3. The structure of Watson-Crick base pairing. Adenine pairs with thymine through two hydrogen bonds, and guanine pairs with cytosine through three hydrogen bonds.

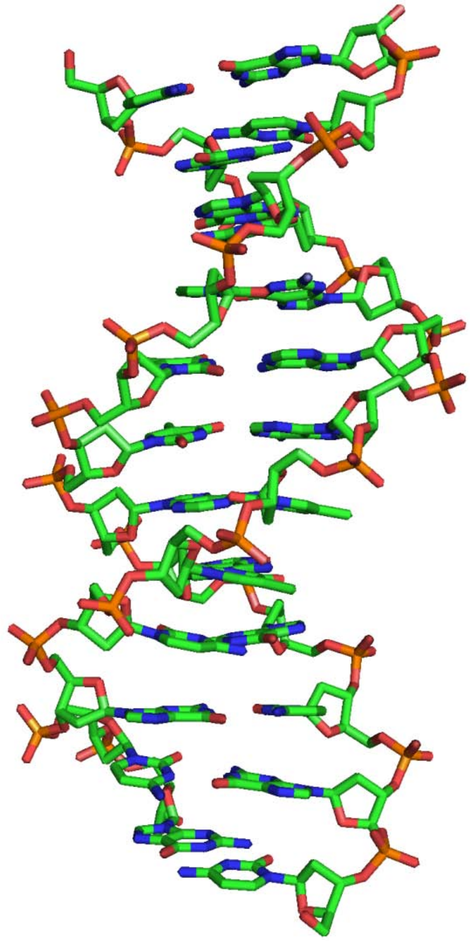

Figure 1.4. The stereo-view of a B-form DNA double helix. The two component strands are anti-parallel to each other. The double helix and the two component strands follow a right-handed spiral. PDB ID: 1BNA.[5]

The predominant secondary structure observed under physiological conditions is B-form DNA, which is the double helical structure proposed by Watson and Crick. In B-form DNA, the two component strands hybridize with each other in an anti-parallel fashion, which means the directions of the two component strands are opposite. The double helix and each component strand in the double helix all adopt a right-handed conformation. (Figure 1.4) The bases between complementary strands in the duplex form base pairs according to the Watson-Crick pairing rule.[4] As the base pairs gradually rotate from the neighboring pairs along the helical axis, the inner angle between the two backbones forms the minor groove of the double helix, and the outer angle forms the major groove of the double helix. In B-form DNA, the diameter of a duplex is 2 nm. Each turn of the double helix contains 10.5 base pairs on average. The length of one full turn of the double helix is 3.4 nm. (Figure 1.5B)

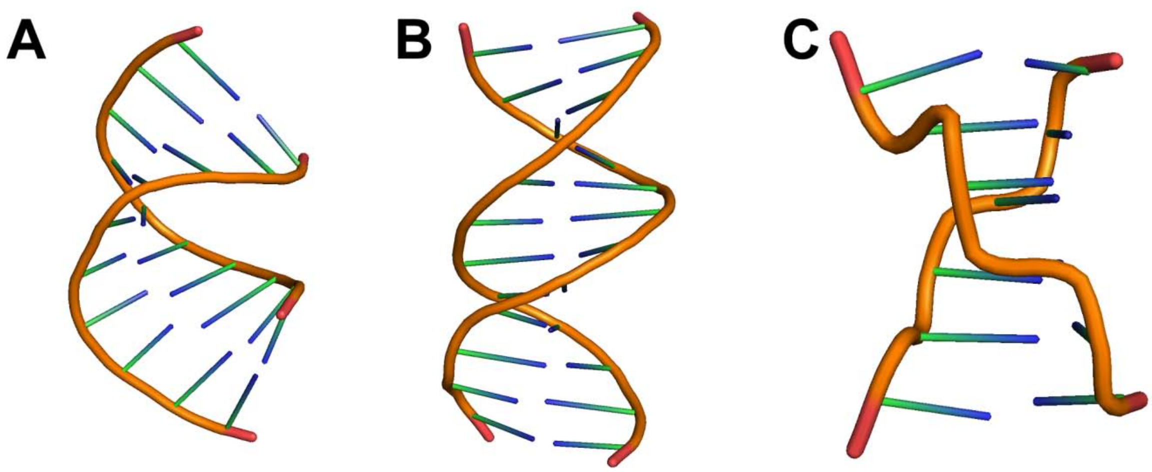

Figure 1.5. A comparison between structures of A-form, B-form, and Z-form DNA. **(A)** Structure of A-form DNA. PDB ID: 213D.[6] **(B)** Structure of B-form DNA. PDB ID: 1BNA.[5] **(C)** Structure of Z-form DNA. PDB ID: 2DCG.[7]

Besides B-form DNA, there are two other forms of DNA double helices that are well characterized. One is A-form DNA, and the other is Z-form DNA. A-form DNA is favored in dehydrated conditions, thus is also often seen in crystals. A-form DNA is also a right-handed structure. But there are several structural differences between A-form and

B-form DNA. One difference is that the diameter of an A-form DNA double helix is 2.6 nm, which is larger than that of B-form DNA. Another difference is that one full turn in A-form DNA contains 11 base pairs, instead of the 10.5 base pairs in B-form DNA. The length of a full turn in A-form DNA is 2.8 nm, which is shorter than one turn of B-form DNA. (Figure 1.5A) The origin of the conformational difference between A-form and B-form DNA is the different conformation of the sugar pucker. In A-form DNA, the sugar pucker conformation is C3' endo, while it is C2' endo in B-form DNA.[5]

Z-form DNA is a left-handed spiral structure. The predominant sequence pattern of Z-form DNA is an alternating purine-pyrimidine sequence. The sugar pucker conformation of the pyrimidines is C2' endo, while the purine sugar pucker is C3' endo, thus, the sugar-phosphate backbone displays a zig-zag conformation. The diameter of a Z-form double helix is 1.8 nm. Each full turn has 12 base pairs, and each full turn is 4.4 nm in length.[5] (Figure 1.5C).

The tertiary structure of DNA is a higher structure order than the secondary structure. It corresponds to the precise three-dimensional structure of DNA. One example of DNA tertiary structure is supercoiled DNA. A DNA supercoil is a coil of DNA double helices.

1.2.3 DNA Strand Displacement Reactions. Two DNA strands with partially or fully complementary domains hybridize with each other, and then displace one or more pre-hybridized domains in the two strands. This process is called DNA strand displacement. This reaction can occur either between two double-stranded DNAs (dsDNA) or one ssDNA and one dsDNA.[8]

Figure 1.6 shows the strand displacement reaction process between an ssDNA and dsDNA. The DNA duplex displays a single-stranded overhang, which is called toehold.[9] The toehold first binds another ssDNA with a complementary region. Then, if they have the same sequence, the segment of DNA next to the toehold region on the ssDNA migrates along the duplex and replaces the opposite strand. This step is called branch migration. Branch migration is a random displacement process that contains a series of reversible single nucleotide dissociation and hybridization steps.[10] When the branch migrates to the point that one strand dissociates from the complex, strand displacement is complete. The reaction is driven by the enthalpy change in the system as the end product has more base pairs.

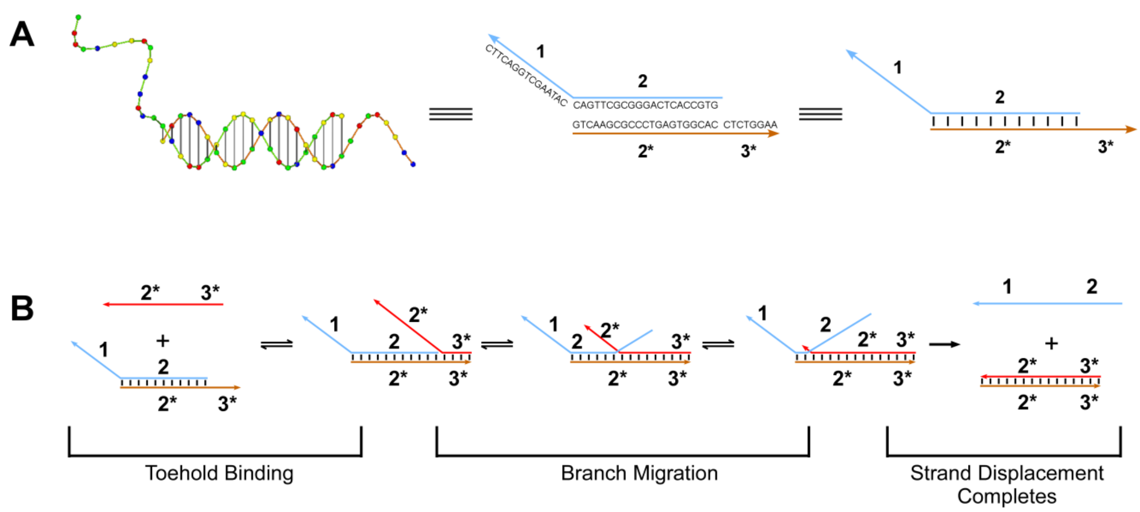

Figure 1.6. The process of a strand displacement reaction. **(A)** DNA is represented by directional lines with the arrow pointing to the 3’ end. **(B)** The strand displacement starts with the binding of the toehold domains. The braches migrate after the hybridization of the toeholds. The strand displacement is complete when the branch migration reaches the end and the pre-hybridized strand dissociates.

The kinetics of strand displacement reactions can be tuned by varying the length and sequences of the toehold domain as the toehold binding step is the rate limiting step.[11-13] The second order reaction rate constant ranges from 1 $M^{-1} \cdot s^{-1}$ to 6×10^6 $M^{-1} \cdot s^{-1}$. Increasing the length of toeholds and the G/C content in the toeholds can increase the reaction rate constant. And generally, the reaction rate constant stops increasing when the length of the toehold reaches >7 nucleotides.[13]

1.3 DNA Nanotechnology

In the early 1980's, Nadrian Seeman created an artificial DNA tile structure containing four ssDNAs rationally designed to form a four-way branched junction.[14] This work marks the beginning of DNA nanotechnology. DNA nanotechnologists engineer the interactions between DNA strands to fabricate and study nanoscale materials composed of DNA. Since the double-crossover (DX) DNA tile, which has a rigid conformation, was developed in 1993,[15] numerous tile-based DNA nanostructures have been designed and realized, including multi-helix bundles, cross shaped tiles or 3- and 5-point stars that assemble into 3D geometric polyhedrons, like cubes,[16] tetrahedra,[17] octahedra, icosahedra, and buckyballs.[18] Many periodic structures, such as nanotubes[19,20] and 2D lattice arrays,[21] have also been assembled utilizing the tile structures as repeating units.[22] (Figure 1.7)

In 2006, an important DNA nanostructure, DNA origami, was first developed.[23] DNA origami structures contain one long ssDNA as a scaffold. This scaffold is usually single stranded viral genomic DNA, and M13mp18 DNA is the most widely used. Through a specific design, hundreds of short ssDNA oligomers are mixed with the scaffold strand. These short ssDNA are usually called staple strands or helper strands, and are usually 30-50 nucleotides long. Each staple strand is a specifically designed sequence that hybridizes to multiple regions of the scaffold strand, thus brings specific regions into the desired adjacent positions. Finally, after all the staple strands hybridize to the correct complementary regions, the scaffold strand is folded into a well-defined shape based on the initial design. With this approach, many well controlled 2D structures with definite shapes and sizes are demonstrated on the sub-hundred nanometer scale.[23] Soon after that, many reports of 3D origami and origami with curvatures were published, thus making DNA origami a versatile and highly customizable material.[24-28]

DNA origami is a type of highly addressable structure. By modifying the staple strands, DNA origami can easily host other functional molecules or particles, such as proteins, peptides, virus capsids, nanoparticles, and carbon nanotubes.[29] This makes DNA origami a powerful tool in many research areas.

DNA origami and other types of structural DNA engineering have revealed their capability in scientific endeavors, but still face many future challenges. These challenges include gaining finer spatial control, expression and assembly *in vivo*, and reducing the cost of assembly. There are also potential new applications of DNA nanotechnology, like biomimetic systems and diagnostics and therapeutics for human health.[29]

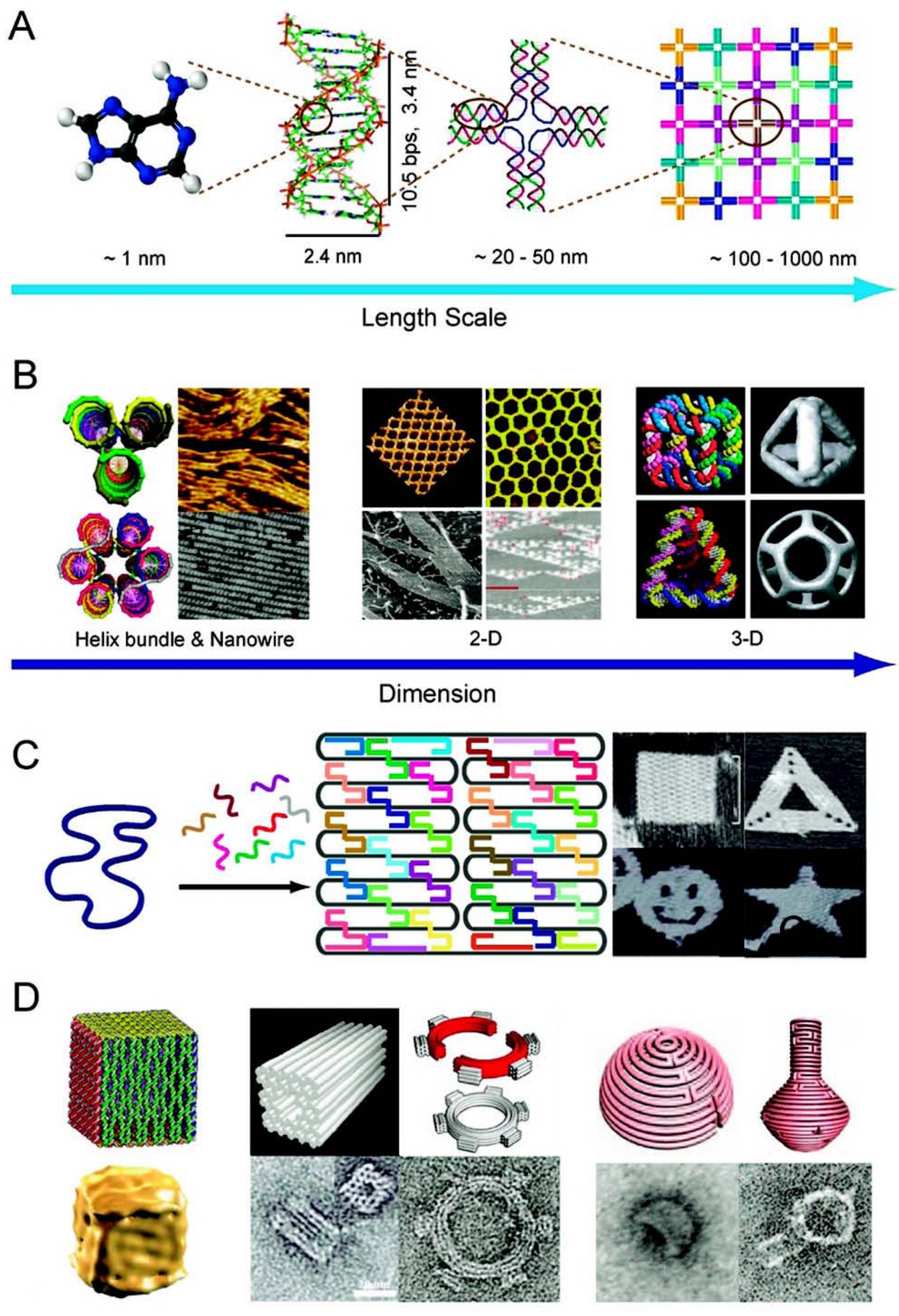

Figure 1.7. Structural DNA Nanotechnology. (A) DNA nanostructures based on DNA base pairing. (B) DNA multi-helix bundle, 2D lattice array of DNA tiles, and 3D DNA polyhedral structures. (C) The formation of DNA origami. One long ssDNA scaffold,

usually viral genomic DNA, and multiple staple strands are used. The staple strands are programmed to bind to specific positions on the scaffold, thus folding the scaffold strand into a pre-designed shape. (D) 3D DNA origami and DNA origami with curvature on their component DNA double helices. Panel A, Panel B, left and part of the middle image reproduced with permission from refs 22, 20, 19, and 21. Copyright 2012, 2005, and 1999 American Chemical Society. Parts of panel B, middle and right, and panel D, right and part of middle image, reproduced with permission from refs 30, 17, 25, and 27. Copyright 2003, 2005, 2009, and 2011 AAAS. Part of panel B, right, panel C, panel D, left, and part of panel D, middle, reproduced with permission from refs 31, 16, 18, 23, and 26. Copyright 2009, 1991, 2008, 2006, and 2009 Nature Publishing Group.

1.4 DNA Computation

1.4.1 DNA Computation and Its History. DNA computation and other forms of biological computation are interdisciplinary subjects that bridge chemistry, biology, and computer science. Compared to traditional silicon-based computation, DNA computation utilizes DNA and other biomolecules, and the interactions between these molecules to realize logical and mathematic functions. DNA is generally considered the best candidate for molecular level computation. One of the advantages of DNA over other types of biomolecules is that DNA is a very robust molecule. It is stable under a wide range of chemical conditions. DNA also has a relatively simple structure, and the behaviors of DNA molecules are highly predictable and programmable because of Watson-Crick base pairing. Another reason for DNA being popular in molecular programming is the easy accessibility of synthetic DNA.

The idea of molecular computation was first introduced by R. P. Feynman in his visionary presentation, *There's Plenty of Room at the Bottom*, at the 1959 annual meeting of the American Physical Society.[32] Feynman talked about miniaturizing computers in his talk. Although he did not propose any practical methods, he first pointed out the direction of developing computational system at molecular level. In 1994, 35 years after Feynman's talk, the first DNA computing system was developed by Leonard Adleman.[33] He solved the Hamiltonian path problem with a set of DNA strands and series of ligation, amplification, and purification operations on the DNA strands. In the two decades after this work, DNA computation has developed rapidly. In 2000, the idea of using enzyme free DNA strand displacement reactions to program molecular machines and reaction networks was developed.[9] Boolean logic circuits based on enzyme free DNA reaction system were realized in 2006.[34] Since then, developing complicated and functional logic circuits have been popular research topics in DNA computation.[35,36]

1.4.2 Methods Used in DNA Computation. There are many methods scientists have applied to DNA computation. One method is enzyme catalyzed DNA reactions. This method has the advantage of being able to select from various enzymes and reaction types, thus it makes the programming of computing operations easy and versatile. However, with enzymes in the system, the reactions are often restricted to the optimal conditions of the enzyme, such as narrow ranges of temperature, buffer concentration, light intensity, etc. The procedures also often involve multiple steps of separation of the enzymes and DNA.

The first DNA computation research, the Hamiltonian path problem by Leonard Adleman, was realized with multiple enzyme-catalyzed reactions of DNA. Figure 1.8

shows the Hamiltonian path graph Adleman used to demonstrate the process of DNA computation. For a graph with multiple vertices and directional edges going from one vertex to another, if there is a path composed of existing edges in the graph that goes through all vertices and only once through any individual vertex, that path is a Hamiltonian path of the graph. Adleman assigned a random 20 nucleotide long DNA single strand to each vertex *i* in the graph. These strands are named O_i, with complementary strands O_i*. Specifically, the starting vertex and ending vertex are referred to as vertex 0 and vertex 6, respectively, in Figure 1.8. Every edge *i-j*, which is directional from vertex *i* to vertex *j*, is represented by a 20 nucleotides ssDNA named $O_{i\text{-}j}$, which starts with the ten terminal 3' end bases of O_i, and ends with the ten terminal 5' end bases of O_j. All O_i* and $O_{i\text{-}j}$ are mixed and annealed for hybridization. At this point, every path in the graph has a corresponding DNA duplex in the system. The nicks in these duplexes are ligated with DNA ligase. Then the mixture solution is amplified by polymerase chain reaction (PCR), only using O_0 and O_6* as primers, such that only the paths starting at the entrance and ending of the exit are amplified. Then gel electrophoresis is used to purify the paths with the correct length. In the case shown in Figure 1.8, the expected Hamiltonian path should contain six edges, so the corresponding dsDNA should be 120 nucleotides long. The strands with the correct starting/ending points and correct length are then subjected to multi-step purification with magnetic beads modified with O_i*. In each step, only beads modified with a single O_i* sequence are used. Until all six O_i* are used once, any correct length strands missing any O_i domain, which means the path missing a vertex *i*, are removed. At the end, the remaining strands are sequenced to prove it represents the Hamiltonian path.[33]

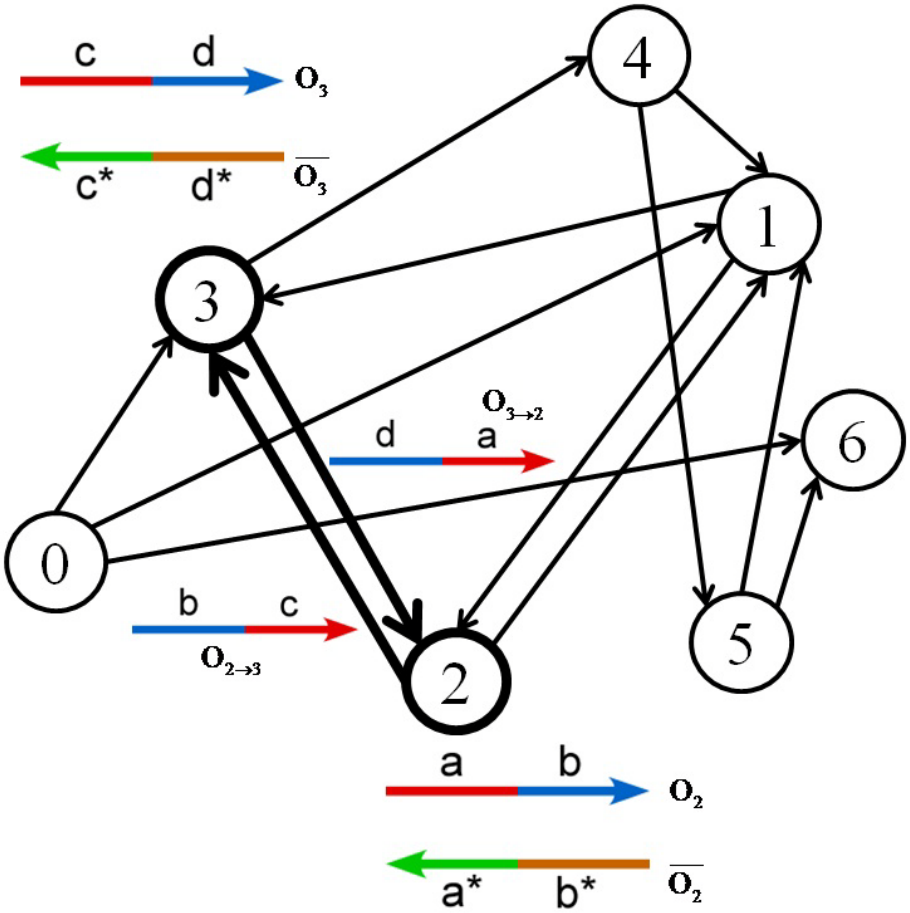

Figure 1.8. The Hamiltonian path. The graph with the same vertices and edges was used as the example in Adleman's work.[33] A Hamiltonian path exists in the graph, which is 0-1-2-3-4-5-6. Each vertex is assigned a random 20 nucleotide long ssDNA. For example, Vertex 2 is assigned as Strand a-b, and Vertex 3 is assigned as c-d. Each edge is represented by a 20 nucleotide ssDNA, which starts with ten terminal bases the 3' end of the starting vertex, and ends with the ten terminal bases of the 5' end of the ending vertex. For example, Edge 2-3 is represented as Strand b-c, as Domain b is the 3' end domain of the starting Vertex 2, and Domain c is the 5' end domain of the ending Vertex 3. Edge 3-2 is represented as Strand d-a following the same rule.

Another method in DNA computation is enzyme-free DNA reactions. The most powerful and well-studied reaction used in this category is toehold mediated strand displacement. A representative example of research utilizing this method is a binary square root calculation developed in 2011.[35] The authors designed a DNA strand displacement reaction network with two inputs, which are both ssDNA. The two input strands react and produce the same reactive species. By tuning the relative concentration of threshold dsDNA, which can consume the reactive species produced by the inputs, the function of the strand displacement reaction network can be switched between an AND gate and an OR gate of the two input strands. In this design of the logic gates, the input and output signals are all ssDNA, and the presence or absence of the signal DNA molecule means the signal is true or false, respectively. (Figure 1.9A) The goal was to construct the logic circuit shown in Figure 1.9C, which functions as a binary square root calculation. However the circuit contains a NOT function, which is difficult to realize with molecular computation, because once the downstream signal molecules are consumed, the output cannot be reversed by the upstream signal molecules. So instead, the authors constructed the logic circuit shown in Figure 1.9D to implement the function of the circuit shown in Figure 1.9C. The circuit shown in Figure 1.9D is a dual-rail input system. Each input or output signal in Figure 1.9C is divided into two signals. For example, input X_1 is divided into X_1^0 and X_1^1. These two signals are exclusive to each other. They cannot be true and false at the same time. If X_1^1 is true and X_1^0 is false, X_1 is true. Otherwise X_1 is false. The authors successfully realized a four-digit binary square root calculation with this strategy. And more importantly, they demonstrated a practical method to scale up DNA logic systems for complicated applications.[35]

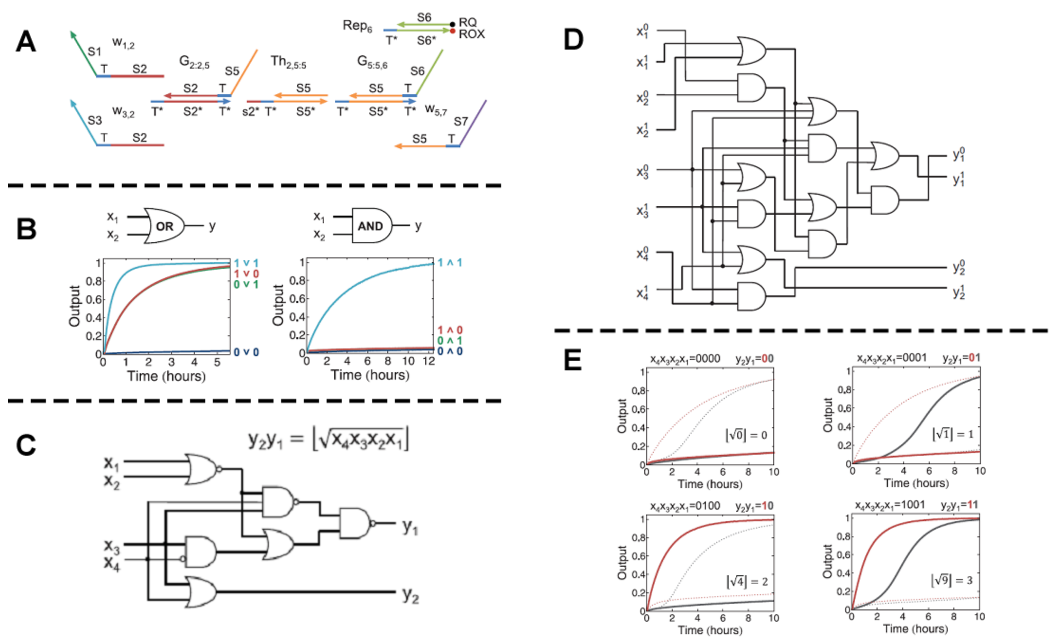

Figure 1.9. A square root calculation based on a DNA strand displacement reaction network. **(A)** The design of a single logic gate which can be switched between AND and OR gates by tuning the relative concentration of duplex Th. **(B)** Fluorescence kinetic results of the OR gate and AND gate. **(C)** The diagram of a four-digit binary square root logic circuit. **(D)** A dual-rail input logic circuit implementing the circuit in panel C. **(E)** Fluorescence kinetic results of the square root calculation. Figure reproduced with permission from ref 35. Copyright 2011 AAAS.

DNA computation and DNA nanotechnology are two naturally compatible areas. Although the goals of the two areas are different, they both use DNA molecules as materials, and the programming strategies are usually the same. As a result, DNA nanotechnology can be utilized for presenting mathematical and logical systems. In 2004, a DNA Sierpinski triangle constructed from DNA tiles was published. The authors used a set of unique DX tiles with carefully designed sticky ends and a long ssDNA template as a nucleation seed to achieve a binary XOR function between each neighboring tile pair and thus created a Sierpinski triangle fractal pattern. The system has a moderate error rate of 1% to 10%. Although it is not perfect, the starting points of assembly errors are traceable. Also, this work demonstrated the Turing-universal capability of engineered DNA self-assembly.[37] (Figure 1.10)

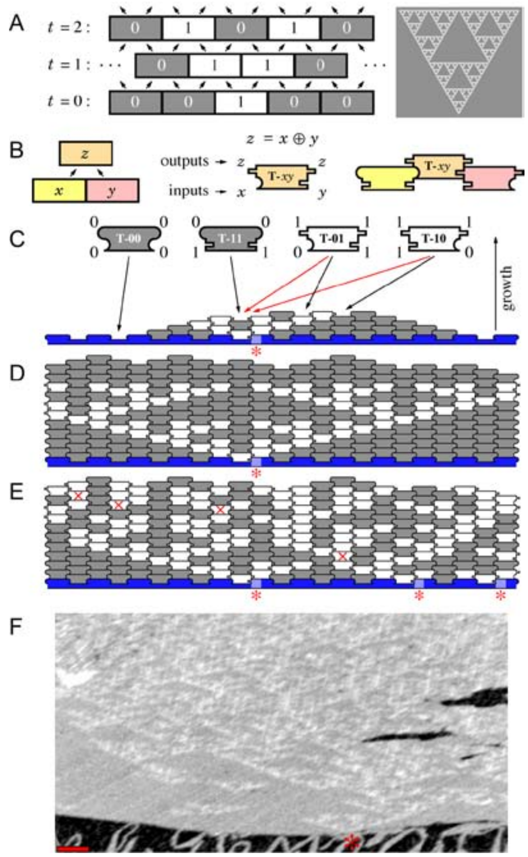

Figure 1.10. DNA tiles self-assembling into a Sierpinski triangle pattern following the XOR function. **(A)** Two groups of DNA tiles are employed in the system. One group of tiles shown in grey represents a binary 0. The other group of tiles shown in white represents a binary 1. A pair of neighboring tiles yields an output tile in the next row. The value of the output tile is the result of the XOR function of the values of the parent tiles. The tiles following the designed rule form a Sierpinski triangle pattern of the tiles of the

value of 1. **(B)** Translating the model in Panel A into DNA tiles. **(C)** Four types of tiles, of which two tiles have the value 1 and the other two tiles have the value 0, are used. **(D)** The expected pattern with no errors. **(E)** The expected error-prone pattern. **(F)** AFM result of the pattern. The scale bar is 100 nm. Figure reproduced with permission from ref 37. Copyright 2004 Rothemund et al.

Besides these three methods, another interesting method has also been used in DNA computation - programmed reactions catalyzed by DNAzymes, which is not discussed further.[38,39]

1.4.3 Comparison between DNA Computation and Silicon-Based Computing. Since people are very familiar with silicon-based computers, and the development of DNA computation is still at an early stage, people always tend to compare DNA computation with silicon-based computations. This topic can be discussed in two ways, one is the pros and cons of DNA computation, and the other is the applications of the two types of computations.

The biggest disadvantage of DNA computation is the low reaction or assembly rate. The typical time required by a DNA system to finish a simple logic operation ranges from a couple of hours to one day. The long time required by DNA and other biomolecular computation and programming techniques renders these systems far inferior to silicon-based computers in terms of calculation capability. This disadvantage is determined by the nature of DNA molecules, thus it is very difficult to overcome, even with an expectation of the development of DNA computation.

Another limiting factor of DNA computation is the lifetime of the materials being used. The lifetime of biological molecules is usually much shorter than inorganic materials used in traditional computers, even if they are stored under proper conditions. DNA is a relatively robust biomolecule, but it is still prone to degradation in the presence of small amounts of proteins, micro-organisms, or metal ions. The physical stability issue makes the operating conditions of DNA and other biomolecular computing systems limited to those proper for biochemical reactions. Also, long term information storage is difficult to achieve.

Currently, programmed DNA computing systems cannot be built up and characterized without the help of silicon-based computers. The artificial synthesis of the DNA components, concentration measurements for adjusting the component stoichiometry, and signal detection to read out the computation results all depend on instruments that are controlled by silicon-based computers. Even with the rapid development of biological and chemical sciences, it is not realistic to think that an independent bio-computer that can rival silicon-based computers will be developed. However, replacing or realizing the same functions of traditional computers is not necessary or practical.

Traditional computers utilized the bi-stable properties of materials to realize the binary function. There is no intermediate state between “0” and “1”. In DNA operations, the molecular signals have continuous intensities. The up side of this is that continuous signal intensities have a better tolerance for error. The down side is the dilemma of having a signal not significantly distinct enough to be assigned either “0” or “1”.

While bearing the disadvantages above, DNA computation has a significant natural advantage: DNA is biocompatible. This makes DNA a perfect tool for programming and regulating other biochemical reaction systems both *in vivo* and *in vitro*. DNA can be used to sense a biological signal, compute, return a result and actuate, e.g. release a drug.[40-44]

The other advantage of DNA computation is the different performance routine from that of traditional computers that can sometimes significantly simplify a problem. For example, in the Hamiltonian path work by Adleman, the author used a single DNA solution to generate all possible paths in the graph, which is a massively parallel processing strategy. This is superior to the brute force strategy used in traditional computers.

The pros and cons of DNA computation determine that its application area is different from that of the silicon-based computers. DNA computation and molecular programming are aimed to be applied in biological systems, which are currently developed in bioengineering and nanomedicine.[45,46]

1.5 References

(1) Watson, J. D.; Crick, F. H. C. *Nature* **1953**, *171*, 737.

(2) Dahm, R. *Dev. Biol.* **2005**, *278*, 274.

(3) Hecht, S. M. *Bioorganic Chemistry: Nucleic Acids*; OUP USA, 1996.

(4) Lehninger, A. L.; Nelson, D. L.; Cox, M. M. *Lehninger Principles of Biochemistry*; W. H. Freeman, 2005.

(5) Drew, H. R.; Wing, R. M.; Takano, T.; Broka, C.; Tanaka, S.; Itakura, K.; Dickerson, R. E. *Proc. Natl. Acad. Sci.* **1981**, *78*, 2179.

(6) Ramakrishnan, B.; Sundaralingam, M. *Biophys. J.* **1995**, *69*, 553.

(7) Wang, A. H. J.; Quigley, G. J.; Kolpak, F. J.; Crawford, J. L.; van Boom, J. H.; van der Marel, G.; Rich, A. *Nature* **1979**, *282*, 680.

(8) Zhang, D. Y.; Seelig, G. *Nat. Chem.* **2011**, *3*, 103.

(9) Yurke, B.; Turberfield, A. J.; Mills, A. P.; Simmel, F. C.; Neumann, J. L. *Nature* **2000**, *406*, 605.

(10) Radding, C. M.; Beattie, K. L.; Holloman, W. K.; Wiegand, R. C. *J. Mol. Biol.* **1977**, *116*, 825.

(11) Yurke, B.; Mills, A., Jr. *Genet. Program Evolvable Mach* **2003**, *4*, 111.

(12) Li, Q.; Luan, G.; Guo, Q.; Liang, J. *Nucleic Acids Res.* **2002**, *30*, e5.

(13) Zhang, D. Y.; Winfree, E. *J. Am. Chem. Soc.* **2009**, *131*, 17303.

(14) Seeman, N. C. *J. Theor. Biol.* **1982**, *99*, 237.

(15) Fu, T. J.; Seeman, N. C. *Biochemistry* **1993**, *32*, 3211.

(16) Chen, J.; Seeman, N. C. *Nature* **1991**, *350*, 631.

(17) Goodman, R. P.; Schaap, I. A. T.; Tardin, C. F.; Erben, C. M.; Berry, R. M.; Schmidt, C. F.; Turberfield, A. J. *Science* **2005**, *310*, 1661.

(18) He, Y.; Ye, T.; Su, M.; Zhang, C.; Ribbe, A. E.; Jiang, W.; Mao, C. *Nature* **2008**, *452*, 198.

(19) Mathieu, F.; Liao, S.; Kopatsch, J.; Wang, T.; Mao, C.; Seeman, N. C. *Nano Lett.* **2005**, *5*, 661.

(20) Park, S. H.; Barish, R.; Li, H.; Reif, J. H.; Finkelstein, G.; Yan, H.; LaBean, T. H. *Nano Lett.* **2005**, *5*, 693.

(21) Mao, C.; Sun, W.; Seeman, N. C. *J. Am. Chem. Soc.* **1999**, *121*, 5437.

(22) Fu, J.; Liu, M.; Liu, Y.; Yan, H. *Acc. Chem. Res.* **2012**, *45*, 1215.

(23) Rothemund, P. W. K. *Nature* **2006**, *440*, 297.

(24) Ke, Y.; Douglas, S. M.; Liu, M.; Sharma, J.; Cheng, A.; Leung, A.; Liu, Y.; Shih, W. M.; Yan, H. *J. Am. Chem. Soc.* **2009**, *131*, 15903.

(25) Dietz, H.; Douglas, S. M.; Shih, W. M. *Science* **2009**, *325*, 725.

(26) Andersen, E. S.; Dong, M.; Nielsen, M. M.; Jahn, K.; Subramani, R.; Mamdouh, W.; Golas, M. M.; Sander, B.; Stark, H.; Oliveira, C. L. P.; Pedersen, J. S.; Birkedal, V.; Besenbacher, F.; Gothelf, K. V.; Kjems, J. *Nature* **2009**, *459*, 73.

(27) Han, D.; Pal, S.; Nangreave, J.; Deng, Z.; Liu, Y.; Yan, H. *Science* **2011**, *332*, 342.

(28) Han, D.; Pal, S.; Liu, Y.; Yan, H. *Nat. Nano.* **2010**, *5*, 712.

(29) Pinheiro, A. V.; Han, D.; Shih, W. M.; Yan, H. *Nat. Nano.* **2011**, *6*, 763.

(30) Yan, H.; Park, S. H.; Finkelstein, G.; Reif, J. H.; LaBean, T. H. *Science* **2003**, *301*, 1882.

(31) Douglas, S. M.; Dietz, H.; Liedl, T.; Hogberg, B.; Graf, F.; Shih, W. M. *Nature* **2009**, *459*, 414.

(32) Feynman, R. P. *J. Microelectromechanical Systems* **1992**, *1*, 60.

(33) Adleman, L. M. *Science* **1994**, *266*, 1021.

(34) Seelig, G.; Soloveichik, D.; Zhang, D. Y.; Winfree, E. *Science* **2006**, *314*, 1585.

(35) Qian, L. L.; Winfree, E. *Science* **2011**, *332*, 1196.

(36) Li, W.; Yang, Y.; Yan, H.; Liu, Y. *Nano Lett.* **2013**, *13*, 2980.

(37) Rothemund, P. W. K.; Papadakis, N.; Winfree, E. *PLoS. Biol.* **2004**, *2*, e424.

(38) Elbaz, J.; Lioubashevski, O.; Wang, F.; Remacle, F.; Levine, R. D.; Willner, I. *Nat. Nano.* **2010**, *5*, 417.

(39) Kahan-Hanum, M.; Douek, Y.; Adar, R.; Shapiro, E. *Sci. Rep.* **2013**, *3*.

(40) Parker, J. *EMBO reports* **2003**, *4*, 7.

(41) Douglas, S. M.; Bachelet, I.; Church, G. M. *Science* **2012**, *335*, 831.

(42) Benenson, Y. *Curr. Opin. Biotech.* **2009**, *20*, 471.

(43) Surana, S.; Bhat, J. M.; Koushika, S. P.; Krishnan, Y. *Nat. Commun.* **2011**, *2,* 340.

(44) Hemphill, J.; Deiters, A. *J. Am. Chem. Soc.* **2013**, *135*, 10512.

Chapter 2

Multi-Functional DNA Logic Circuit: 3-Input Majority Logic Gate and Multiple Input Logic Circuit Based on DNA Strand Displacement

Adapted with permission from Li, W.; Yang, Y.; Yan, H.; Liu, Y., Three-Input Majority Logic Gate and Multiple Input Logic Circuit Based on DNA Strand Displacement. *Nano Lett.* **2013,** *13*, 2980-2988. Copyright 2013 American Chemical Society.

2.1 Abstract

In biomolecular programming, the properties of biomolecules such as proteins and nucleic acids are harnessed for computational purposes. The field has gained considerable attention due to the possibility of exploiting the massive parallelism that is inherent in natural systems to solve computational problems. DNA has already been used to build complex molecular circuits, where the basic building blocks are logic gates that produce single outputs from one or more logical inputs. We designed and experimentally realized a 3-input majority gate based on DNA strand displacement. One of the key features of a 3-input majority gate is that the 3 inputs have equal priority, and the output will be true if any of the two inputs are true. Our design consists of a central, circular DNA strand with 3 unique domains between which are identical joint sequences. Before inputs are introduced to the system, each domain and half of each joint is protected by one complementary ssDNA that displays a toehold for subsequent displacement by the corresponding input. With this design the relationship between any two domains is analogous to the relationship between inputs in a majority gate. Displacing two or more of the protection strands will expose at least one complete joint and return a true output; displacing none or only 1 of the protection strands will not expose a complete joint and

will return a false output. Further, we designed and realized a complex 5-input logic gate based on the majority gate described here. By controlling 2 of the 5 inputs the complex gate can realize every combination of OR and AND gates of the other 3 inputs.

2.2 Introduction

The ability to program interactions between biomolecules can help us to understand life processes and activities at the molecular level. DNA is an ideal candidate for molecular programming that facilitates both *in vivo* and *in* **vitro** applications[1] because of its biological and physical properties. The behavior of DNA molecules with particular sequences can be reliably predicted according to the Watson-Crick base-pairing principle. The recent developments in the field of structural DNA nanotechnology[2] provide many different platforms onto which logically programmed DNA interactions can be combined and organized.

The first employment of DNA as molecular programming reagent resulted in a solution to the seven-city Hamilton path problem.[3] Since then, several enzyme-catalyzed[4-6] and enzyme-free[7-10] DNA automata systems have been designed and realized. In the enzyme-free systems single-stranded DNA (ssDNA) molecules are used as input signals. Introducing the input signals to a system containing other double-stranded DNA (dsDNA) molecules displaying ssDNA toeholds results in a series of toehold directed strand displacement reactions[11-15] and the release of an ssDNA molecule as a detectable output signal. Computing circuits based on DNA strand displacement that demonstrate complicated computations such as binary square root [16] and network computations[17] were achieved with high efficiency and accuracy. In these computing circuits both AND and OR gates were utilized.

In this work we achieved the construction of a 3-input majority logic gate by programming DNA interactions. A majority logic gate with multiple inputs returns true outputs, if and only if more than half of the inputs are true. A 3-input majority gate is one of the most basic logic gates and has been demonstrated using magnetic quantum-dot cellular automata (MQCA).[18] With multiple inputs this gate can accept and produce a high volume of information; thus, on the molecular level a 3-input majority gate can serve as a basic and versatile building block for constructing more complex circuits. Here we experimentally realized a 3-input majority gate with programmed DNA strand displacement reactions for the first time, and demonstrated that it reliably produces all the correct outputs with different combinations of the inputs. We further constructed a 5-input computing circuit implemented solely by linking two 3-input majority gates together. This circuit can be tuned to accomplish four different computing patterns among the various combinations of the inputs.

2.3 Architecture Design

2.3.1 Single 3-input Majority Gate. For a 3-input majority gate (see Figure 2.1A), if any 2 or all of the 3 inputs are true, the output is true. The truth table (Table 2.1) specifies that the 3 inputs have the same priority among one another. Thus, for a 3-input majority gate the outputs between any combinations of 2 or 3 inputs should not be distinguishable. To construct a 3-input majority gate from DNA molecules we implemented a circular DNA strand consisting of 3 distinct segments, A, B, and C (Figure 2.1B); in each segment the middle portion is unique (M1, M2 and M3, 16 nts each), and the 3 joints are identical (RS2 18 nts and RS1, 8 nts). Before performing the computation segments A, B, and C each hybridize to a complementary ssDNA molecule

(A*, B* and C*, respectively) forming a circular (quasi-triangular) duplex. Strands A*, B*, and C* each have two domains: one domain is fully complementary to A, B, and C, respectively, and the other domain displays a toehold (T1*, T2*, and T3*, 10 nts each) for initiating the strand displacement reaction. This circular duplex structure is referred to as a “Calculator” herein.

Table 2.1. Truth table of a 3-input majority logic gate

Input A	Input B	Input C	Output
0	0	0	0
1	0	0	0
0	1	0	0
0	0	1	0
1	1	0	1
1	0	1	1
0	1	1	1
1	1	1	1

Three unique input strands (Inputs A, B, and C) are designed to be fully complementary to A*, B* and C* (both domains). When the inputs are introduced to the computing system toehold-mediated strand displacement reactions are initiated. For those cases in which there are 2 or 3 inputs (i.e. majority input) (Figure 2.1C), ssDNA from 2 or 3 sides of the Calculator are released. The release events expose a single joint (for 2 inputs), or all three joints (for three inputs), in the Calculator structure and Segments A, B, and C is/are concurrently exposed as ssDNA. The exposure of at least one joint domain (all with the same sequence) is defined as a positive output. A "Detector" is utilized to recognize and report the output. The detector is composed of two strands that form a duplex displaying a toehold, and is labeled with a fluorescence dye and a corresponding dark quencher on the two component strands. The strand that is modified with the dark quencher carries the toehold that is fully complementary to the output. When it hybridizes with the output, the fluorescence-dye-modified strand is released to the solution and an increase in the fluorescence intensity of the dye is detected as proof of a true output.

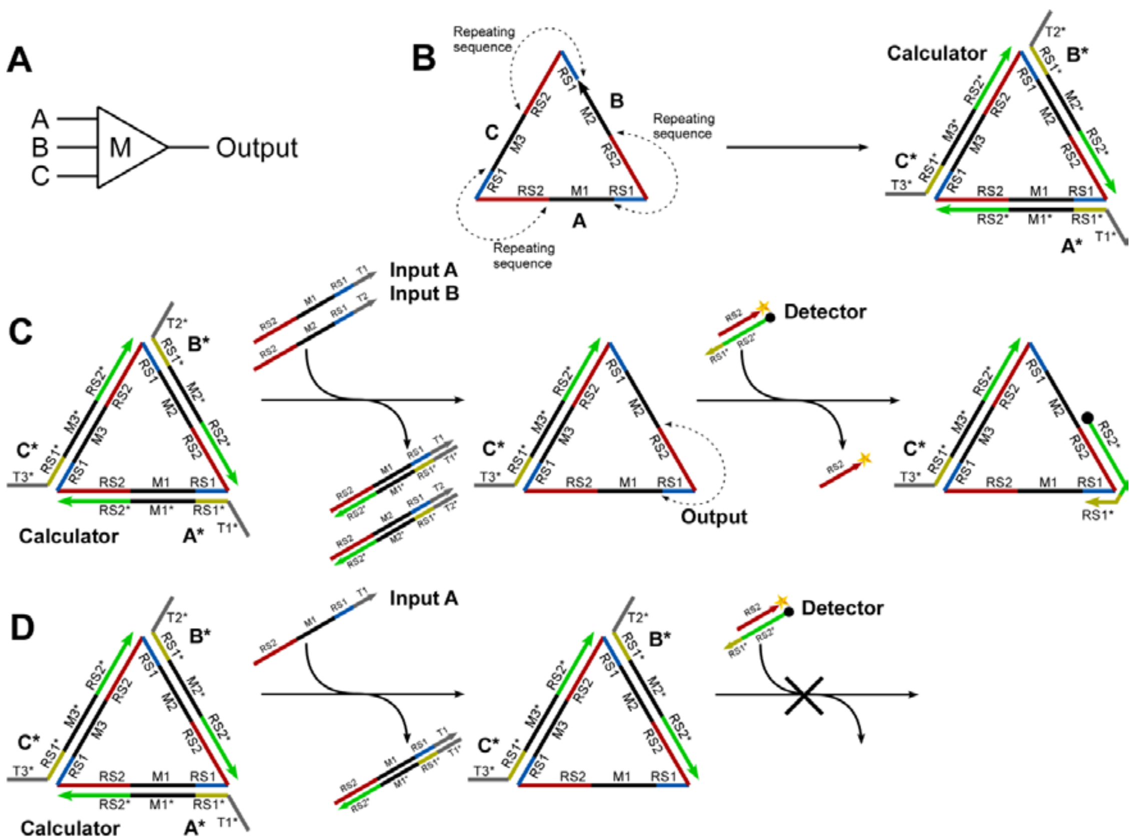

Figure 2.1. Architectural design of a 3-input majority gate based on DNA strand displacement reactions. (**A**) Symbolic representation of the majority logic gate. (**B**) Design of the Calculator structure. The circular ssDNA (left) is composed of 3 segments, A (RS2-M1-RS1), B (RS2-M2-RS1), and C (RS2-M3-RS1). Each segment has 42 nts.

RS1 and RS2 are 8 and 18 nts long, respectively. The RS1-RS2 joint sequence is repeated in the circular structure 3 times. M1, M2, and M3 are each 16 nts long and have distinct sequences. ssDNA A*, B*, and C* are hybridized with A, B, and C, respectively, forming the Calculator structure (right). A*, B*, and C* each have 2 domains: one domain, RS1*-M1(2,3)*-RS2*, is fully complementary to A, B or C. The other domain, T1(2,3)*, is a unique sequence toehold for initiating the computation process. (**C**) 2 or 3 inputs lead to a true output. Here a representative 2 input model is shown. Input A and Input B are fully complementary to A* and B*, respectively. The toeholds, T1 and T2, first hybridize with T1* and T2*. Next, the input strands fully displace A* and B* from the circular structure. Finally A* and B* hybridize with Input A and Input B and are displaced from the Calculator. The RS1-RS2 joint (output) on the circular strand is then fully exposed, yielding a true output. A "Detector" is pre-mixed with the Calculator. The Detector is a duplex of RS2 and RS2*-RS1*. RS2 is modified with 6-carboxyfluorescein (FAM) at the 3' end. RS2*-RS1* is modified with Iowa Black^{TM} dark quencher (IABk) at the 5' end. RS1 in the output and RS1* in the Detector serve as toeholds and RS2-FAM is displaced from the dark quencher, thus the true output is revealed by a fluorescence increase. (**D**) One or no input leads to a false output. A representative 1 input (e.g. Input A) case is shown. Only A* is released by Input A, thus no continuous RS1-RS2 is exposed and the output is 0. The Detector duplex is highly stable and the fluorescence remains quenched through the computation process.

When only 1 or no input (minority input) is introduced (Figure 2.1D), none of the joint domains of the 3 segments is fully exposed. Even though 2 joint domains may be partially exposed, because they are operating separately at opposite ends of a segment they cannot disassemble the detector duplex and the output remains 0.

2.3.2 Logic Gate Cascade. As indicated by the truth table (Table 2.1), an important property of a 3-input majority gate is that if any of the 3 inputs is preset as 1, the logic gate becomes an OR gate for the remaining 2 inputs (Figure 2.2A), and if any of the 3 inputs is preset as 0, the logic gate becomes an AND gate for the remaining 2 inputs (Figure 2.2B). This ability to switch between OR and AND gates makes the 3-input majority gate a versatile building block for constructing more complex computing circuits.

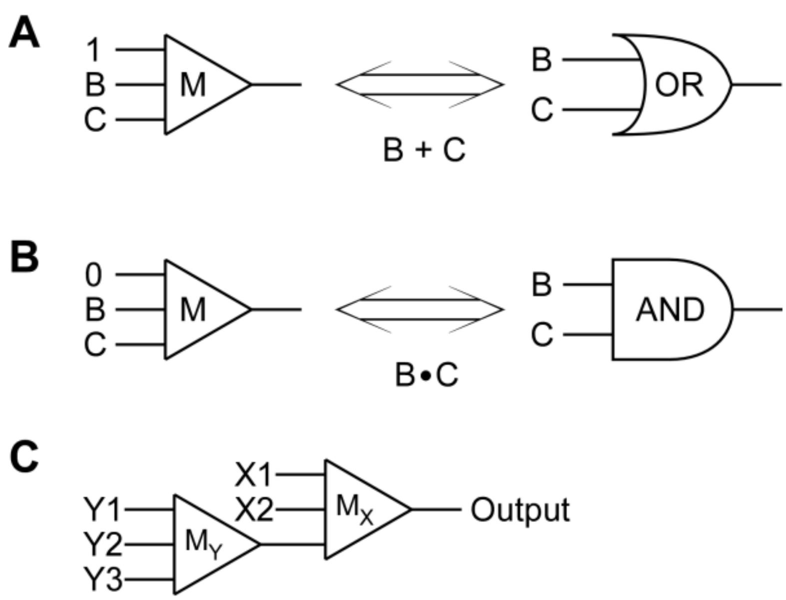

Figure 2.2. Properties of a 3-input majority gate and the design of a multi-functional circuit. (**A**) If any 1 of the 3 inputs of a majority gate is preset as 1, the gate becomes an OR gate of the remaining 2 inputs. In the figure, Input A is preset as 1. The relationship between Inputs B and C becomes an OR function (B + C). (**B**) If any 1 of the 3 inputs of a majority gate is preset as 0, the gate becomes an AND gate of the remaining 2 inputs. In

the figure, Input A as 0 is shown. The relationship between Inputs B and C becomes an AND function (B · C). (**C**) The multi-functional circuit contains 2 majority gates and has a depth of 2. The output of the first generation, Majority Gate Y (M_Y), is employed as one input of the second generation, Majority Gate X (M_X). There are 5 input of the circuit: Y1, Y2, and Y3 to M_Y; X1, and X2 to M_X. The output of the second generation is the output of the entire circuit.

Table 2.2. Computing patterns of the multi-functional circuit under different preset values of X1 and Y1

X1	Y1	Computation Pattern
0	0	Y2 · Y3 · X2
1	0	Y2 · Y3 + X2
0	1	(Y2 + Y3) · X2
1	1	Y2 + Y3 + X2

To demonstrate switching of a 3-input majority gate we assembled a computing circuit composed of 2 majority gates arranged sequentially (Figure 2.2C). Majority Gate Y (M_Y) is the first generation gate. The output of M_Y is utilized as one of the inputs of Majority Gate X (M_X), which is the second generation gate. The output from M_X is read as the final output of the circuit. The circuit has 5 inputs in total: Y1, Y2, and Y3 in M_Y; X1, and X2 in M_X. By assigning values of 0 or 1 to any one of the inputs in each majority gate, this circuit can be switched between 4 different computing patterns for the remaining 3 inputs (Table 2.2). These 4 logical computing patterns represent all the combinations of OR and AND functions between the 3 inputs.

Based on the success of the single majority gate design described above (shown in Figure 2.1C, D), we engineered a 2-generation circuit as shown in Figure 2.3. Similarly, the Calculator structures in both generations feature a circular (quasi-triangular) design. The sequences of the joint domains between any 2 arms of Calculator Y (first generation) are all the same such that fully exposing any of the joints results in a true output of M_Y. Each joint domain is fully complementary to arm X3 in Calculator X (the second generation). Therefore, the output of M_Y acts as an intermediate of the circuit and can be used as an input for the next generation calculator. For example, if the output of M_Y is true, M_X receives a true input from M_Y; and if the output of M_Y is false, M_X receives a false input from M_Y. Depending on the output of M_Y and the additional 2 inputs of M_X (X1 and X2) Calculator X produces the final output of the circuit. For example, if any 2 or 3 of the inputs for M_X are present, 2 or 3 of the arm strands (X1*, X2*, and X3*) are displaced from Calculator X, exposing at least one joint domain of the circular strand as ssDNA which yields a true final output. Conversely, if only 1 or none of the inputs for M_X is present, the final output is false. The output reacts with the “Detector”, binding with the dark quencher labeled strand and releasing the fluorescence of the dye modified strand. The output is visualized by an increase in the fluorescence intensity of the dye, following the same mechanism as for the single majority gate.

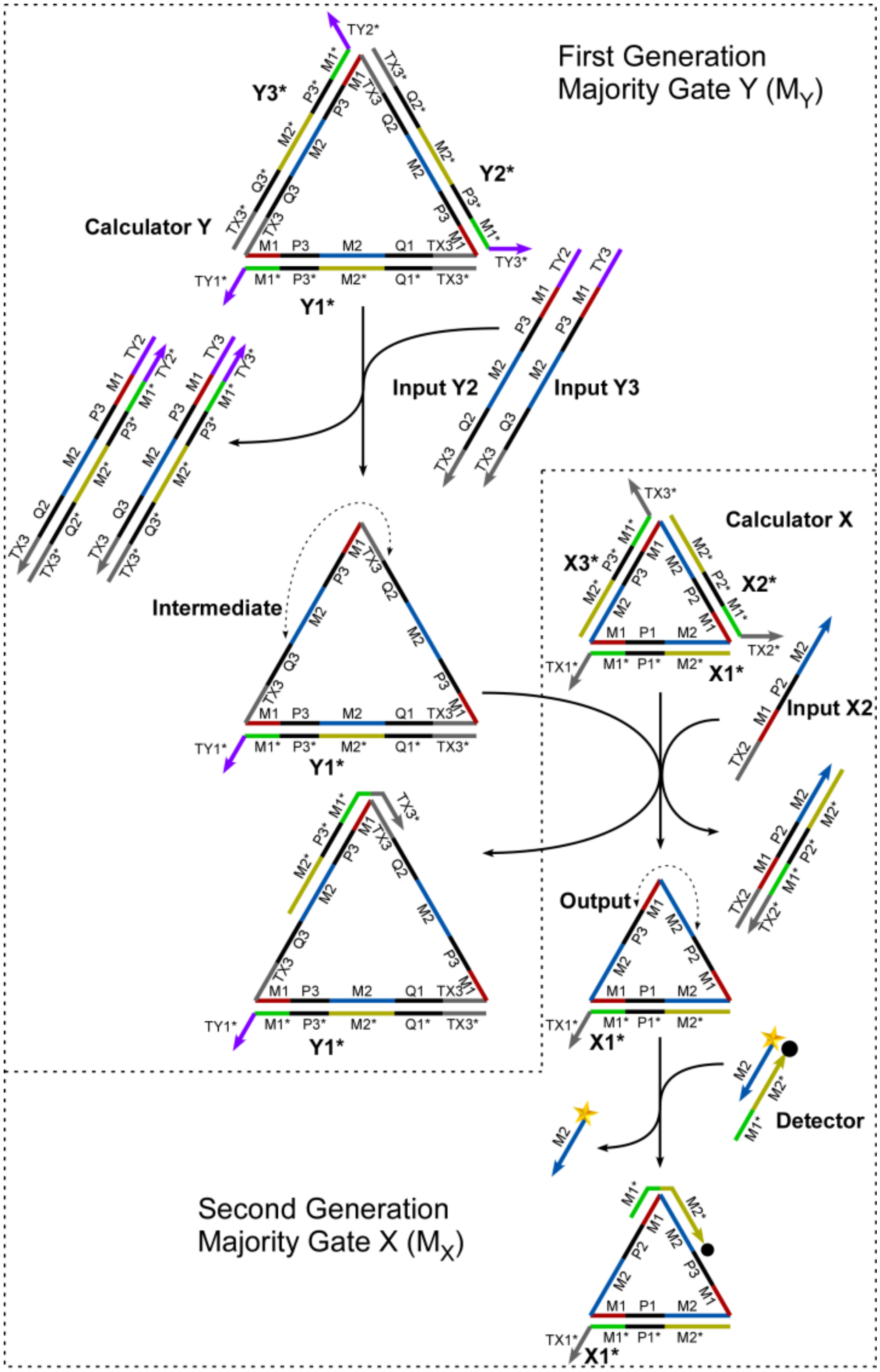

Figure 2.3. Designed reaction flow of the multi-functional circuit. Majority Gate Y (M_Y), the first generation in the circuit, is shown in the upper-left. Majority Gate X (M_X), the

second generation in the circuit, is shown in the lower-right. For M_Y, there are 3 segments in circular Calculator Y, each with 3 domains. One domain of the circular strand is M1-P3-M2. A second domain is Q1(2,3); Q1, Q2, and Q3 are each a unique sequence. The third domain is TX3. The 3 joint segments of the circular strand are all TX3-M1-P3-M2. Once Calculator Y has 2 or 3 arms displaced it will return a true M_Y output, exposing the Intermediate (TX3-M1-P3-M2) as ssDNA. This Intermediate is fully complementary to arm strand X3* in Calculator X, and can therefore serve as an input of M_X. TX3 in the Intermediate functions as a toehold and M1-P3-M2 displaces the remainder of X3* from Calculator X. For M_X, there are also 3 segments in Calculator X. The design of Calculator X is similar to the design of the single gate shown in Figure 2.1, except for the length of each domain. The intermediate, and the other 2 Inputs of M_X, Input X1 and Input X2, determine the output of the overall circuit. The ssDNA output signal is the repeating joint sequence of the circular strand in Calculator X, M2-M1. Similar to the single gate design the output of the circuit can be detected via changes in the fluorescence of a dye molecule. A representative computing pattern example is shown in the figure. Input Y1 is preset as 0, which means that no ssDNA Input Y1 is introduced to the reaction. Input X1 is also preset as 0. As a result of the preset values of Inputs Y1 and X1, the computing pattern in the figure is Y2 · Y3 · X2. Inputs Y2, Y3, and X2 are all present in the reaction system so the logical computing result is 1· 1 · 1 = 1. The lengths (in base pairs) of the domains in the figure: TX1(2,3) = TX1(2,3)* = 10. P1(2,3) = P1(2,3)* = 9. M1 = M1* = 8. M2 = M2* = 15. TY1(2,3) = TY1(2,3)* = 10. Q1(2,3) = Q1(2,3)* = 11.

2.4 Results and Discussion

2.4.1 Assembly of the Calculators. The central circular ssDNA molecules (126 nts long for the single 3-input majority gate, 159 nts long for M_Y and 96 nts for M_X) in the calculators are prepared by ligating one or two linear ssDNAs end to end (See APPENDIX A for Figure S2.1). T4 DNA ligase is used to catalyze the circularization reactions. The termini of the ssDNA fragments are specifically paired and joined by hybridizing to 20-nt ssDNA templates and the resulting nicks are then sealed with T4 DNA ligase. The circular ssDNA is purified and recovered by denaturing polyacrylamide gel electrophoresis (PAGE). The overall recovery yield of the purified circular ssDNA is 30% to 50% (APPENDIX A, Figure S2.2A); note that the circularized strands are resistant to degradation by exonuclease I (APPENDIX A, Figure S2.2B). The purified central circular ssDNA is hybridized with the 3 arm strands, forming the Calculator (Figure 2.4). The molar ratio between the circular ssDNA and each arm strand is 1:1.1.

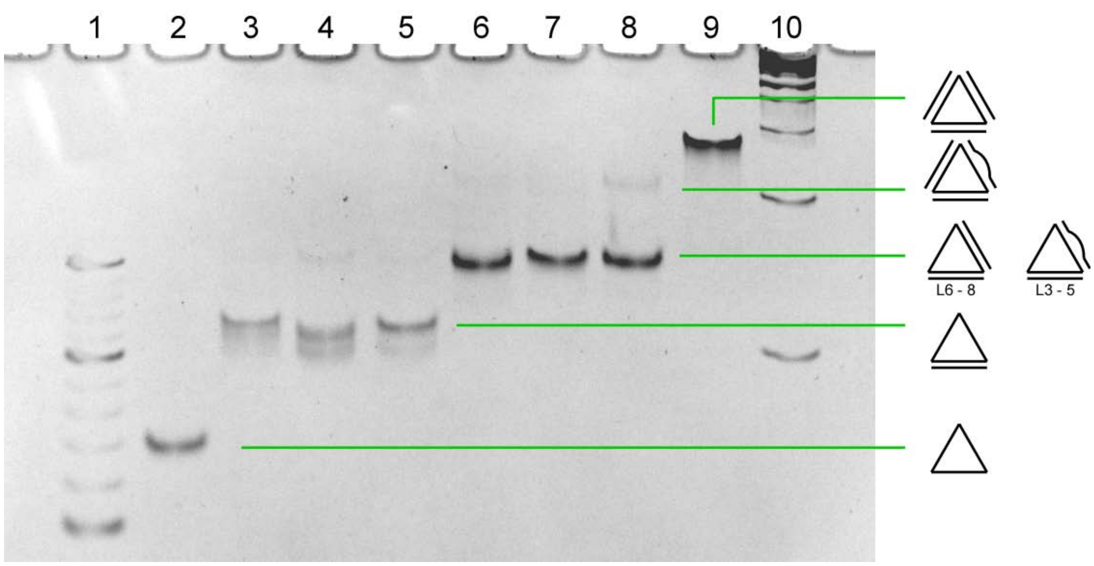

Figure 2.4. Native polyacrylamide gel electrophoresis confirming the formation of the single gate Calculator of the single gate. **Lane 1:** 10 bp DNA ladder. The three intense

bands are 50 bps, 100 bps and 150 bps from bottom to top, respectively. **Lane 2:** center circular strand. **Lanes 3 – 5:** center strand with one arm strand: A*, B* or C*, respectively. **Lanes 6 – 8:** center strand with two arm strands: A* + B*, A* + C*, or B* + C*, respectively. **Lane 9:** center strand with three arm strands: A* + B* + C*, forming the complete Calculator structure. **Lane 10:** 100 bp DNA ladder. For each segment of the center circular strand, the two termini are portions of the repeating sequence. As a result, if a segment of the center strand does not have a fully complementary arm strand present in the system, its two ends may hybridize with the excess arm strands intended to interact with other segments such that with the middle portion of the segment is not bound. This process may result in species with retarded mobility as shown in Lanes 3 to 8.

2.4.2 Gel Characterization of Calculator Formation and Operation with Inputs. The Calculators are prepared with excess arm strands that do not need to be removed before use. After a Calculator is prepared the specific input strands are mixed with the Calculator at a molar ratio of 1.2:1. The input strands displace the arm strands from the central circular strand of the Calculator. The structural changes of the Calculator corresponding to single gate reactions were characterized by native PAGE (Figure 2.5).

The gel image shown in Figure 2.5 clearly demonstrates the difference between true and false outputs of the logic gate for different input combinations. Lane 2 corresponds to no inputs and the intact Calculator migrates as a single band. Lanes 3, 4, and 5 correspond to systems with a single input. Multiple bands are present in the gel image, but the emergence of species with fully exposed circular strand joints was not observed. Lanes 6 to 9 correspond to systems with 2 or 3 inputs where at least one output ssDNA is evident.

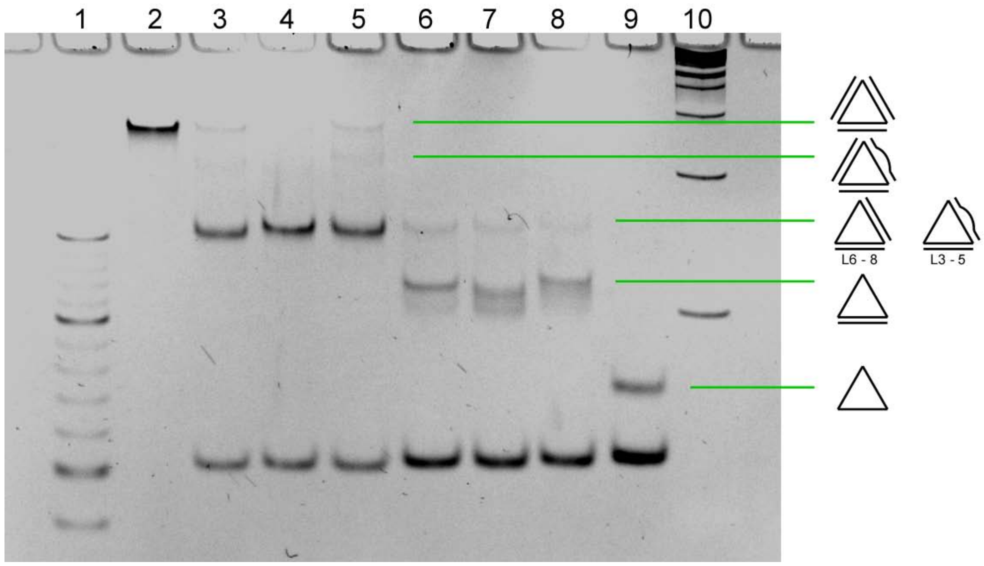

Figure 2.5. Native PAGE demonstrating the single gate design Calculator. **Lane 1**: 10 bp DNA ladder. The three intense bands are 50 bps, 100 bps and 150 bps from bottom to top, respectively. **Lane 2:** the fully assembled Calculator. **Lanes 3 – 5:** the Calculator with a single input: Inputs A, B, or C respectively. **Lanes 6 – 8:** the Calculator with two inputs: Inputs A + B, Inputs A + C, or Inputs B + C, respectively. **Lane 9:** the calculator with all three inputs. **Lane 10:** 100 bp DNA ladder. For each segment of the center circular strand, the two termini are portions of the repeating sequence. As a result, if a segment of the center strand does not have a fully complementary arm strand present in the system, its two ends may hybridize with the excess arm strands intended to interact with other segments such that with the middle portion of the segment is not bound. This process may result in species with retarded mobility as shown in Lanes 3 to 8.

2.4.3 Detecting the Operation of a Single Majority Gate. A fluorescent dye molecule was used to detect the products of the 3-input majority gate and to follow the kinetics of the logic computing reactions (Figure 2.6). The Calculator, a specific combination of inputs, and the FAM - Iowa Black^{TM} modified Detector are mixed and the fluorescence intensity of FAM (Ex 490 nm, Em 520 nm) is measured every 30 seconds at constant temperature of ~ 20°C.

At the beginning of the reaction the fluorescence intensities of all input combinations are low because the FAM modified strand in the detector remains hybridized to the dark quencher modified strand. For reactions with one or no input, no output ssDNA is produced as the reaction proceeds. Thus, the FAM strands are never released from interaction with the dark quencher. The fluorescence intensities of these reactions remain at a low level throughout the experiment, indicating a false output of the majority logic gate.

For reactions with two or three inputs, one or three ssDNA output domains of the Calculators are exposed. The outputs are subsequently recognized by the Detector through toehold hybridization events. Next, the output displaces the FAM modified strand (toehold mediated displacement) from the dark quencher modified strand. As a result the fluorescence intensity increases, indicating the true output. The reaction rates are high at the initial stages of the reaction and slow down considerably as more and more Calculator species and ssDNA inputs are consumed. After the reaction reaches equilibrium the fluorescence intensity of that system remains constant. The computation of each input combination finishes in 0.5 to 1.5 hours.

From the design shown in Figure 2.1 it is apparent that if all 3 inputs are introduced to the Calculator, 3 ssDNA output domains would be exposed. Therefore, the molar ratio between the output and the Calculator is 3:1. However, for the three cases with combinations of 2 inputs the molar ratio between the output species and the Calculator is 1:1 because there is only one output domain exposed per Calculator. Thus, when there is 3 or more fold excess of the Detector present, the final fluorescence intensity of the 3-input model is expected to be 3 times higher than the 2-input cases (Figure 2.6B). If the amount of the Detector in the system is decreased to the same level as that of the Calculator, the final fluorescence intensities of the true output cases will be limited by the availability of the Detector. Figure 2.6A illustrates such a scenario in which four true outputs yield similar fluorescence intensity levels. The reaction kinetics is the fastest for the system with all three inputs, and for the 2-input systems the rates are similar when input B is absent, but become much slower when either input A or C is missing. The 1- to 2-fold difference in the reaction kinetics is not well understood. We speculate that it may originate from sequence-specific interactions between the DNA strands, especially in the toehold regions.

The raw data collected from the fluorescence experiments is the absolute intensity of the detector bound dye at each time point in the reaction. The fluorescence increase for each reaction is calculated by subtracting the initial intensity from the final intensity. For cases with a 1:1 Detector to Calculator ratio, the fluorescence increase is normalized to 1 (Figure 2.6A). The curves corresponding to reactions with 2 or 3 inputs plateau above 0.75, while the curves with one or no input reach equilibrium very close to 0.

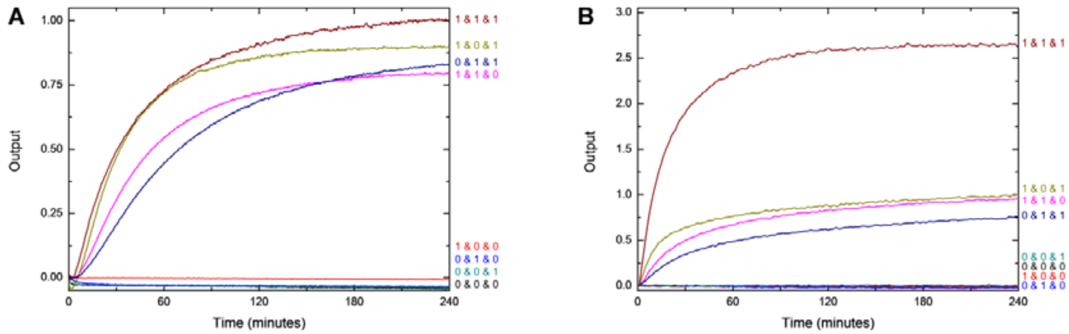

Figure 2.6. Kinetic characterization of the single 3-input majority gate. (**A**) The ratio between the Detector and the Calculator is 1:1. (**B**) The ratio between the Detector and the Calculator is 4:1. Each curve in these two graphs represents a reaction corresponding to the inputs specified next to each curve. The fluorescence measurement begins at the moment that the Calculator, the Detector, and the inputs of each reaction are mixed. The fluorescence intensity is collected every 0.5 minutes. The fluorescence increase is calculated by subtracting the initial intensity from the final intensity, normalized and plotted. For a 1:1 or 4:1 Detector to Calculator ratio, single or no input cases all return an output of 0. The 2 or 3 input cases all return an output above 0.75. The 3 inputs case for a 4:1 Detector to Calculator ratio returns an output of 2.7, very close to the theoretically predicted value of 3.

For cases with a 4:1 Detector to Calculator ratio, the fluorescence increase is normalized to the largest intensity increase of the 2-input reactions (Figure 2.6B). Notably, the curve corresponding to the 3-input reaction plateaus at more than 2.5, while the curves corresponding to the 2-input reactions all plateau around 1. These results, in accordance with the 3-input majority gate truth table, validate that our DNA based logic gate functions as designed.

2.4.4 Assembling a Multi-Functional Circuit. Based on the success of the single 3-input majority gate, we went on to construct a two-generation majority gate circuit. The circuit is composed of two majority gates operated in series (Figure 2.3). These two majority gates were individually verified and the kinetics were examined (APPENDIX A, Figure S2.4). As shown in Table 2.2, by presetting one input in each gate of the circuit (Y1 and X1, for example), the circuit can realize four different computational patterns depending on the identities of the preset inputs. For each computation pattern there are eight unique operations, depending on the combinations of the other three inputs. Figure 2.7 presents the kinetics of these computing systems with different input combinations, with each panel of graphs representing one computing pattern. In each panel the fluorescence output versus time plots represent the reaction kinetics of a combination of inputs (specified next to each curve). The specific combinations of inputs are represented by three numbers that correspond to Y2, Y3 and X2, respectively. The output of Y2 and Y3 serves as the intermediate that passes information from the first generation (M_Y) to the second generation (M_X). For example, the operation 1 + 1 + 0 implies the following information: 1) the relationship between Y2 and Y3 is “OR”, which only occurs when Input Y1 is preset as 1; 2) the relationship between (Y2 + Y3) and X2 is “OR”, which only occurs when Input X1 is preset as 1; 3) the intermediate between the 2 generations is the result of Y2 + Y3 = 1 + 1 = 1. Therefore, the expected final output is 1. In another example, the operation (1 + 0)· 1 implies the following information: 1) the relationship between Y2 and Y3 is “OR”, which only occurs when Input Y1 is preset as 1; 2) the relationship between (Y2 + Y3) and X2 is "AND", which only occurs when Input X1 is preset as 0; 3) the intermediate between the 2 generations is the result of Y2 + Y3 = 1 + 0 = 1. Here, the final output is 1.

Figure 2.7A depicts the results of presetting both Y1 and X1 as 0. Thus, the circuit functions as Y2 · Y3 · X2. For all the input combinations of Y2, Y3 and X2, only the system in which all three inputs are true returns a true output. The other seven input combinations should all return false. We experimentally confirmed this for all situations, except for 0· 1 · 1, where we observed minimal signal leakage. If we specify a > 0.5 threshold for a true value, the result can be considered to be false.

In Figure 2.7B, Y1 is preset as 1 and X1 is preset as 0. The circuit functions as (Y2 + Y3) · X2. For this computing pattern, input combinations of (1 + 0) · 1, (0 + 1) · 1, and (1 + 1) · 1, return true. The other five combinations of inputs, (0 + 0) · 0, (1 + 0) · 0, (0 + 1) · 0, (0 + 0) · 1, and (1 + 1) · 0, return false. As shown in the figure the reaction rate is the highest for the system with all 3 true inputs. Here, the reactions are monitored for 12 hours. Within this time the fluorescence intensity of the other 2 true output systems reaches 75% of that of the highest output, thus representing successful true outputs. The remainder of the operations yield different levels of fluorescence intensities all below 0.3, thus can be considered to be false outputs.

In Figure 2.7C, Y1 is preset as 0 and X1 is preset as 1. The circuit functions as Y2 · Y3 + X2. Five combinations of inputs of this circuit return true, and the other three combinations return false. The combinations leading to the true output are 0 · 0 + 1, 1 · 1 + 0, 1 · 0 + 1, 0 · 1 + 1, and 1 · 1 + 1. Among the five true outputs, three reactions are relatively fast. The fastest reactions finish in approximately 4 hours, while the two slower reactions reach 70% intensity (of the fastest) in 12 hours. The operations with false outputs all plateaued below 0.3.

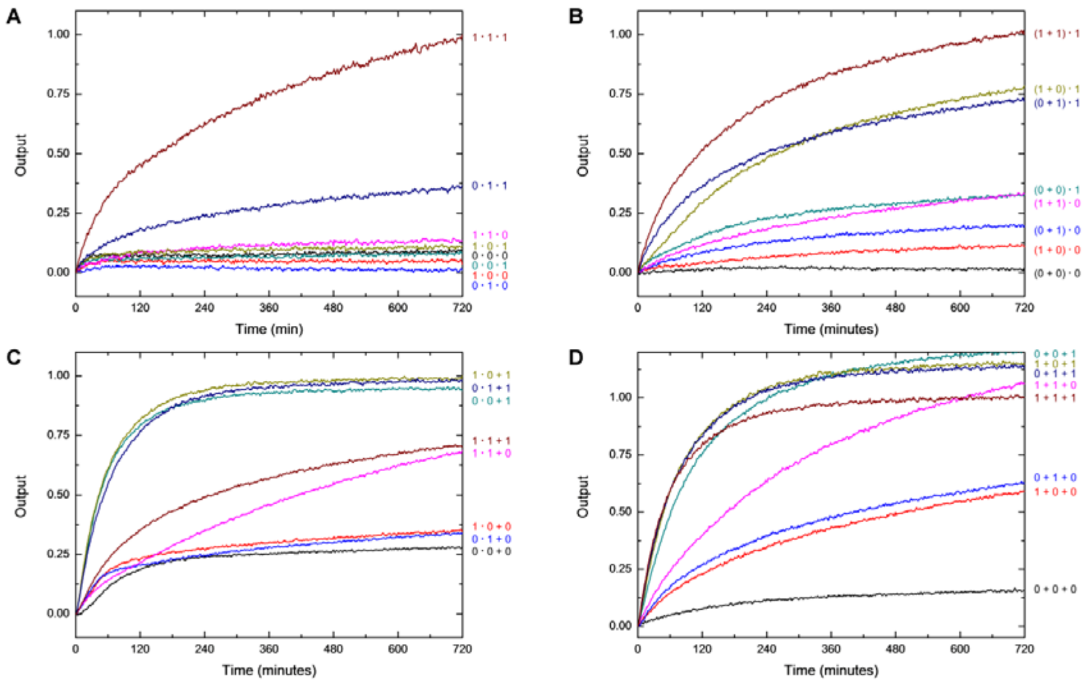

Figure 2.7. Kinetic characterization of the multi-functional circuit composed of two 3-input majority gates. (**A**) Input Y1 is preset as 0; Input X1 is preset as 0. The computation pattern is Y2 · Y3 · X2. Only when Y2, Y3, and X2 are all true does the circuit return true. (**B**) Input Y1 is preset as 1; Input X1 is preset as 0. The computation pattern is (Y2 + Y3) · X2. Three input combinations return true outputs. **(C)** Input Y1 is preset as 0; Input X1 is preset as 1. The computation pattern is Y2 Y3 + X2. Five input combinations return true outputs. **(D)** Input Y1 is preset as 0; Input X1 is preset as 1. The computation pattern is Y2 + Y3 + X2. Seven input combinations return true outputs. Only when Y2, Y3, and X2 are all false does the circuit return false. Each curve in these four graphs represents a reaction where the input combination is labeled at the end of the curve. The fluorescence measurement begins at the moment that the Calculator, the Detector, and the inputs of

each reaction are mixed. The fluorescence intensity is measured every minute. The fluorescence increase is calculated by subtracting the initial intensity from the final intensity, normalized and plotted.

The final computing pattern of the circuit is Y2 + Y3 + X2, which can be realized by presetting Input Y1 and X1 both 1 (Figure 2.7D). If any input among Y2, Y3, and X2 is true, the circuit returns true. Indeed, only 0 + 0 + 0 returns a false output. Five input combinations that have at least one true input from the second generation gate, or both true inputs from the first generation gate, have similar kinetics and produce final fluorescence intensities between 1.0-1.1, representing a true output. The fluorescent intensity of the curves corresponding to the other two cases (with a true input from only one of the first majority gates) plateaus at 0.6 in 12 hours with slower kinetics, and also represents a true output.

The 4 plots shown in Figure 2.7 demonstrate that the signal leakage of each false computation pattern is controlled below 30%. The true outputs all reach intensities higher than 60%. This suggests that the 2-generation logic gate cascade is functioning properly. However, some reactions are obviously slower and result in lower intensities than others. Generally, the more true inputs (including the controlled two preset inputs, Y1 and X1) in a system, the faster the reaction is. For example, in Figure 2.7B, (1 + 1)· 1 is faster than both (1 + 0) 1 and (0 + 1) · 1. In addition, if the true output depends on a true intermediate transferred from the first generation (M_Y) to the second generation (M_X), the reaction is slower. The different rates of each computation reaction can be easily explained. The intermediate that is transferred from M_Y to M_X is within the circular strand of the M_Y Calculator. Its exposure induces the strand displacement reaction between the intermediate segment in the middle of the circular strand on M_Y and the strands bound to the circular M_X Calculator to expose the final output. Both circular structures in this step experience a crowed physical environment for the reaction, thus slowing down the strand displacement reaction in the M_X Calculator.

The main source of leakage of the system is the “cross talk” between the two generations. Specifically, the three inputs of M_Y all have the whole sequence of the intermediate from M_Y to M_X, except the toehold. An ssDNA domain can displace an identical domain from a dsDNA, although the reaction rate is magnitudes lower than toehold directed strand displacement.[9,10] The inputs of M_Y can displace the X3* strand in M_X. So when there are inputs of both the two generations present at the same time and the output should be 0, there is possible outstanding leakage. The strategy used to control the leakage is to use higher concentration of the first generation than the second generation, so the reaction rate ratio between the toehold-directed strand displacement and the undesired non-toehold-directed reaction is increased. In preliminary experiments, the concentration ratio between M_Y and M_X was 1:1. The outstanding leakage was about 50%. The concentration ratio between M_Y and M_X is 2:1 in the experiments of Figure 2.7. The leakage is well controlled below 30%.

2.5 Conclusion

We experimentally realized a 3-input majority gate based on enzyme free DNA strand displacement reactions. A 3-input majority gate is a basic and a versatile logic gate that can be switched between OR and AND gates. The circular structural design presented here provides a new route for designing complex logic gates and may serve as an efficient candidate in designing efficient DNA computing circuits. By combining two 3-input majority gates in series, we realized a multi-functional circuit that can be employed in four different forms according to the demand.

Although our design does require a change in the length of strands (which may cause slower reaction kinetics) when scaling up computing circuits, it still provides an alternative strategy for constructing complex circuits. Due to the nature of our majority gate where the inputs and outputs are all ssDNA, it is foreseeable that a circular logic gate can be combined with other existing DNA logic gates[13,16] for construction of larger circuits for more advance computation.

2.6 References

(1) Liu, X.; Yan, H.; Liu, Y.; Chang, Y. *Small* **2011**, *7*, 1673.

(2) Pinheiro, A. V.; Han, D.; Shih, W. M.; Yan, H. *Nat. Nano.* **2011**, *6*, 763.

(3) Adleman, L. M. *Science* **1994**, *266*, 1021.

(4) Stojanovic, M. N.; Stefanovic, D. *Nat. Biotech.* **2003**, *21*, 1069.

(5) Elbaz, J.; Lioubashevski, O.; Wang, F.; Remacle, F.; Levine, R. D.; Willner, I. *Nat. Nano.* **2010**, *5*, 417.

(6) Benenson, Y.; Gil, B.; Ben-Dor, U.; Adar, R.; Shapiro, E. *Nature* **2004**, *429*, 423.

(7) Yurke, B.; Turberfield, A. J.; Mills, A. P.; Simmel, F. C.; Neumann, J. L. *Nature* **2000**, *406*, 605.

(8) Turberfield, A. J.; Mitchell, J. C.; Yurke, B.; Mills, A. P., Jr.; Blakey, M. I.; Simmel, F. C. *Phys. Rev. Lett.* **2003**, *90*, 118102.

(9) Yurke, B.; Mills, A., Jr. *Genet Program Evolvable Mach* **2003**, *4*, 111.

(10) Zhang, D. Y.; Winfree, E. *J. Am. Chem. Soc.* **2009**, *131*, 17303.

(11) Soloveichik, D.; Seelig, G.; Winfree, E. *Proc. Natl. Acad. Sci.* **2010**, *107*, 5393.

(12) Phillips, A.; Cardelli, L. *J. R. Soc. Interface* **2009**, *6*, S419.

(13) Seelig, G.; Soloveichik, D.; Zhang, D. Y.; Winfree, E. *Science* **2006**, *314*, 1585.

(14) Zhang, D. Y.; Turberfield, A. J.; Yurke, B.; Winfree, E. *Science* **2007**, *318*, 1121.

(15) Yin, P.; Choi, H. M. T.; Calvert, C. R.; Pierce, N. A. *Nature* **2008**, *451*, 318.

(16) Qian, L. L.; Winfree, E. *Science* **2011**, *332*, 1196.

(17) Qian, L. L.; Winfree, E.; Bruck, J. *Nature* **2011**, *475*, 368.

(18) Imre, A.; Csaba, G.; Ji, L.; Orlov, A.; Bernstein, G. H.; Porod, W. *Science* **2006**, *311*, 205.

Chapter 3

DNA Based Arithmetic Functions: 1-Bit Full Adder and Half Adder Based on DNA Strand Displacement

3.1 Abstract

Biomolecular programming utilizes the reactions and information stored in biological molecules such as proteins and nucleic acids for computational purposes. DNA has proven itself as a perfect candidate for building biomolecular logic operating systems due to its highly predictable molecular behavior. In this work we designed and realized an XOR logic gate and an AND logic gate based on DNA strand displacement reactions. These logic gates utilize ssDNA as input and output signals. The XOR gate and AND gate were used as building blocks for constructing half adder and full adder logic circuits. An adder is a basic arithmetic unit in computing. This work provides the DNA molecular programming field a potential universal arithmetic tool.

3.2 Introduction

Programming reaction networks of biological systems is an important way for scientists to understand the secret of life at the molecular level. These biological systems with computational functions have been applied in bioengineering and nanomedicine.[1,2] DNA is an ideal biomolecular candidate for building up molecular automata, because the behavior of DNA molecules can be precisely predicted according to Watson-Crick base pairing. This advantage has promoted DNA systems to facilitate both *in vivo* and *in vitro* applications.[3] The rapidly developing field of structural DNA nanotechnology also mutually benefits from programmed DNA interactions by providing various structural platforms [4-8] and adopting programming principles.[9,10]

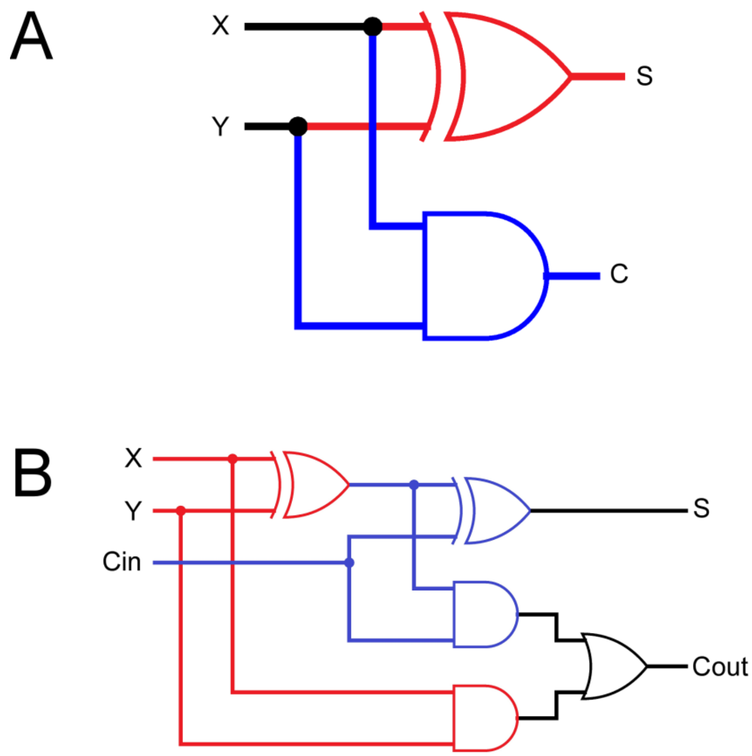

Figure 3.1. Logic diagrams of a half adder and a full adder. **(A)** The logic diagram of a half adder. The easiest construction of a half adder contains one XOR gate (drawn in red) and one AND gate (drawn in blue). The two logic gates share the same two inputs. The output of the AND gate is the "carry" of the result. The output of the XOR gate is the "sum" of the result. **(B)** The logic diagram of a full adder. The easiest construction of a full adder is composed of two half adders as shown in Panel A. The first half adder drawn in red uses Input X and Input Y as inputs. One of the two inputs of the second half adder (drawn in blue) is the output of the XOR gate in the first half adder. The other input of the second half adder is Cin, which is usually a bit carried from the previous stage. The "sum" bit in the output is the output of the XOR gate in the second half adder, and is abbreviated as "S". The "carry" bit in the output is the result of an OR operation of the

outputs of the two AND gates. This bit is usually used as the input carry in the next stage, and it is abbreviated as “Cout”.

Since the first example of DNA computation solved a seven-city Hamiltonian path problem,[11] several molecular DNA automata systems have been designed and developed. These systems include enzyme catalyzed[12,13] and enzyme-free[10,14-17] DNA reaction networks, DNAzyme facilitated reactions,[18,19] and programmed self-assembly of DNA nanostructures.[6,8] In enzyme-free computation systems, the input signals and output signals are usually designed in the same form, which is typically single-stranded DNA (ssDNA). Upon mixing the input ssDNA with a system containing a set of programmed double-stranded DNA (dsDNA) molecules, a series of toehold directed DNA strand displacement reactions occur and yield a ssDNA product as a detectable output.[7,20-25] A few complicated computations including binary square root[26] and neural network mimicry[27] have been demonstrated using the DNA strand displacement strategy.

Table 3.1. Truth Table of a Half Adder

Input X	Input Y	C	S
0	0	0	0
1	0	0	1
0	1	0	1
1	1	1	0

In this work we aim to construct a half adder digital circuit and a full adder digital circuit based on programmed DNA reactions. An adder is a digital circuit that functions as the addition of numbers. A binary half adder performs the addition of its two inputs, and yields two outputs, a sum and a carry (Figure 3.1A, Table 3.1). A binary full adder adds three numbers. In addition to the two inputs of a half adder, a full adder has one more input, which is usually a bit carried over from the previous stage. A full adder also has two outputs, a sum and a carry for the next stage (Figure 3.1B, Table 3.2). A 1-bit adder is a basic arithmetic logic unit. It is an important and fundamental operation in computation.

Table 3.2. Truth Table of a Full Adder

Input X	Input Y	Input Cin	Cout	S
0	0	0	0	0
1	0	0	0	1
0	1	0	0	1
0	0	1	0	1
1	1	0	1	0
1	0	1	1	0
0	1	1	1	0
1	1	1	1	1

3.3Architectural Design

The designs of the half adder and full adder circuits are based on the logic diagrams shown in Figure 3.1. The two logic circuits are mainly constructed from two types of logic gate building blocks, an XOR gate and an AND gate. We anticipate that once an XOR gate and an AND gate are designed and realized, with ssDNA representing the input and output signals (the input and output strands all have the same length), we can implement the half adder and full adder based on these single logic gates. The OR gate, after the two AND gates in the full adder (Figure 3.1B), is spontaneously realized if the two AND gates are designed with the same output sequence.

Table 3.3. Truth Table of an XOR Gate

Input X	Input Y	Output
0	0	0
1	0	1
0	1	1
1	1	0

3.3.1 Design of XOR Gate. A two-input XOR gate (red in Figure 3.1A) performs an exclusive OR function of the inputs. The logic operation returns true if one and only one of the inputs is true. If the two inputs are the same, false or true, the logic gate returns false. The truth table of an XOR gate is shown in Table 3.3. From the truth table, it is easy to imagine that the two input strands or the active species generated by each input strand can be designed to be fully complementary to each other, so that when both inputs are present, the fully complementary species hybridize with each other and render the product inactive, thus yielding no output strands.

Figure 3.2 shows our design of the XOR gate based on DNA strand displacement reactions. The two input signals are represented by two ssDNAs. The logic gate program contains four linear dsDNAs and one DNA hairpin structure. The output is one domain in the hairpin stem, which is protected if the hairpin is not opened. The output domain in the hairpin structure has the same length as the input strands. This design makes the XOR logic gate easy to implement in logic gate cascades, where the output of one gate can be directly utilized by the next logic gate as an input. If the output is not passed to the next logic gate, the output domain can be detected by a reporter duplex modified with fluorescent dye and dark quencher on the two component strands, respectively.

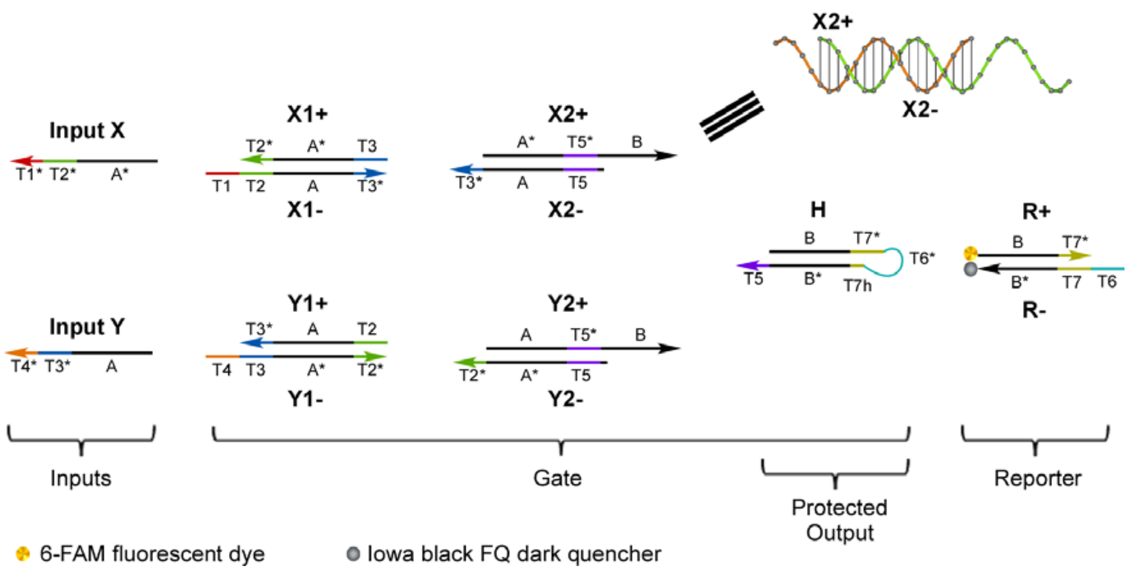

Figure 3.2. Architectural design of an XOR gate. The input signals of the logic gate are represented by two ssDNAs referred to as Input X and Input Y, respectively. The programmed gate contains four linear dsDNAs (X1, X2, Y1, Y2) and one hairpin structure (H). Each component strand and the hairpin strand are individually named and labeled in the figure. Each domain in the strands are also named and labeled. The output sequence is the 5' stem and the loop portion of the hairpin, which is protected if the hairpin is not opened by the upstream reactions. If the logic gate operation yields a true output, which is represented by the B-T7*-T6* domain in the opened hairpin, the output sequence can react with a fluorescent dye and dark quencher modified Reporter duplex (R) and displace the fluorescent dye strand from the dark quencher strand. The true

output can thus be detected by a fluorescence intensity increase. The domains referred to as “T” and a number are designed to function as toeholds, and are each 5 nucleotides (nts) long, except that the T7h domain in the hairpin is 2 nts. The domains A, A*, B, and B* are 12 nts long. There is a one nucleotide “cap” on the 5’ end of T5 in both Strands X2- and Y2-. (See supporting information for details.) The fluorescent dye is 6-carboxyfluorescein (6-FAM), λ_{Ex} = 495 nm, λ_{Em} = 520 nm. The dark quencher is Iowa Black FQ, with an absorbance spectrum ranging from 420 nm to 620 nm with an absorbance maximum at 531 nm.

In the absence of any input strands, the dsDNA and hairpin in the program do not react with each other, thus the output domain remains protected during the entire computing process, yielding no fluorescence increase. If any single input strand is added to the system, the output domain is deprotected from the hairpin structure after three steps of strand displacement reactions, thus the XOR gate returns a true output. Figure 3.3A shows the operation with the presence of Input X as an example. When the two inputs are both added to the system, each input strand releases another ssDNA after the first strand displacement reaction. The two ssDNA released by the inputs are fully complementary to each other. At this step, these two strands hybridize to each other and lose the ability to execute the downstream reactions. The reaction network stops and yields no output strand. Figure 3.3B shows the detailed reactions with both of the inputs. The overall design features a seesaw pattern at every strand displacement reaction except for the reaction of the final fluorescence reporter. The seesaw pattern incorporates an extra toehold domain on the end of the migration domain of each strand displacement reaction. At the end of branch migration, the extra five-base long toehold is not stable enough to maintain hybridization, thus, self-dissociates to finish the strand displacement reaction. This toehold can also initiate the reverse strand displacement reaction. Making each step in the reaction network reversible benefits the system with a self-correction function.[27]

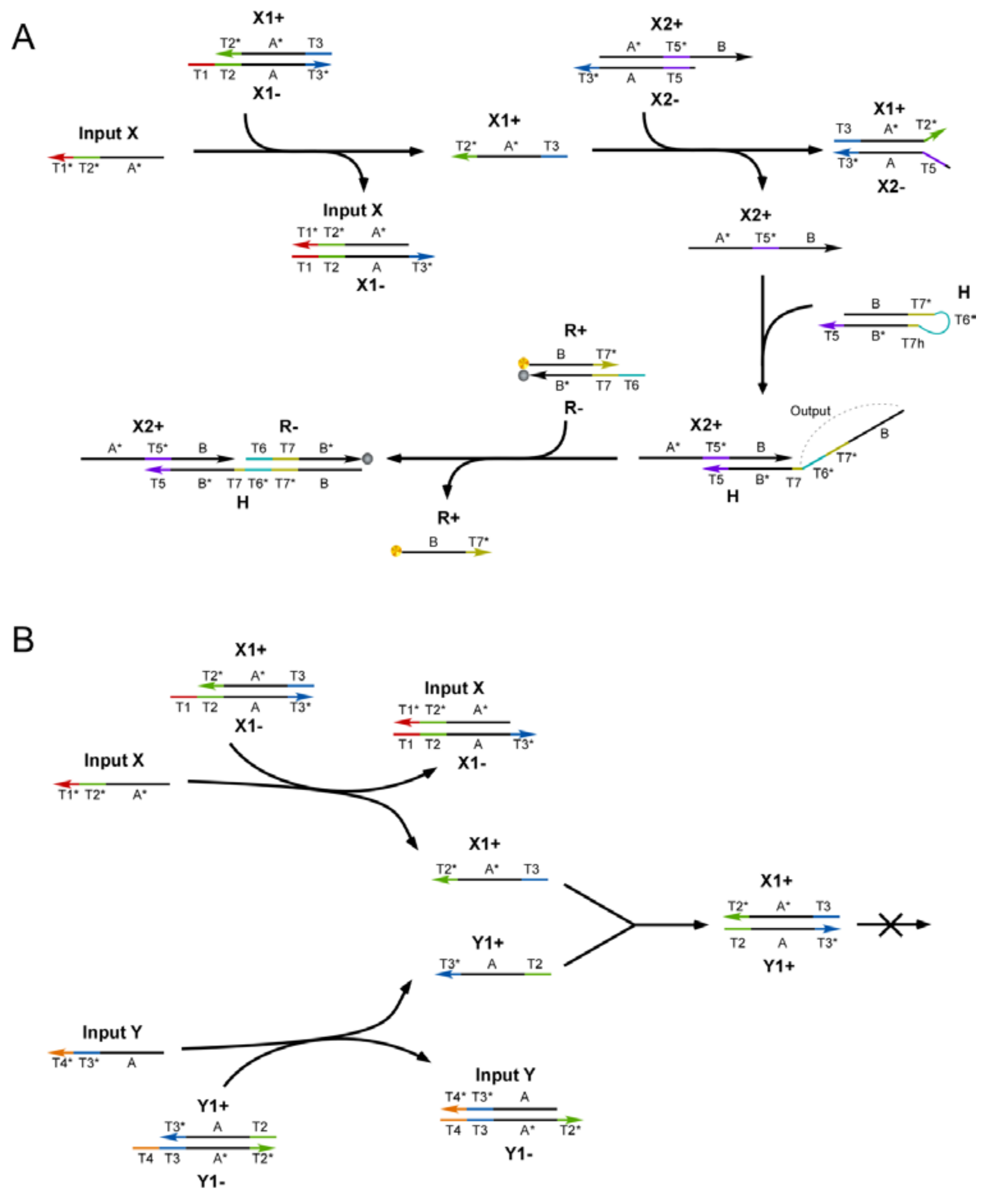

Figure 3.3. Reaction scheme of the XOR gate under conditions with one input strand, and with two input strands. **(A)** Reaction of the XOR gate with only one input. Input X is

shown in the figure as an example. T1* domain in Input X and T1 domain in X1- strand work as toeholds and initiate the strand displacement reaction. As Input X migrates along X1-, X1+ is finally dissociated from X1-. Similarly, X1+ displaces X2+ from X2-. X2+, with active toehold T5*, opens the hairpin structure and exposes the output sequence B-T7*-T6*. This output displaces the fluorescence dye strand from the dark quencher strand, thus increases the fluorescence intensity of the system. **(B)** Reaction of the XOR gate with both of the inputs. The first reaction step of the two input strands is the same as in Panel A. Input X and Input Y produce single-stranded X1+ and Y1+. X1+ and Yi+ are fully complementary to each other. These two strands hybridize and form a dsDNA without any active toehold. The reaction stops at this step and the output domain in the hairpin is not exposed, thus, there is no fluorescence intensity increase.

One important feature in the design of the XOR gate is that the two input stands are not fully complimentary to each other. Although Domain A* in Input X and Domain A in Input Y are complementary to each other and are expected to hybridize as they are mixed, the active toeholds in the two inputs are not protected and are still expected to initiate the downstream strand displacement reactions. The two strands produced by the two inputs individually after the first step of reactions are then fully hybridized to each other and have all toeholds blocked. This design can avoid potential difficulties in two different conditions. The first condition is when the relative concentration of one input is higher than the other. If the inputs are designed to fully hybridize to each other, the excess amount of one input may continue to yield an unexpected true output. With the current design, even if one input is in excess, X1+ and Y1+ are produced in equal amounts, thus, the excess of an individual input will not sabotage the result. The second condition is for the half adder and full adder circuits (Figure 3.1): there is always an AND gate sharing the same input strands with the XOR gate. For AND gates, we do not want the two inputs to inactivate each other when they co-exist.

Another feature of the design of the XOR gate is that a hairpin structure is used to shield the output. From Figure 3.3 we can see that for each input strand, the active toehold domain is on the 3' end of the migrating domain. However, after the second step of reaction, the active toehold domain is moved to the 5' end of the migrating domain in the resulting active species. A hairpin structure can be employed to easily reverse the relative position of the toeholds so that migrating domains in the output strand have the same polarity as the input strands. However, a hairpin structure is usually more thermodynamically stable than a linear DNA duplex. The melting temperature of a hairpin with a loop of five to eight nucleotides and a five-base-pair stem is much higher than room temperature,[28] which is the typical operating temperature of DNA strand displacement reactions. So if a true output is expected, and if toehold T7h in hairpin strand H is as long as other toehold domains, T7h-T7* hybridization will not be able to spontaneously dissociate at the end of the branch migration to open the hairpin, thus, the active toehold T6* of the output domain will be still protected within the hairpin loop. In order to solve this problem, we reduced the length of T7h in the hairpin by several bases at the 5' end. For every base removed from T7h, the stem of the hairpin is reduced by one base pair and the loop increased by one nucleotide. We carefully examined the effect of the length of T7h, and found the optimal length of T7h is 2 nucleotides. This length allows sufficient opening of the hairpin, and a toehold long enough to initiate reversible strand displacement reaction for self-correction. The effect of the length of T7h is discussed in detail in the supporting information.

3.3.2 Design of AND gate. An AND gate (blue in Figure 3.1A) is a basic logic gate that returns true only if both of its two inputs are true. If neither or only one input is true, the output of the AND gate is false. The truth table of an AND gate is shown in Table 3.4.

Table 3.4. Truth Table of an AND Gate

Input X	Input Y	Output
0	0	0
1	0	0
0	1	0
1	1	1

The design strategy of the AND gate is based on DNA strand displacement and involves converting the two input strands into the same active intermediate species with an equivalent of the total inputs. If one input is added, the amount of the intermediate is one equivalent. If both inputs are added, the amount of the intermediate is two equivalents. Then a threshold dsDNA is used to consume one equivalent of the reactive intermediate. Thus, only when there are two inputs yielding two equivalents of the intermediate will one equivalent of the intermediate surpass the threshold and finally produce a true output strand.[26]

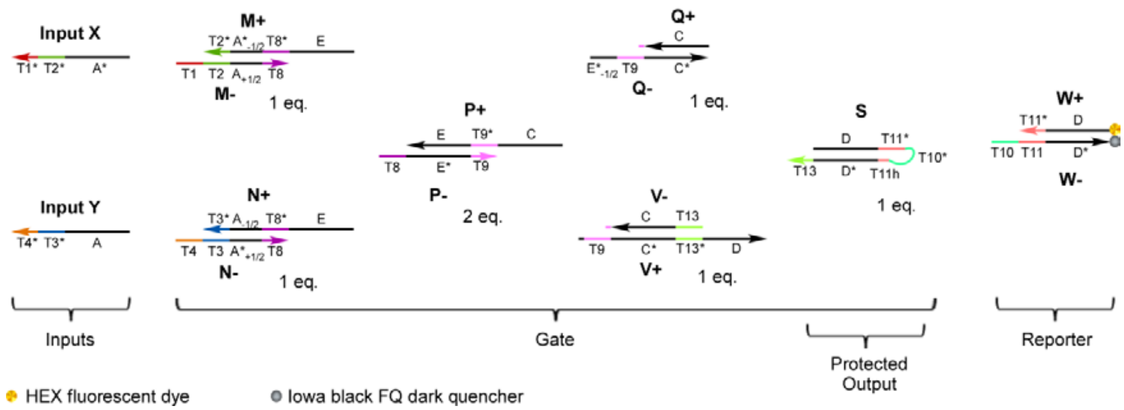

Figure 3.4. Architectural design of an AND gate. The input signals of the logic gate are represented by two ssDNA named Input X and Input Y, respectively. The programmed gate contains five linear dsDNA (M, N, P, Q, V) and one hairpin structure (S). Each component strand and the hairpin strand are individually named and labeled in the figure. Each domain in the strands are also named and labeled. The output sequence is the 5' stem and the loop of the hairpin, which is protected if the hairpin is not opened by the upstream reactions. If the logic gate yields a true output, which is represented by the D-T11*-T10* domain in the opened hairpin, the output sequence will react with a fluorescent dye and dark quencher modified Reporter duplex (W) and displace the fluorescent dye strand from the dark quencher strand. The true output can thus be detected by a fluorescence intensity increase. The domains referred to as "T" and a number are designed to function as toeholds, and are 5 nts long each, except that T11h in the hairpin is 2 nts. The Domains A, A*, C, C*, D, D*, E, and E* are 12 nts long. Domains $A_{+1/2}$ and $A_{-1/2}$ are 6 nts at the 5' end and 3' end, respectively. Domains $A^*_{+1/2}$ and $A^*_{-1/2}$ are 6 nts at the 5' end and 3' end, respectively. Domain $E^*_{-1/2}$ is 6 nts at the 3' end of Domain E*. There is a one nucleotide "cap" on the 3' end of Domain C in Strand

Q+. (See supporting information for details.) The fluorescent dye is hexachlorofluorescein (HEX), $\lambda_{Ex} = 538$ nm, $\lambda_{Em} = 555$ nm.

The design of the AND gate with DNA strands is shown in Figure 3.4. The system is similar to that of the XOR design. The two inputs are represented by two ssDNAs. The programmed gate contains five linear dsDNA and a hairpin structure. The output is also the 5' stem and the loop in the hairpin, which is protected if the hairpin is not opened by the upstream reactions. A Reporter DNA double helix modified with fluorescent dye and dark quencher is added in the system to detect the output strand by an increase in fluorescence. In order to realize the function of an AND gate, a hairpin structure is not necessary. Here, the hairpin keeps the input and output strands of the AND gate in the same format of those in the XOR gate. In addition, the rate hairpin opening is expected to be slower than the strand displacement reaction of a linear dsDNA. Thus, introducing a hairpin structure brings the operating time of the AND gate in the same range as the XOR design, which is preferred in multiple gate logic circuits.

The detailed operation with each input combination is shown in Figure 3.5. The first two steps of the reactions of each input are designed to convert the different input strands into the same reactive species, single-stranded P+. If only one input is added, one equivalent of P+ is produced. If both inputs are added, two equivalents of P+ are produced. There is a threshold structure in the system, which binds to ssDNA P+ quickly, and converts one equivalent of P+ to waste. As a result, if only one input is added, the reactive strand P+ is completely consumed and no downstream reaction occur, thus, no output strand is produced. If both of the two inputs are added, after one equivalent of P+

is consumed, the surviving equivalent of P+ participates in the downstream reactions and finally yields a true output that is detected by an increase in fluorescence.

Strands M+, M-, N+, and N- all have only half of the corresponding domain A or A*. This strategy is used to avoid interaction between M+ and N+ when the two inputs are present. In our preliminary experiments, we used full-length A and A* domains in these four strands and observed that the reaction with two inputs does not produce any output in a reasonable time period. We then tried to remove the threshold from the system, expecting the reactions with one input and two inputs would all show a fluorescence increase. To our surprise, the total reaction rate with two inputs is slower than the rates of reactions with only one input. We propose that the hybridization between Domain A* in M+ and Domain A in N+ significantly slow down the reaction. Next we removed half of Domain A and Domain A* in these strands, leaving the strand displacement reactions with the inputs still possible, but avoiding hybridization between M+ and N+. Domain $A^*_{-1/2}$ in M+ has the same sequence as the terminal 6 bases at the 3' end of Domain A*, so $A^*_{-1/2}$ is complementary to the terminal 6 bases at the 5' end of Domain A. However, Domain $A_{-1/2}$ in Strand N+ is the same as the terminal 6 bases at the 3' end of Domain A. As a result, M+ and N+ do not interact with each other, thus, the reaction rate did not decrease as observed in the preliminary experiments.

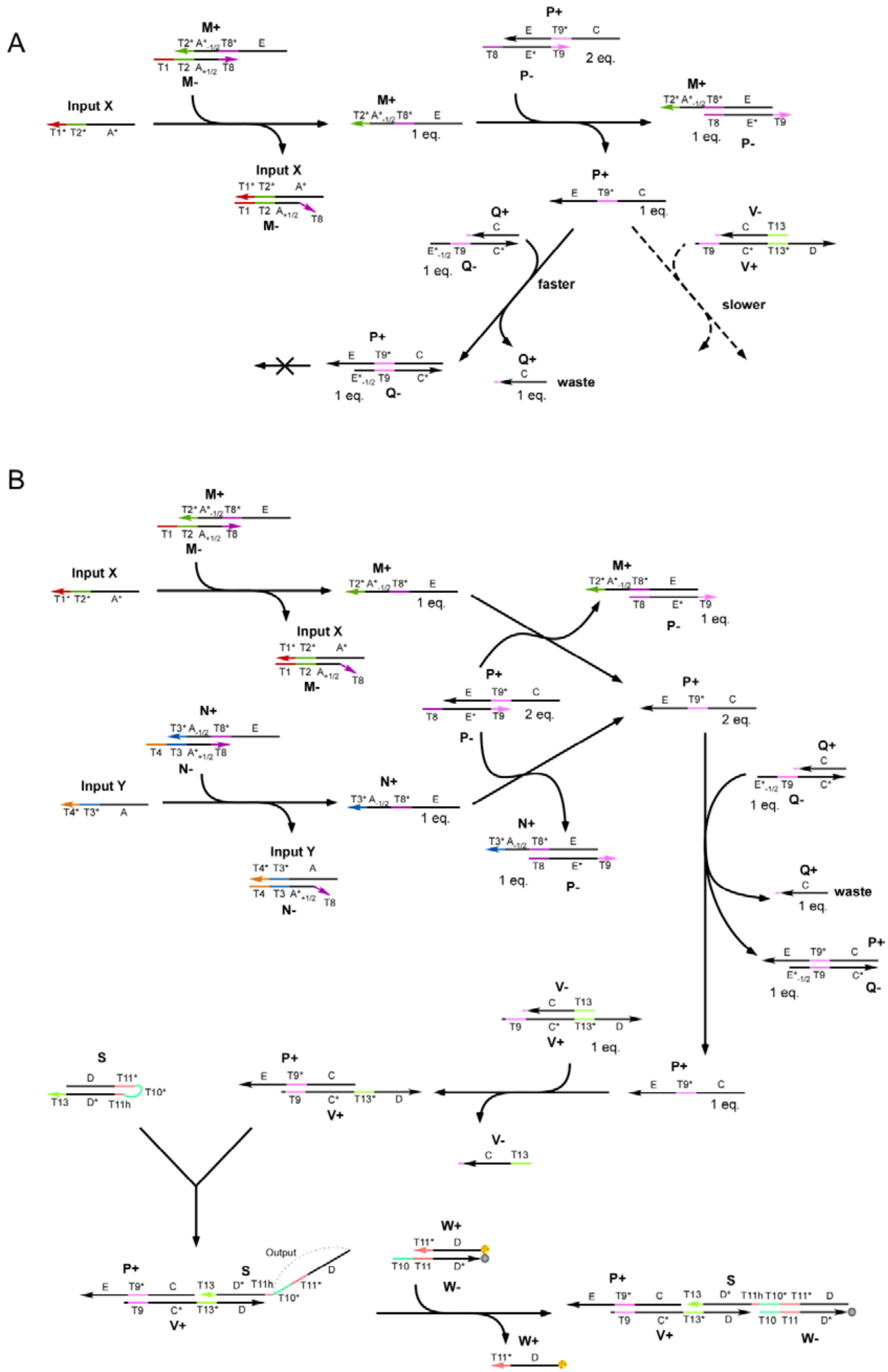
A
Input X
M+
M-
P+
P-
2 eq.
1 eq.
Q+
Q-
V-
V+
faster
slower
waste
B
Input Y
N+
N-
S
W+
W-
Output

Figure 3.5. Reaction of the AND gate under conditions with one input strand, and with two input strands. **(A)** Reaction of the AND gate with only one input. Input X is shown in the figure as an example. T1* domain in Input X and T1 domain in X1- strand work as toeholds and initiate the strand displacement reaction. As Input X migrates along M-, M+ is finally dissociated from M-. Similarly, M+ displaces P+ from P-. Only one equivalent of P+ is generated at this step. ssDNA P+ can either bind to Q- or V+. Strand Q- displays an $E^*_{-1/2}$ domain as a part of a longer toehold compared to V+, so P+ prefers to bind to Q- and is so consumed by the threshold duplex formed from Q+ and Q-. The reaction stops at this step and the output domain in the hairpin is not exposed, thus, there is no fluorescence intensity increase. **(B)** Reaction of the AND gate with both of the inputs. The first reaction step of the two input strands is the same as in Panel A. Input X and Input Y produce single-stranded M+ and N+. The relative concentrations of M+ and N+ are both one equivalent. M+ and N+ displace P+ from P- at the same time, and produce two equivalents of ssDNA P+. One equivalent of P+ is consumed by the threshold Q+/Q- structure, and the remaining equivalent continues to the downstream reactions and finally opens the hairpin structure, exposing the output domain in the hairpin. This output displaces the fluorescence dye strand from the dark quencher strand, thus increases the fluorescence intensity of the system.

3.3.3 Design of Half Adder. The half adder circuit in Figure 3.1 does not require cascading logic gates. The XOR gate and the AND gate in the circuit are in the same layer. A pair of XOR and AND gates with the same input sequences mixed in the same system can function as a half adder. Here the reactive species in the reaction network of each logic gate do not interact with the strands in the other logic gate to any considerable extent (any consecutive sequence similarity < 4 nt). Since the fluorescent dyes used in the two gates are different with no spectral overlap in their absorbance and emission, there will be no significant fluorescence signal interference.

3.3.4 Design of Full Adder. The logic diagram of the full adder shown in Figure 3.1B involves one cascading logic gate in the circuit. The output of the XOR gate in the first half adder is used as one input of the two logic gates in the second half adder. This logic gate cascade requires the sequence of one input of the second half adder to be designed as the same as the output of the first XOR gate.

One of the two outputs of the full adder is the “carry”, which is the result of an OR function of the result of the two AND gates in the circuit. This OR gate does not require any special design. If the output sequences of the two AND gates are designed to be the same, they spontaneously realize the OR gate function. If any one or both of the two AND outputs is true, the carry output is true.

3.4 Results and Discussion

3.4.1 Operation of a Single XOR Gate. The dsDNA in the XOR gate are all individually annealed from the component ssDNA. The assembled dsDNA are then mixed together. In order to monitor the fluorescence intensity change of each reaction with a specific input combination, the measurement of the fluorescence intensity at the emission wavelength starts immediately after the input strand combination is added to the solution. The fluorescence intensity is measured once every minute. The relative concentrations of each input strand and the dsDNA in the solution are all the same. The final concentration of each species is 0.5 μM. The solution is controlled under a constant temperature of 25 ^{o}C during the whole measurement process.

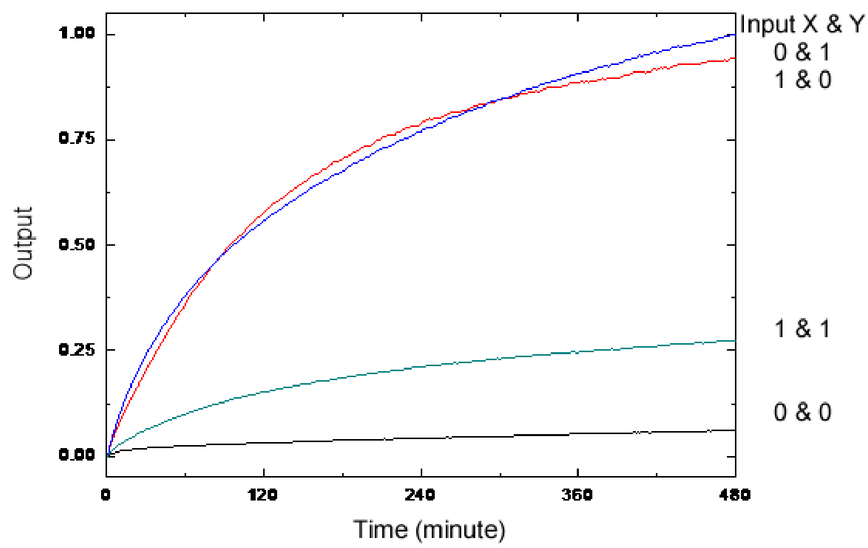

Figure 3.6. Kinetic characterization of the XOR gate. The fluorescence measurement starts at the moment the inputs strand(s) is mixed with the other strands in each reaction. The input combination corresponding to each curve is labeled on the right. The fluorescence intensity is collected once each minute. The data is normalized to the intensity level of the true output sample at 8 hours. The reactions with single inputs both return true outputs. The reaction with no input strand shows no significant fluorescence change, indicating a false output. The reaction with two inputs returns a false output as designed. It shows a leakage of about 27%, which is acceptable.

The kinetics of the XOR logic gate is shown in Figure 3.6. The fluorescence intensities in the four reactions with different input combinations all started from a low level. The reaction system without any input strands does not show any significant fluorescence intensity change over eight hours. The reaction with both of the inputs shows an observable fluorescence increase. The total intensity increase over eight hours is not significant compared to the fluorescence change of the reactions with a single input. The result of the reaction with both inputs should be considered as a negative output, as well as the result of the reaction without any input strand. The two reactions with a single input show a steady fluorescence increase over the eight hour measurement period. The increase slows down after two hours. The two reactions nearly finish within eight hours. The final fluorescence intensities are significantly higher than those of the reactions with both or neither of the inputs, and should be considered to be true outputs.

The data shown in Figure 3.6 are normalized. In each reaction, the initial intensity is subtracted from the intensity at each time point to calculate the fluorescence increase. The fluorescence increase at each time point is then divided by the highest final level (at 8 hours), which is the fluorescence increase of one of the two reactions with a single input. The reaction kinetics of the two single-input reactions are similar to each other. The final fluorescence intensities are at the same level, within 10% of one another.

The fluorescence increase of the reaction with both inputs shows moderate leakage, which is about 27% of the true output. This leakage level is entirely acceptable. Figure 3.3B shows that Strand X1+ and Y1+ should fully hybridize to each other and form non-reactive dsDNA as designed. The origin of the leakage might be that although the hybridization between Strand X1+ and Y1+ should be fast, a small portion of Strand X1+ and/or Y1+ still goes on to the slower downstream reactions.

3.4.2 Operation of a Single AND Gate. The experimental operation of a single AND gate is the same as the XOR gate. All the double helical structures or the hairpins are pre-annealed. The pre-assembled double strands are then mixed. The fluorescence of the solution is monitored as soon as the input strands are added and mixed. The final concentration of each strand is 0.5 μM. The experiment is conducted and kept at 25 °C. The fluorescence intensities of each reaction with different input combinations are collected every minute.

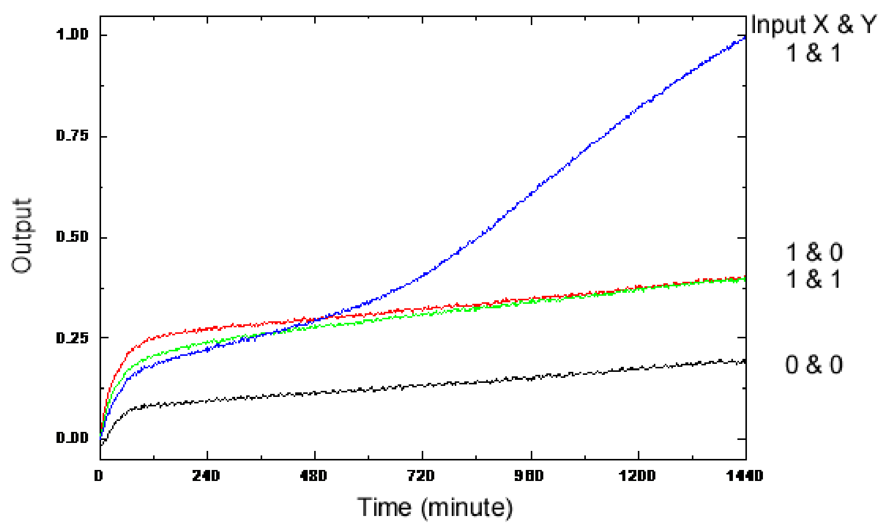

Figure 3.7. Kinetic characterization of a single AND gate. The fluorescence measurement starts at the moment when the inputs strands are mixed with the other strands in each reaction. The input combination corresponding to each curve is labeled on the right. The fluorescence intensity is collected once each minute. The data are normalized to the intensity level of the true output sample at 24 hours. The reaction with both inputs returns a true output. The reactions with only one input strand shows no significant fluorescence change, indicating a false output. The reaction with no input returns a false output as designed. All reactions show a fast, non-specific fluorescence

increase over the first hour of the reactions. The reason for this fluorescence change is not clear.

The fluorescence kinetics of the AND gate is shown in Figure 3.7. There is a fast fluorescence increase at the beginning of all the reactions. The reason for this small intensity increase is not clear. Despite the small fluorescence change in the first hour of the reactions, the reactions with one input or no input do not exhibit fluorescence increases over the measurement time. These indicate the false output of the AND gate when any one of the inputs is absent. The reaction with two input strands shows a significant fluorescence increase, which indicates a true output. The fluorescence intensity of the true output increased more slowly for the first eight hours than later. The slow increase in this period corresponds to the threshold being consumed. The whole reaction process is slower than the operation of the XOR gate shown in Figure 3.6. One reason for the slow AND gate operation might be that the design of the AND gate involves five steps of reactions from the input strands to the separation of the fluorescent dye from the dark quencher, which is one additional step than the reaction of the XOR gate. In addition, consuming the threshold in the AND gate takes extra time.

The data shown in Figure 3.7 are normalized in the same way as the XOR gate. The final relative intensities of the reactions with a single input are relatively high and reach a level of nearly 40%. However, the high final fluorescence level originates from the non-specific fluorescence increase that occurs during the first hour. Despite the initial issue, the fluorescence intensities of the false-output reactions do not shown significant change over the remainder of the measurement period. On the other hand, at the 24 hour time point, the fluorescence intensity of the true-output reaction is still steadily increasing. If observed for a longer time, the difference between the positive and negative outputs would be larger than what is shown in Figure 3.7.

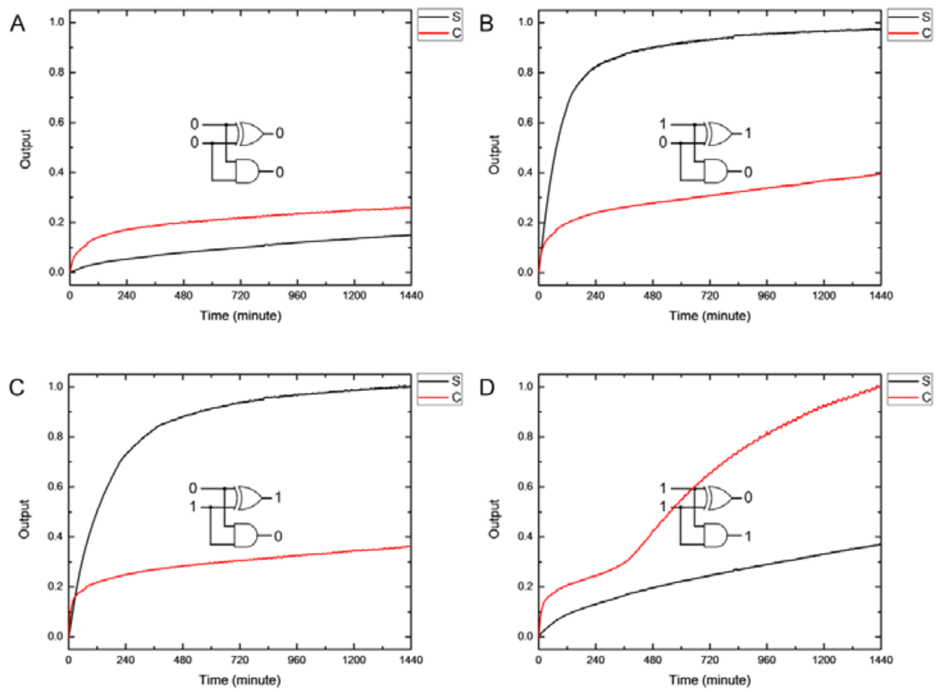

Figure 3.8. Implementation of a half adder with kinetics for a single XOR gate and a single AND gate. **(A)** The result of 0 + 0. The carry and sum outputs are both 0, indicating 0 + 0 = 0. **(B)** The result of 1 + 0. The sum output is 1, and the carry output is 0, indication 1 + 0 = 1. **(C)** The result of 0 + 1. The sum output is 1, and the carry output is 0, indication 0 + 1 = 1. **(D)** The result of 1 + 1. The sum output is 0, and the carry output is 1, indication 1 + 0 = 10. The results shown in the four panels correspond to successful implementation of individually operated single gates. The fluorescence intensities of each logic gate are normalized individually.

3.4.3 Operation of a Half Adder. The half adder does not contain any cascading logic gates, so we expected that the construction of a half adder could be achieved by simply mixing the XOR and AND gates. However, we found after mixing the two systems together, each strand in a single gate is diluted. The designs are sensitive to concentration changes because the hairpin opening depends on the strand concentration (see supporting information for details). Thus, we have not yet achieved adequate experimental result with both gates in the same solution.

However, if we combine the results of the single gates to implement a half adder, the correct half adder operation can be simulated based on the operation of the individual gates. The combination of single AND and XOR gates is shown in Figure 3.8. The four panels individually show input combinations. The result clearly demonstrates a binary adding function of two digits.

3.4.3 Operation of a Full Adder. The experiments are still ongoing. The operation of a full adder faces the same difficulties as the half adder. The concentration of each strand is significantly diluted after mixing multiple gates in the same solution, making the reaction kinetics difficult to predict and control. We are developing a plausible approach to increase the concentration of each strand, so that the logic operation can be carried out without significant errors in a reasonable time period.

3.5 Conclusion

In summary, we have designed and experimentally realized an XOR logic gate and an AND logic gate based on DNA strand displacement reactions. The XOR gate is an important logic gate in digital circuits. It functions as an essential role in basic arithmetic circuits, such as adders and subtractors. We also explored the construction of a half adder and full adder with our designs of the XOR gate and the AND gate. The experiments are still ongoing. The main difficulty in the operation of scaled-up systems is that the reactions of the hairpin structures are kinetically and thermodynamically affected by the concentration. We are still looking for methods to improve the reaction of the hairpins, either by adding supporting strands, similar to fuel strands, to the systems, or by experimentally increasing the operating concentration of the DNA strands.

An adder is a basic arithmetic unit. Our work provides a potential approach to the construction of large scale arithmetic systems with DNA strands. This may largely broaden the potential applications in the field of DNA molecular programming.

3.6 References

(1) Simmel, F. C. *Nanomedicine* **2007**, *2*, 817.

(2) Riehemann, K.; Schneider, S. W.; Luger, T. A.; Godin, B.; Ferrari, M.; Fuchs, H. *Angewandte Chemie International Edition* **2009**, *48*, 872.

(3) Liu, X.; Yan, H.; Liu, Y.; Chang, Y. *Small* **2011**, *7*, 1673.

(4) Pinheiro, A. V.; Han, D.; Shih, W. M.; Yan, H. *Nat Nano* **2011**, *6*, 763.

(5) Lin, C.; Liu, Y.; Yan, H. *Biochemistry* **2009**, *48*, 1663.

(6) Barish, R. D.; Schulman, R.; Rothemund, P. W. K.; Winfree, E. *Proceedings of the National Academy of Sciences* **2009**, *106*, 6054.

(7) Li, W.; Yang, Y.; Jiang, S.; Yan, H.; Liu, Y. *J Am Chem Soc* **2014**, *136*, 3724.

(8) Rothemund, P. W. K.; Papadakis, N.; Winfree, E. *PLoS Biol* **2004**, *2*, e424.

(9) Zhang, F.; Nangreave, J.; Liu, Y.; Yan, H. *Nano Letters* **2012**, *12*, 3290.

(10) Yurke, B.; Turberfield, A. J.; Mills, A. P.; Simmel, F. C.; Neumann, J. L. *Nature* **2000**, *406*, 605.

(11) Adleman, L. M. *Science* **1994**, *266*, 1021.

(12) Benenson, Y.; Gil, B.; Ben-Dor, U.; Adar, R.; Shapiro, E. *Nature* **2004**, *429*, 423.

(13) Stojanovic, M. N.; Stefanovic, D. *Nat Biotech* **2003**, *21*, 1069.

(14) Turberfield, A. J.; Mitchell, J. C.; Yurke, B.; Mills, A. P., Jr.; Blakey, M. I.; Simmel, F. C. *Physical Review Letters* **2003**, *90*, 118102.

(15) Yurke, B.; Mills, A., Jr. *Genet Program Evolvable Mach* **2003**, *4*, 111.

(16) Zhang, D. Y.; Winfree, E. *J Am Chem Soc* **2009**, *131*, 17303.

(17) Li, W.; Yang, Y.; Yan, H.; Liu, Y. *Nano Letters* **2013**, *13*, 2980.

(18) Elbaz, J.; Lioubashevski, O.; Wang, F.; Remacle, F.; Levine, R. D.; Willner, I. *Nat Nano* **2010**, *5*, 417.

(19) Kahan-Hanum, M.; Douek, Y.; Adar, R.; Shapiro, E. *Sci. Rep.* **2013**, *3*.

(20) Soloveichik, D.; Seelig, G.; Winfree, E. *Proceedings of the National Academy of Sciences* **2010**, *107*, 5393.

(21) Chen, Y.-J.; Dalchau, N.; Srinivas, N.; Phillips, A.; Cardelli, L.; Soloveichik, D.; Seelig, G. *Nat Nano* **2013**, *8*, 755.

(22) Phillips, A.; Cardelli, L. *J R Soc Interface* **2009**, *6*, S419.

(23) Seelig, G.; Soloveichik, D.; Zhang, D. Y.; Winfree, E. *Science* **2006**, *314*, 1585.

(24) Zhang, D. Y.; Turberfield, A. J.; Yurke, B.; Winfree, E. *Science* **2007**, *318*, 1121.

(25) Yin, P.; Choi, H. M. T.; Calvert, C. R.; Pierce, N. A. *Nature* **2008**, *451*, 318.

(26) Qian, L. L.; Winfree, E. *Science* **2011**, *332*, 1196.

(27) Qian, L. L.; Winfree, E.; Bruck, J. *Nature* **2011**, *475*, 368.

(28) Rentzeperis, D.; Alessi, K.; Marky, L. A. *Nucleic Acids Research* **1993**, *21*, 2683.

Chapter 4

Controlled Nucleation and Growth of DNA Tile Arrays within Prescribed DNA Origami Frames and Their Dynamics

4.1 Abstract

Controlled nucleation of nanoscale building blocks with seeds programmed on geometrically defined nanoscaffold provides a unique strategy to study and understand the dynamic processes of molecular self-assembly. Here we utilize a two dimensional (2D) DNA origami frame with a hollow interior and selectively positioned DNA hybridization seeds to control the self-assembly of DNA tile building blocks, where the small DNA tiles are directed to fill the hollow interior of the DNA origami frame, guided through sticky end interactions at prescribed positions. This design facilitates the construction of an origami-DNA array hybrid that adopts the overall shape and dimensions of the origami frame and contains a 2D array in the core consisting of a large number of simple repeating DNA tiles. The formation of the origami-array hybrid was characterized with Atomic Force Microscopy (AFM), and the nucleation dynamics were monitored with time-series AFM scanning and fluorescence spectroscopy, revealing a faster kinetics of growth within a frame compared to those without a frame. Our study provides insights for understanding the fundamental processes of DNA based self-assembling systems.

4.2 Introduction

DNA tiles composed of a small number of short synthetic DNA oligomers have been employed as building blocks for the assembly of two-dimensional (2D) and three dimensional (3D) nanostructures.[1-3] Various current and potential future applications of these DNA nanostructures have been demonstrated in biosensing, nanoelectronics, and molecular programming.[4-11] 2D arrays of repeating small DNA tiles with designed sticky ends (single stranded overhangs) can grow into large arrays that reach micrometer to sub-millimeter scales.[3,12,13] However, the lack of a defined boundary renders the 2D arrays of DNA tiles less than adequate when precise size control is desired.

DNA origami[2,14,15] contains normally one long scaffold DNA strand (e.g. a single stranded DNA viral genome) and many (~ 200) short staple strands with designed sequences that hybridize to different part of the scaffold strand and help it to form a desired shaped nanostructure. Intrinsically, DNA origami will have well defined shapes and dimensions. Other scaffold-less non-repeating DNA nanostructures[16,17] also can achieve the precise size and shape control. However, hundreds or even thousands of unique DNA strands are required to reach ~ 100 nm size scale. Expanding the size of DNA origami without sacrificing assembly yield and cost is an ongoing problem.[18-21] Here we utilize a hollow 2D DNA origami structure as a frame to direct the assembly of a 2D array of double-crossover (DX) tiles with high assembly yields and fixed dimensions, and at the same time to investigate how controlled nucleation of DNA tiles with programmed seeds can help understand the dynamic processes of DNA self-assembly. This hybrid structure adopts the advantages of fixed dimensions from DNA origami and large sizes from DNA tile arrays.

4.3 Architecture Design

4.3.1 Design of the DNA DX Tiles and 2D Array. The 2D array we utilized is composed of four unique DX tiles (Figure 4.1A, Figure S4.1). Each tile has a length of four full DNA helical turns (42 bp), which is ~ 13.6 nm. The four sticky ends displayed from each tile are specifically designed to be complementary to one another so that the four tiles spontaneously self-assemble into a 2D array when mixed together, where Tiles A and B are arranged alternately to form one column, and Tiles C and D are arranged alternatively to form a second column. The two columns alternately bind to each other to form the 2D array (interior part of Figure 4.1C).

4.3.2 Design of the DNA Origami Frame. The DNA origami designed here consists of two distinct scaffold strands, using ssDNA from M13mp18 (7249 nts long) and phi X 174 (5286 nts long) (Figure 4.1B, Figure S4.3). By combining the two scaffolds within a single structure we were able to significantly increase the size of the origami frame (~73% larger than origami structures assembled from M13mp18 DNA alone), such that a relatively large number of DX tiles could be incorporated into the DNA origami. However, a larger frame is likely to suffer from slow assembly rates and result in low yield of the frame alone. To overcome these difficulties we maximized the contact between the two scaffolds that compose the frame. We assumed this strategy would increase the probability of effective cooperative assembly between the two long scaffold strands.[18,19] In order to demonstrate that the growth of the 2D array within the origami frame can be asymmetric, the origami frame was designed with one half wider than the other half (resembling an L-shape).

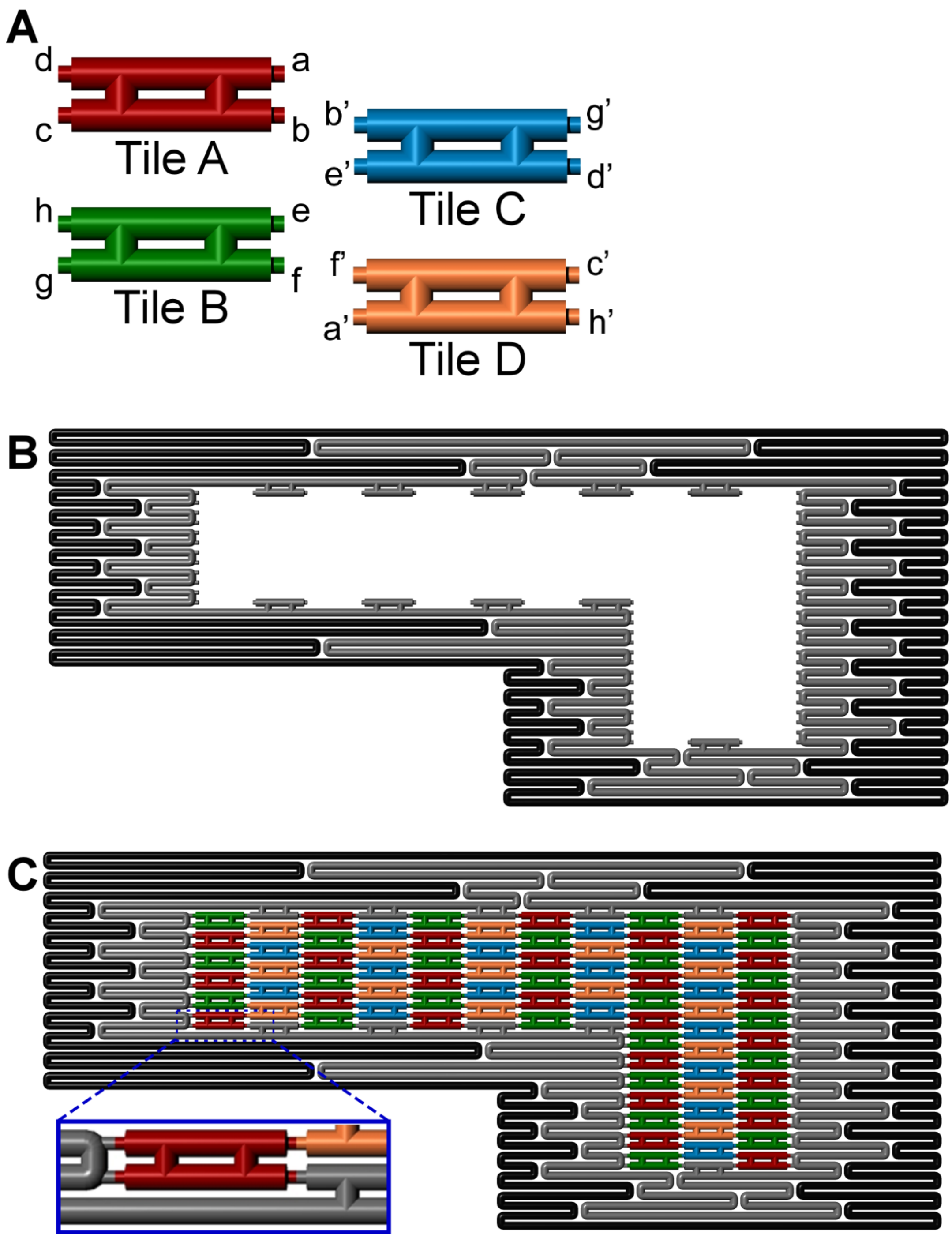

Figure 4.1. DNA origami controlled assembly of a 2D DX tile array within a DNA origami frame of fixed size. (A) The four unique DX tiles employed to assemble the 2D array. Each tile is four full helical turns along the helical axes. Unique sticky ends on Tile A and Tile B are denoted as a-h. The complementary sticky ends on Tile C and Tile D are

denoted as a'-h', respectively. (B) The origami frame structure. The origami frame is 210 nm long along the helical axis. The wider edge is 95 nm. The narrower edge is 60 nm. The hollow interior is 150 nm long and 15 or 32 nm wide. Sticky ends are located along the inner edges to initiate and direct the nucleation of DX tiles within the frame. The origami frame is scaffolded by two different single strands: M13mp18, which is shown in black, and phi X 174, which is shown in grey. (C) The origami frame directed assembly of a 2D array of DX tiles. The origami frame is designed to accommodate 82 DX tiles. The sticky ends displayed from the origami frame only associate with Tile A or B, so that nucleation begins with Tile A and B (but not with Tile C or D). The tiles are arranged in alternating columns of Tiles A and B, and Tiles C and Tile D, respectively. The inset in C shows the tile-origami connection and the tile-tile connection.

4.3.3 Design of the Frame-Array Hybrid Structure. The DNA origami frame has a hollow interior. At several locations along the inner face of the top and bottom edges of the origami we pre-positioned 42 bp long DNA duplexes linked to the frame through two crossovers (the same size as half of a DX tile). Both ends of these duplexes displayed a sticky end, with an inter-molecular distance equal to the length of a DX tile. Besides these sticky ends along the top and bottom edges, the inner face of each of the DNA helices comprising the origami frame displayed a pair of sticky ends with designed sequences. Upon mixing of the origami frame and small DX tiles, the sticky ends along the inner edge of the frame serve as nucleation sites for the growth of a 2D array within the origami structure (Figure 4.1C). The specific sequences of the sticky ends facilitate the association of either Tile A or Tile B, starting from the inner corners (with three sticky end interactions required to realize each tile attachment) and along the inner edges of the frame (with two sticky end interactions required for each tile attachment). After one Tile A and one Tile B from consecutive rows are securely positioned, the sticky ends displayed from the two tiles work cooperatively to bind either Tile C or Tile D. As the nucleation and growth process continue, the origami frame is gradually filled by a 2D array of DX tiles (Figure 4.1C).

4.4 Results and Discussion

4.4.1 Preparation and Characterization of the Origami and Tiles. The DNA origami frame was prepared by mixing the two scaffold strands (1:1 molar ratio) with 430 helper strands. The mixture was then cooled from 90 ^{o}C to 4 ^{o}C over 12 hours. The excess helper strands were removed by Amicon spin columns (Millipore) with 100KD molecular weight cut off membrane filters. The formation of the origami frame was evaluated by atomic force microscopy (AFM) (Figure 4.2A). The origami frame formed well, as designed in Figure 4.1B. Since the two scaffold strands are in contact with one another in many areas of the structure there is a chance that more than one of each scaffold could be linked together to form larger aggregations with ill- defined shapes (Figure S4.4). Increasing the molar ratio between the helper strands and the scaffold strands helped to reduce the occurrence of aggregation. With 30 fold excess of helper strands, the formation yield of the origami frame is ~70% based on AFM images.

The four unique DX tiles were prepared separately by annealing the respective strands mixtures (5 strands each) from 90 ^{o}C to 4 ^{o}C over two hours. When the tiles are mixed in the absence of the origami frame structure, they form 2D arrays of various sizes and unregulated boundaries (Figure S4.5).

4.4.2 Directed Self-Assembly Process, Purification, and Characterization. The DNA origami frame directed assembly of a 2D array of DX tiles was achieved by mixing the origami frame with Tiles A-D. As shown in Figure 4.1C, the assembly ratio of each of the individual tiles to the origami frame varied from 16:1 to 25:1. Considering the possibility of spontaneous formation of "unframed" 2D arrays that are not initiated and directed by the origami structure, all tiles were mixed with the origami frame at a molar ratio of 100:1 which ensured that there was a large excess of tiles in solution. The tile and origami frame mixture was incubated at 25 ^{o}C overnight. Next, the origami frame-2D array hybrid was purified by agarose gel electrophoresis to remove the excess free DX tiles and "unframed" tile arrays (Figure S4.6). The band corresponding to the framed arrays was cut and extracted from the gel and then characterized by AFM (Figure 4.2B). The AFM images show that the DX tiles fit well into the origami frame as designed. Approximately 70% of the origami frames were fully filled with the 2D array without any deformation. Most of the defective frame-array hybrids were grown in deformed frames. Only a few were incompletely filled.

The frame-array hybrids cannot be sufficiently separated from the frame-free 2D arrays using agarose gel electrophoresis (Figure S4.7) due to their similarity in size. In order to obtain a cleaner separation, the origami frame was modified with biotin by covalently label one help strand with a biotin, and subsequently separated from the frame-free 2D arrays and individual tiles using monomeric avidin resin (Thermo Scientific), finally eluded by washing with extra free biotin. The AFM images show that the frame-array hybrids purified by this method (Figure 4.2C) are well-formed with fewer impurities visible in the background (Figure S4.8). Note that in Figure 4.2C, every origami frame has a bright spot at the inner corner position, which is the position of the helper strand with biotin modification protruding from the origami surface. The yield and defects observed are similar to those purified using the gel electrophoresis method.

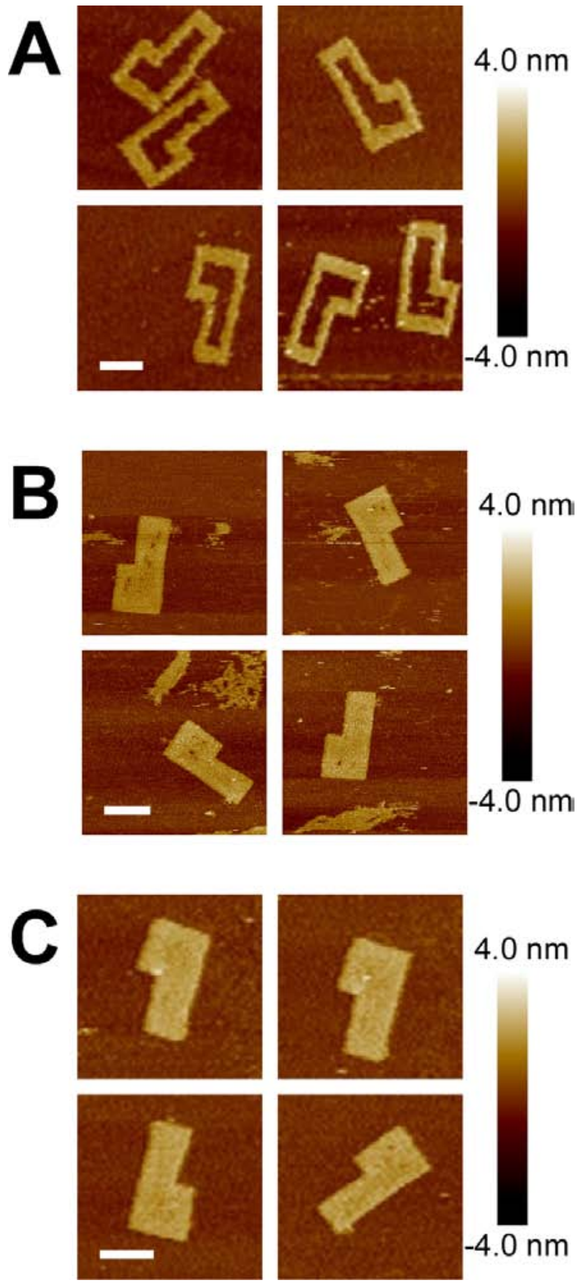

Figure 4.2. AFM images of the DNA origami frame and the frame – DX tile array hybrid. (A) Empty DNA origami frame. (B) Origami frame – array hybrid, after

purification by agarose gel electrophoresis. (C) Origami frame – array hybrid. Here, the frames are modified with biotin. The frame-array hybrid is purified by binding to mono-avidin beads and then eluting with excess biotin. The scale bars in the three figures are 100 nm.

The sources of defects in the frame-array hybrids required careful examination (Figure S4.10). We propose that one major origin of the defects is a "cross-talk" between the complementary sticky ends in different rows of the tile array. Because the inner corner positions of the frame each provide three sticky ends for the tiles to attach with, and the positions along the inner edges each provide two sticky ends, we envision that the first step of the self-assembly process is the association of the tiles at the inner corners of the frame, followed by association with the inner edges, effectively creating a new boundary one layer inward. At the same time, this process exposes additional sticky ends that allow tiles in a second row (or column) to attach. It is at this stage, due to the flexibility of DX tiles at the crossover points, that two sticky ends on tiles in non-neighboring rows within the same column (with a gap the width of one- or two-tiles) may be able to hybridize to the corresponding sticky ends displayed from a single tile in the next column such that the frame shrinks in width and bends inwards (thus, the frame-array hybrid would appear thinner). Similarly, but oppositely, there could be more rows of tiles inserted than designed, causing the frame-array hybrid to appear wider than designed.

4.4.3 Kinetics Characterized with FS-AFM. In order to better understand the self-assembly process of the DX tiles within the DNA origami frame, the nucleation and growth process was monitored using real-time AFM scanning which allows imaging of a liquid sample consecutively when it is deposited on a flat mica surface. Each scan can be collected in a short time (< 1 min per 516x516 pixel image) without compromising the image quality. First, the empty DNA origami frame, together with Tiles C and D (in a ratio of 1:100:100, respectively) were deposited on a mica surface. Because the sticky ends displayed from the frame are all designed to associate with Tiles A and B but not Tiles C or D, and Tiles C and D do not associate each other, the nucleation does not start at this stage. Next, a mixture of Tiles A and B (100 fold excess to the origami frame) was injected into the sample droplet. Nucleation is expected to begin immediately and continuous AFM imaging in the same area was initiated. Figure 4.3 shows the consecutive AFM images collected at constant time intervals (87 seconds per image) that monitor the dynamic self-assembly of DX tiles within the origami frame. From the images, we observed that the nucleation of DX tiles starts in the direction parallel to the DNA helices along the left and right inner edges as well as in the direction perpendicular to the helices along the top and bottom inner edges. We should point out that the excess tiles may undergo spontaneous nucleation in solution, and small sections of frame-free 2D arrays appear nearby, as first observed in the second image. Spontaneous nucleation in solution is apparently slower than nucleation within the frame. It is also possible that nucleation happens in solution at an earlier time and is deposited between collection of the first and second image. Regardless, growth outside the frame does appear to occur more rapidly than within the frame possibly due to less structural constrains as the tiles grow outwards instead of inwards. As the concentration of free DX tiles quickly decreases after the nucleation step the growth of the tile array within the origami frame significantly slows down before the frame is completely filled. Nevertheless, the nucleation and growth process within the origami frame is finished within 1 hour. The same process is expected to be faster in solution without the restriction of the surface.

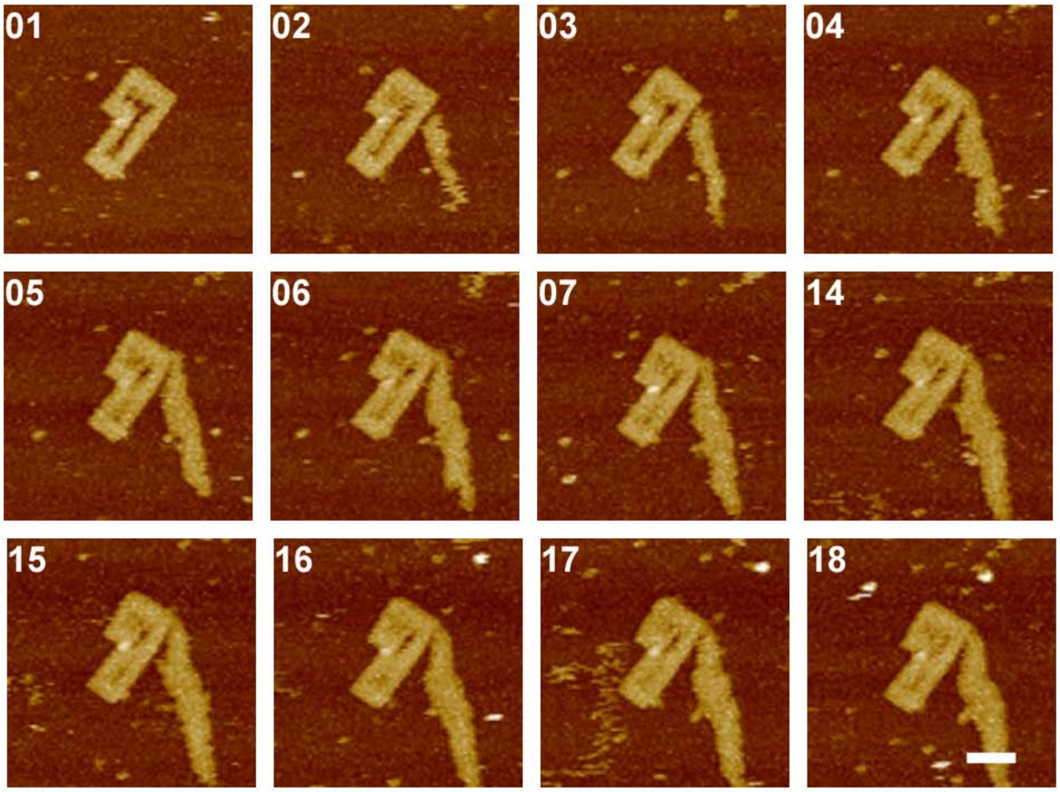

Figure 4.3. FS-AFM images showing the dynamic nucleation and growth of DX tiles within the DNA origami frame. As soon as the reactants are all deposited on the mica surface, scanning begins. The total scan time for each image is 87 seconds. Frame 8 to Frame 13 is not shown because there is little change of the images in the time period. The sequential images reveal that nucleation along the DNA helices is faster than in the direction perpendicular to the helices. The scale bar is 100 nm.

4.4.4 Kinetics Characterized with Fluorescence. While time-series AFM scanning establishes direct observation of the nucleation process, it is likely that the mica surface restricts the ability of the tiles to enter the origami frame, thus making the nucleation kinetics different from that in solution. Therefore, we modified one of the DX tiles with a fluorescent dye and a neighboring tile with a dark quencher, and studied the nucleation kinetics in solution by monitoring the change in fluorescence intensity of the dye with time. Specifically, the ssDNA located comprising sticky end d' on Tile C was modified with 6-carboxyfluorescein (6-FAM), and the ssDNA comprising sticky end d on Tile A was modified with an Iowa Black dark quencher (Figure 4.4A, Figure S4.12A). Upon association of the four tiles within the 2D array (with our without the DNA origami frame) 6-FAM is positioned adjacent to the dark quencher, and its fluorescence intensity should decrease as the self-assembly proceeds (Figure 4.4B).

This fluorescence change with time was monitored using a fluorometer (λex = 495 nm, λem = 520 nm), which reflects the kinetics of the tile-tile assembly process (Figure 4.4C, and additional data shown in Figure S4.12B). In Figure 4.4C, four curves are shown to represent four different experiments. The slowest decay represents the self-assembly of the four tiles in the absence of origami frame. This very slow reaction rate indicates that the spontaneous nucleation process in solution is significantly slower than with a seed. The remaining three curves represent the reaction kinetics with varying molar ratios between each tile and the origami seed (100:1, 100:2, and 100:3, respectively). As expected, as the concentration of the nucleation seed increases, the initial rate of the reaction becomes higher.

The concentration of the origami seed and the DX tiles used for fast-scan AFM experiment were 4 fold smaller than those used for the fluorescence measurements. Therefore, the spontaneous nucleation and growth rate observed in solution is apparently much slower than on the mica surface. The rapid emergence of seed-free nucleation in the FS-AFM image (Figure 4.3) could result from a surface mediated process, where the mica may also act as a nucleation point, aiding the tile-tile assembly.[22-24] For surface mediated assembly on mica, with the exception of a short delay time (between image frames 1 and 2), the spontaneous nucleation and growth rate outside the frame seems comparable with the seeded nucleation and growth within the frame. Meanwhile, for the assembly process in solution, the seeded nucleation and growth rate within the origami frame is much faster than the spontaneous nucleation and growth rate without the frame. This result indicates the importance of the nucleation in the kinetics of tile array assembly.[25]

In order to characterize the kinetics of the nucleation, we built a reaction model to calculate the reaction rate constant, *k*, from our data. The reaction rate between Tile C and the origami frame can be expressed by

$$-\frac{d[C]}{dt} = k \cdot [origami] \cdot [C] \quad (1)$$

We assume that at the initial stages of seeded nucleation, a small number of tiles assembled inside the origami frame do not affect the accessibility or diffusion of the origami significantly, thus, we may treat the concentration of origami in Equation (1) as a constant. At a certain time *t*, the concentration of unassembled Tile C is

$$-\frac{d[C]}{dt} = k \cdot [origami] \cdot [C] \quad (2)$$

This assumption fails when the origami is more thoroughly filled, which would change the properties of the frame, and thus, the reaction rate constant *k*. Therefore, we only collected and analyzed the fluorescence change in the early stages (the first 10 minutes) where only a small percentage of the assembly process is complete.

The fluorescence intensity observed is the sum of fluorescence intensities from the free and associated Tile C, which are linear to the concentrations of each species,

$$I_t = a \cdot [C]_t + b \cdot ([C]_0 - [C]_t) = (a - b) \cdot [C]_t + b \cdot [C]_0 \quad (3)$$

Here, a and b are constants. We normalized the fluorescence intensity by dividing both sides of Equation (3) by the initial intensity, $a \cdot [C]_0$, and obtained

$$\frac{I_t}{I_{ini}} = \frac{a-b}{a \cdot [C]_0} \cdot [C]_t + \frac{b}{a} = \frac{a-b}{a} \cdot e^{-k \cdot [origami] \cdot t} + \frac{b}{a} \quad (4)$$

Therefore, a linear equation can be obtained:

$$\ln\left(\frac{I_t}{I_{ini}} - \frac{b}{a}\right) = -k \cdot [origami] \cdot t + \ln\frac{a-b}{a} \quad (5)$$

The ratio of b/a is experimentally measured as 0.399, which equals the ratio of the fluorescence intensity of the fully assembled structure of all four tiles, to that of individual Tile C in the presence of the same concentration of Tiles A and C. The data in Figure 4.4C and Figure S4.12B were fit by Equation (5), and the nucleation rate constant k obtained from the slope is $(2.3 \pm 0.4) \times 10^5$ $M^{-1} \cdot s^{-1}$. We should note that in the actual self-assembly process, we experimentally follow the change of the occupancy status at one of the sticky end on Tile C (where the fluorescence dye is labeled). The nucleation sites for Tile C in the origami frame must be first generated by the binding of A and B tiles first and then regenerated by the self-assembly of other three types of tiles. Each regeneration cycle requires the attachment of three to five tiles of other types. Thus, the time that it takes for the attachment of a random individual tile in the origami frame is expected to be, on average, one third to one fifth of the nucleation time of Tile C. Therefore, the nucleation rate constant for random tile association should be 3-5 times the value of constant k that we determined from our model. Considering this factor, the nucleation rate constant falls in the same order of magnitude as 10^6 $M^{-1} \cdot s^{-1}$, consistent with values previously reported in the literature.[25,26]

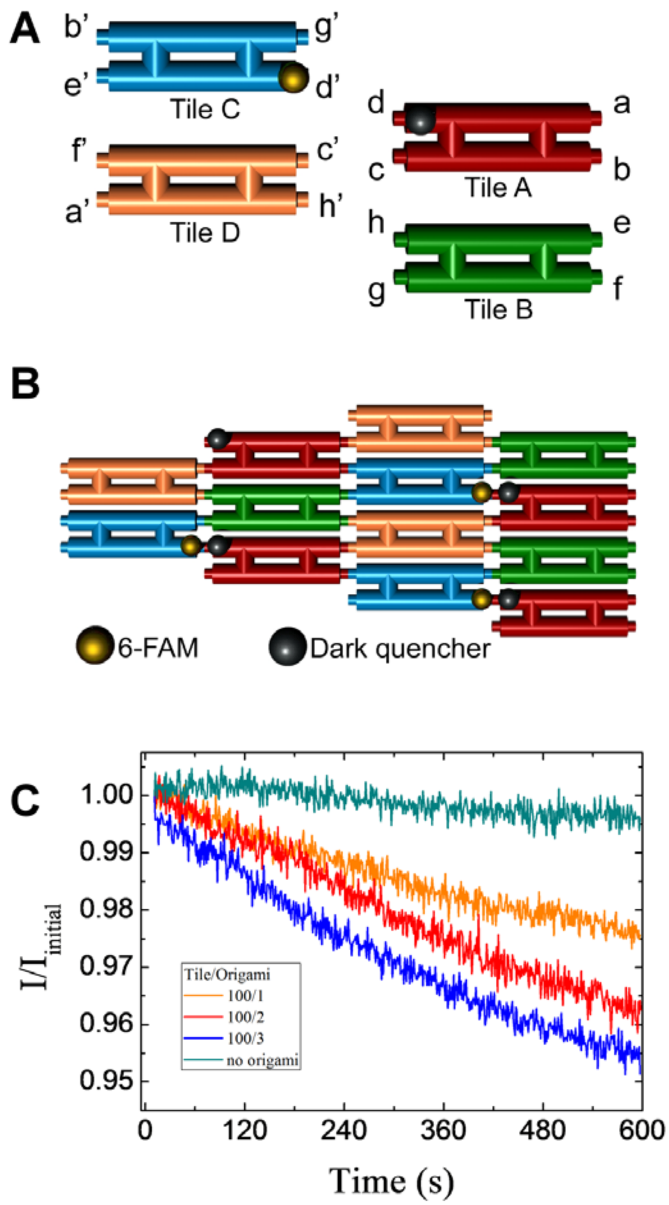

Figure 4.4. Nucleation kinetics monitored by fluorescence. (A) Tile C is modified with the fluorescence dye 6-FAM at sticky end d'. Tile A is modified with Iowa black dark

quencher at sticky end d. Tile B and Tile D are not modified. (B) After assembling the four tiles, either with or without the presence of the origami frame, the fluorescence dye is arranged adjacent to the dark quencher. The fluorescence intensity decreases as the self-assembly process proceeds. In Panels A and B, the yellow dots represent 6-FAM, and the black dots represent the dark quencher. (C) Normalized fluorescence decrease. The normalization is achieved by dividing the fluorescence intensity by the initial intensity of each experiment. With the same amount of tiles present, the initial intensities in each experiment are the same. The cyan curve shows that without the presence of the origami seed, the nucleation exhibits a very slow rate. The orange, red, and blue curves show the reaction process with origami concentrations of 0.2 nM, 0.4 nM, and 0.6 nM, respectively. The tile concentrations are 20 nM for each tile, in all experiments.

4.5 Conclusion

In summary, we successfully utilized a large DNA origami frame to regulate the growth of a 2D array of DX DNA tiles with high yield. The dynamics of nucleation were monitored using time-series AFM and fluorescence kinetics. We obtained the nucleation rate constant of assembly with and without the DNA origami seed. The assembly of the frame-array hybrid structures takes advantage of the properties of DNA origami and 2D arrays such that it has a defined shape and dimensions with aperiodic peripheral sequences and a solid periodic core that consists of a small number of DNA sequences. A fixed number of each DX tile was incorporated into the 2D array, which is variable according to the design of the frame and the identities of the sticky ends. 2D DNA arrays are powerful templates for patterning proteins and inorganic materials.[12] Our approach will be useful and efficient to create DNA based nanodevices when definite boundaries and exact numbers of addressable positions are required.

4.6 References

(1) Seeman, N. C. *J. Theor. Biol.* 1982, *99*, 237.

(2) Rothemund, P. W. K. *Nature* 2006, *440*, 297.

(3) Winfree, E.; Liu, F.; Wenzler, L. A.; Seeman, N. C. *Nature* 1998, *394*, 539.

(4) Seeman, N. C. *Nature* 2003, *421*, 427.

(5) Gothelf, K. V.; LaBean, T. H. *Org. Biomol. Chem.* 2005, *3*, 4023.

(6) Voigt, N. V.; Torring, T.; Rotaru, A.; Jacobsen, M. F.; Ravnsbaek, J. B.; Subramani, R.; Mamdouh, W.; Kjems, J.; Mokhir, A.; Besenbacher, F.; Gothelf, K. V. *Nat. Nano.* 2010, *5*, 200.

(7) Deng, Z.; Samanta, A.; Nangreave, J.; Yan, H.; Liu, Y. *J. Am. Chem. Soc.* 2012, *134*, 17424.

(8) Barish, R. D.; Schulman, R.; Rothemund, P. W. K.; Winfree, E. *Proc. Natl. Acad. Sci.* 2009, *106*, 6054.

(9) Qian, L. L.; Winfree, E. *Science* 2011, *332*, 1196.

(10) Qian, L. L.; Winfree, E.; Bruck, J. *Nature* 2011, *475*, 368.

(11) Li, W.; Yang, Y.; Yan, H.; Liu, Y. *Nano. Lett.* 2013, *13*, 2980.

(12) Yan, H.; Park, S. H.; Finkelstein, G.; Reif, J. H.; LaBean, T. H. *Science* 2003, *301*, 1882.

(13) He, Y.; Chen, Y.; Liu, H.; Ribbe, A. E.; Mao, C. *J. Am. Chem. Soc.* 2005, *127*, 12202.

(14) Dietz, H.; Douglas, S. M.; Shih, W. M. *Science* 2009, *325*, 725.

(15) Han, D.; Pal, S.; Nangreave, J.; Deng, Z.; Liu, Y.; Yan, H. *Science* 2011, *332*, 342.

(16) Wei, B.; Dai, M.; Yin, P. *Nature* 2012, *485*, 623.

(17) Ke, Y.; Ong, L. L.; Shih, W. M.; Yin, P. *Science* 2012, *338*, 1177.

(18) Zhao, Z.; Liu, Y.; Yan, H. *Nano. Lett.* 2011, *11*, 2997.

(19) Yang, Y.; Han, D.; Nangreave, J.; Liu, Y.; Yan, H. *ACS Nano* 2012, *6*, 8209.

(20) Pound, E.; Ashton, J. R.; Becerril, H. c. A.; Woolley, A. T. *Nano. Lett.* 2009, *9*, 4302.

(21) Zhang, H.; Chao, J.; Pan, D.; Liu, H.; Huang, Q.; Fan, C. *Chem. Commun.* 2012, *48*, 6405.

(22) Sun, X.; Hyeon Ko, S.; Zhang, C.; Ribbe, A. E.; Mao, C. *J. Am. Chem. Soc.* 2009, *131*, 13248.

(23) Lee, J.; Hamada, S.; Hwang, S. U.; Amin, R.; Son, J.; Dugasani, S. R.; Murata, S.; Park, S. H. *Sci. Rep.* 2013, *3*.

(24) Hamada, S.; Murata, S. *Angew. Chem., Int. Ed.* 2009, *48*, 6820.

(25) Schulman, R.; Winfree, E. *Proc. Natl. Acad. Sci.* 2007, *104*, 15236.

(26) Pinheiro, A. V.; Nangreave, J.; Jiang, S.; Yan, H.; Liu, Y. *ACS Nano* 2012, *6*, 5521.

Chapter 5

Summary and Outlook

5.1 Summary

DNA computation and biological molecular programming have been under development for two decades.[1] A broad range of molecular programming methods and design strategies have been proposed and realized. These methods and strategies include enzyme catalyzed reaction networks, enzyme-free reactions, and programmed nanoscale DNA self-assemblies. The biological nature of DNA molecules make DNA based molecular programming suitable for applications in bioengineering and nanomedicine.[2,3] Computational DNA systems have also been combined with the fast developing area of DNA nanotechnology, which provides a versatile and highly compatible platform for DNA computation.[4,5]

DNA molecular programming has developed rapidly, yet still faces some technical challenges. One challenge is to develop new types of computational operations based on DNA molecules. The computational operations can be considered as basic tools in the toolbox for solving problems with programmed DNA systems and the more tools that we have, the more versatile the functions that are possible. Another challenge is to build larger scale DNA systems to solve more complicated biological problems. Building large scale DNA computational systems has already been demonstrated to be experimentally practical.[6,7] However, more successful examples and practical optimizations are still highly desired. The third challenge is to incorporate new design rules into DNA and other biological molecular programming systems.

In this dissertation, I discussed three research projects that aimed to tackle the three challenges mentioned above. In Chapter 2 and Chapter 3, new types of logic gates based on DNA strand displacement reactions were described. A three-input majority gate was demonstrated in Chapter 2, and an XOR gate was demonstrated in Chapter 3. A three-input majority gate is a versatile gate, which can function as either a two-input AND gate or a two-input OR gate by changing the value of the third input. The majority gate was utilized to construct a multi-functional logic circuit based on this unique property. An XOR gate is the key logic gate in the simplest half adder and full adder circuits. We aimed to implement the functions of adders with the XOR gate and other logic gates. This would provide a basic building block for arithmetic purposes.

In Chapter 4 we first proposed to construct a programmable nanodisplay system. Large DNA origami and small DNA tiles were hybridized together and the self-assembling behaviors were studied. If it becomes possible to control the assembly pattern of the tiles through programming the sticky-ends of the DNA origami platform and tile pixels, a programmed nanoscale display may be realized.

All the work demonstrated in this dissertation is at the frontier of engineering DNA. The computational DNA molecular programming projects provide new DNA computation tools and design principles, and may be used in artificial manipulation of biochemical reaction systems. The DNA nanotechnology project was aimed at studying the fundamental properties of DNA origami, DNA tiles, and the self-assembly process of DNA nanostructures. The research results provide a new type of DNA nanostructure with remarkable advantages. It also provides a platform for visionary computational DNA self-assembly on the nanometer scale.

5.2 Future Perspectives

In addition to the efforts reported in this dissertation, we have some ideas about how to tackle the challenges of DNA and other biological molecular programming strategies in the future.

5.2.1 Computational Systems with Signal Feedback. Feedback is a process in which information about two factors mutually affect each other. Signal feedback is a common process seen in biology and computer science. Developing biological computation systems with signal feedback functions is important and useful. Current examples of DNA molecular programming systems with feedback functions are usually based on recycling of output strands. This strategy has been used to mimic neural systems[7] and model chemical reaction networks.[8]

Our perspective is to develop a feedback mechanism at nanometer scale. Molecular delivery is a research area that scientists have always been interested in. It is directly associated with drug delivery. Our goal is to design a guest molecule transportation system using DNA nanotechnology, where a DNA robot carries the guest along a series of routes and passes several vortices. With a feedback mechanism that sends a signal when the guest molecule is delivered to the expected destination, that can then in turn direct the release of the second signal further directs the route of the next robot, we can avoid unnecessary vortices. Here, the signal would be reactive DNA strands. The signal strand would be amplified through an enzyme-catalyzed or enzyme-free process so that there would be enough copies of the signal strands reacting with the wrong vortices, thus blocking all unnecessary routes of the DNA nanorobot. This strategy would significantly increase the efficiency of molecular delivery, which is superior to strategies that deliver guest molecules in bulk and only utilize those that arrive at the correct target. In addition, the feedback mechanism would avoid any unnecessary traversing that occurs in traditional targeted molecular delivery.

5.2.2 Programmed Nanodisplay. DNA nanostructures have been used to construct well-defined 2D or 3D structures with high resolution.[9,10] The current strategies use unique DNA units as the pixels and voxels to construct arrays that display particular patterns. Unfortunately, each pattern requires a unique set of DNA units.

Our perspective is to design a program composed of a limited number of DNA tiles with different surface features. These tiles could be programmed to display specific sticky-ends. The tiles can self-assembly to each other through these sticky-ends. Once a nucleation seed with specifically designed nucleation sites is added to the mixture of tiles, the tiles will spontaneously assemble on the seed and display a desired pattern from the surface features of the tile.

Figure 5.1 shows a schematic design of the nanodisplay system. Figure 5.1A and Figure 5.1B demonstrate two sets of programs composed of several four-sticky-end tiles. The tiles feature two values represented by two types of surface structures, representing binary 1 and 0. When the tiles are mix under self-assembly conditions, two tiles can anchor a third tile through the sticky-ends, and the value of the third tile is the calculation result of the first two tiles. The calculation rule is determined by the specifically designed sticky-ends on the tiles. Figure 5.1A shows the tiles defining an AND calculation rule. And Figure 5.1B shows the tiles defining an OR calculation rule.

With the program designed, an input represented by a DNA origami nucleation seed can be introduced. The final pattern of the tile array, which is the output of the process, is based on the sticky-end arrangement on the nucleation seed.

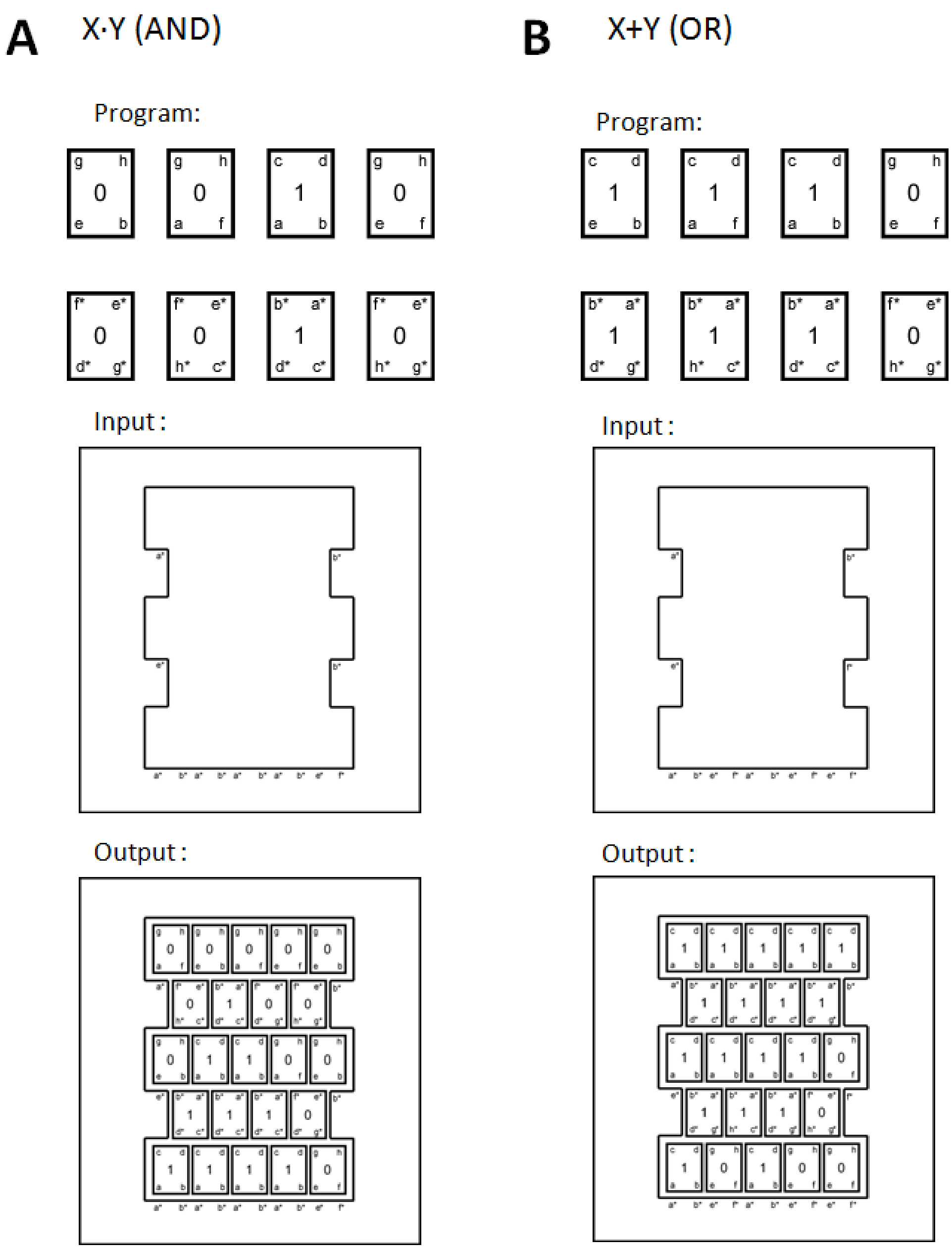

Figure 5.1. Two examples of programmed nanodisplay with limited types of pixels. A set of tiles are designed with two "face values", 0 and 1. Two tiles arranged side by side

(parent tiles) connect to the next tile (daughter tile) through two sticky-ends, of which one sticky-end is from one tile, and the other sticky-end from the other tile. Thus, the tiles can grow into a 2D lattice array. The sticky-ends on the tiles are programmed, so the face value of the daughter tile follows a designed calculation of the parent tile face values. A DNA origami nucleation seed is added to the tiles as the input of the program. The tiles nucleate on the seed and self-assemble into a pattern determined by the sticky-ends on the seed. **(A)** An example when the tiles are programmed to process an AND operation. **(B)** An example when the tiles are programmed to process an OR operation.

With a comparable working principle as liquid crystal displays in which every pixel can be well controlled, this strategy could be developed on a large scale with more adequate controls over the assembly pattern of the DNA tiles. This nanodisplay research would have great potential in miniaturizing computational systems and nanoscale information storage/processing with biological molecules.

5.3 References

(1) Adleman, L. M. *Science* **1994**, *266*, 1021.

(2) Riehemann, K.; Schneider, S. W.; Luger, T. A.; Godin, B.; Ferrari, M.; Fuchs, H. *Angew. Chem., Int. Ed.* **2009**, *48*, 872.

(3) Simmel, F. C. *Nanomedicine* **2007**, *2*, 817.

(4) Rothemund, P. W. K.; Papadakis, N.; Winfree, E. *PLoS. Biol.* **2004**, *2*, e424.

(5) Barish, R. D.; Schulman, R.; Rothemund, P. W. K.; Winfree, E. *Proc. Natl. Acad. Sci.* **2009**, *106*, 6054.

(6) Qian, L. L.; Winfree, E. *Science* **2011**, *332*, 1196.

(7) Qian, L. L.; Winfree, E.; Bruck, J. *Nature* **2011**, *475*, 368.

(8) Chen, Y.-J.; Dalchau, N.; Srinivas, N.; Phillips, A.; Cardelli, L.; Soloveichik, D.; Seelig, G. *Nat. Nano.* **2013**, *8*, 755.

(9) Wei, B.; Dai, M.; Yin, P. *Nature* **2012**, *485*, 623.

(10) Ke, Y.; Ong, L. L.; Shih, W. M.; Yin, P. *Science* **2012**, *338*, 1177.

Bibliography

Chapter 1 References

(1) Watson, J. D.; Crick, F. H. C. *Nature* **1953**, *171*, 737.

(2) Dahm, R. *Dev. Biol.* **2005**, *278*, 274.

(3) Hecht, S. M. *Bioorganic Chemistry: Nucleic Acids*; OUP USA, 1996.

(4) Lehninger, A. L.; Nelson, D. L.; Cox, M. M. *Lehninger Principles of Biochemistry*; W. H. Freeman, 2005.

(5) Drew, H. R.; Wing, R. M.; Takano, T.; Broka, C.; Tanaka, S.; Itakura, K.; Dickerson, R. E. *Proc. Natl. Acad. Sci.* **1981**, *78*, 2179.

(6) Ramakrishnan, B.; Sundaralingam, M. *Biophys. J.* **1995**, *69*, 553.

(7) Wang, A. H. J.; Quigley, G. J.; Kolpak, F. J.; Crawford, J. L.; van Boom, J. H.; van der Marel, G.; Rich, A. *Nature* **1979**, *282*, 680.

(8) Zhang, D. Y.; Seelig, G. *Nat. Chem.* **2011**, *3*, 103.

(9) Yurke, B.; Turberfield, A. J.; Mills, A. P.; Simmel, F. C.; Neumann, J. L. *Nature* **2000**, *406*, 605.

(10) Radding, C. M.; Beattie, K. L.; Holloman, W. K.; Wiegand, R. C. *J. Mol. Biol.* **1977**, *116*, 825.

(11) Yurke, B.; Mills, A., Jr. *Genet. Program Evolvable Mach* **2003**, *4*, 111.

(12) Li, Q.; Luan, G.; Guo, Q.; Liang, J. *Nucleic Acids Res.* **2002**, *30*, e5.

(13) Zhang, D. Y.; Winfree, E. *J. Am. Chem. Soc.* **2009**, *131*, 17303.

(14) Seeman, N. C. *J. Theor. Biol.* **1982**, *99*, 237.

(15) Fu, T. J.; Seeman, N. C. *Biochemistry* **1993**, *32*, 3211.

(16) Chen, J.; Seeman, N. C. *Nature* **1991**, *350*, 631.

(17) Goodman, R. P.; Schaap, I. A. T.; Tardin, C. F.; Erben, C. M.; Berry, R. M.; Schmidt, C. F.; Turberfield, A. J. *Science* **2005**, *310*, 1661.

(18) He, Y.; Ye, T.; Su, M.; Zhang, C.; Ribbe, A. E.; Jiang, W.; Mao, C. *Nature* **2008**, *452*, 198.

(19) Mathieu, F.; Liao, S.; Kopatsch, J.; Wang, T.; Mao, C.; Seeman, N. C. *Nano Lett.* **2005**, *5*, 661.

(20) Park, S. H.; Barish, R.; Li, H.; Reif, J. H.; Finkelstein, G.; Yan, H.; LaBean, T. H. *Nano Lett.* **2005**, *5*, 693.

(21) Mao, C.; Sun, W.; Seeman, N. C. *J. Am. Chem. Soc.* **1999**, *121*, 5437.

(22) Fu, J.; Liu, M.; Liu, Y.; Yan, H. *Acc. Chem. Res.* **2012**, *45*, 1215.

(23) Rothemund, P. W. K. *Nature* **2006**, *440*, 297.

(24) Ke, Y.; Douglas, S. M.; Liu, M.; Sharma, J.; Cheng, A.; Leung, A.; Liu, Y.; Shih, W. M.; Yan, H. *J. Am. Chem. Soc.* **2009**, *131*, 15903.

(25) Dietz, H.; Douglas, S. M.; Shih, W. M. *Science* **2009**, *325*, 725.

(26) Andersen, E. S.; Dong, M.; Nielsen, M. M.; Jahn, K.; Subramani, R.; Mamdouh, W.; Golas, M. M.; Sander, B.; Stark, H.; Oliveira, C. L. P.; Pedersen, J. S.; Birkedal, V.; Besenbacher, F.; Gothelf, K. V.; Kjems, J. *Nature* **2009**, *459*, 73.

(27) Han, D.; Pal, S.; Nangreave, J.; Deng, Z.; Liu, Y.; Yan, H. *Science* **2011**, *332*, 342.

(28) Han, D.; Pal, S.; Liu, Y.; Yan, H. *Nat. Nano.* **2010**, *5*, 712.

(29) Pinheiro, A. V.; Han, D.; Shih, W. M.; Yan, H. *Nat. Nano.* **2011**, *6*, 763.

(30) Yan, H.; Park, S. H.; Finkelstein, G.; Reif, J. H.; LaBean, T. H. *Science* **2003**, *301*, 1882.

(31) Douglas, S. M.; Dietz, H.; Liedl, T.; Hogberg, B.; Graf, F.; Shih, W. M. *Nature* **2009**, *459*, 414.

(32) Feynman, R. P. *J. Microelectromechanical Systems* **1992**, *1*, 60.

(33) Adleman, L. M. *Science* **1994**, *266*, 1021.

(34) Seelig, G.; Soloveichik, D.; Zhang, D. Y.; Winfree, E. *Science* **2006**, *314*, 1585.

(35) Qian, L. L.; Winfree, E. *Science* **2011**, *332*, 1196.

(36) Li, W.; Yang, Y.; Yan, H.; Liu, Y. *Nano Lett.* **2013**, *13*, 2980.

(37) Rothemund, P. W. K.; Papadakis, N.; Winfree, E. *PLoS. Biol.* **2004**, *2*, e424.

(38) Elbaz, J.; Lioubashevski, O.; Wang, F.; Remacle, F.; Levine, R. D.; Willner, I. *Nat. Nano.* **2010**, *5*, 417.

(39) Kahan-Hanum, M.; Douek, Y.; Adar, R.; Shapiro, E. *Sci. Rep.* **2013**, *3*.

(40) Parker, J. *EMBO reports* **2003**, *4*, 7.

(41) Douglas, S. M.; Bachelet, I.; Church, G. M. *Science* **2012**, *335*, 831.

(42) Benenson, Y. *Curr. Opin. Biotech.* **2009**, *20*, 471.

(43) Surana, S.; Bhat, J. M.; Koushika, S. P.; Krishnan, Y. *Nat. Commun.* **2011**, *2*, 340.

(44) Hemphill, J.; Deiters, A. *J. Am. Chem. Soc.* **2013**, *135*, 10512.

Chapter 2 References

(1) Liu, X.; Yan, H.; Liu, Y.; Chang, Y. *Small* **2011**, *7*, 1673.

(2) Pinheiro, A. V.; Han, D.; Shih, W. M.; Yan, H. *Nat. Nano.* **2011**, *6*, 763.

(3) Adleman, L. M. *Science* **1994**, *266*, 1021.

(4) Stojanovic, M. N.; Stefanovic, D. *Nat. Biotech.* **2003**, *21*, 1069.

(5) Elbaz, J.; Lioubashevski, O.; Wang, F.; Remacle, F.; Levine, R. D.; Willner, I. *Nat. Nano.* **2010**, *5*, 417.

(6) Benenson, Y.; Gil, B.; Ben-Dor, U.; Adar, R.; Shapiro, E. *Nature* **2004**, *429*, 423.

(7) Yurke, B.; Turberfield, A. J.; Mills, A. P.; Simmel, F. C.; Neumann, J. L. *Nature* **2000**, *406*, 605.

(8) Turberfield, A. J.; Mitchell, J. C.; Yurke, B.; Mills, A. P., Jr.; Blakey, M. I.; Simmel, F. C. *Phys. Rev. Lett.* **2003**, *90*, 118102.

(9) Yurke, B.; Mills, A., Jr. *Genet Program Evolvable Mach* **2003**, *4*, 111.

(10) Zhang, D. Y.; Winfree, E. *J. Am. Chem. Soc.* **2009**, *131*, 17303.

(11) Soloveichik, D.; Seelig, G.; Winfree, E. *Proc. Natl. Acad. Sci.* **2010**, *107*, 5393.

(12) Phillips, A.; Cardelli, L. *J. R. Soc. Interface* **2009**, *6*, S419.

(13) Seelig, G.; Soloveichik, D.; Zhang, D. Y.; Winfree, E. *Science* **2006**, *314*, 1585.

(14) Zhang, D. Y.; Turberfield, A. J.; Yurke, B.; Winfree, E. *Science* **2007**, *318*, 1121.

(15) Yin, P.; Choi, H. M. T.; Calvert, C. R.; Pierce, N. A. *Nature* **2008**, *451*, 318.

(16) Qian, L. L.; Winfree, E. *Science* **2011**, *332*, 1196.

(17) Qian, L. L.; Winfree, E.; Bruck, J. *Nature* **2011**, *475*, 368.

(18) Imre, A.; Csaba, G.; Ji, L.; Orlov, A.; Bernstein, G. H.; Porod, W. *Science* **2006**, *311*, 205.

Chapter 3 References

(1) Simmel, F. C. *Nanomedicine* **2007**, *2*, 817.

(2) Riehemann, K.; Schneider, S. W.; Luger, T. A.; Godin, B.; Ferrari, M.; Fuchs, H. *Angewandte Chemie International Edition* **2009**, *48*, 872.

(3) Liu, X.; Yan, H.; Liu, Y.; Chang, Y. *Small* **2011**, *7*, 1673.

(4) Pinheiro, A. V.; Han, D.; Shih, W. M.; Yan, H. *Nat Nano* **2011**, *6*, 763.

(5) Lin, C.; Liu, Y.; Yan, H. *Biochemistry* **2009**, *48*, 1663.

(6) Barish, R. D.; Schulman, R.; Rothemund, P. W. K.; Winfree, E. *Proceedings of the National Academy of Sciences* **2009**, *106*, 6054.

(7) Li, W.; Yang, Y.; Jiang, S.; Yan, H.; Liu, Y. *J Am Chem Soc* **2014**, *136*, 3724.

(8) Rothemund, P. W. K.; Papadakis, N.; Winfree, E. *PLoS Biol* **2004**, *2*, e424.

(9) Zhang, F.; Nangreave, J.; Liu, Y.; Yan, H. *Nano Letters* **2012**, *12*, 3290.

(10) Yurke, B.; Turberfield, A. J.; Mills, A. P.; Simmel, F. C.; Neumann, J. L. *Nature* **2000**, *406*, 605.

(11) Adleman, L. M. *Science* **1994**, *266*, 1021.

(12) Benenson, Y.; Gil, B.; Ben-Dor, U.; Adar, R.; Shapiro, E. *Nature* **2004**, *429*, 423.

(13) Stojanovic, M. N.; Stefanovic, D. *Nat Biotech* **2003**, *21*, 1069.

(14) Turberfield, A. J.; Mitchell, J. C.; Yurke, B.; Mills, A. P., Jr.; Blakey, M. I.; Simmel, F. C. *Physical Review Letters* **2003**, *90*, 118102.

(15) Yurke, B.; Mills, A., Jr. *Genet Program Evolvable Mach* **2003**, *4*, 111.

(16) Zhang, D. Y.; Winfree, E. *J Am Chem Soc* **2009**, *131*, 17303.

(17) Li, W.; Yang, Y.; Yan, H.; Liu, Y. *Nano Letters* **2013**, *13*, 2980.

(18) Elbaz, J.; Lioubashevski, O.; Wang, F.; Remacle, F.; Levine, R. D.; Willner, I. *Nat Nano* **2010**, *5*, 417.

(19) Kahan-Hanum, M.; Douek, Y.; Adar, R.; Shapiro, E. *Sci. Rep.* **2013**, *3*.

(20) Soloveichik, D.; Seelig, G.; Winfree, E. *Proceedings of the National Academy of Sciences* **2010**, *107*, 5393.

(21) Chen, Y.-J.; Dalchau, N.; Srinivas, N.; Phillips, A.; Cardelli, L.; Soloveichik, D.; Seelig, G. *Nat Nano* **2013**, *8*, 755.

(22) Phillips, A.; Cardelli, L. *J R Soc Interface* **2009**, *6*, S419.

(23) Seelig, G.; Soloveichik, D.; Zhang, D. Y.; Winfree, E. *Science* **2006**, *314*, 1585.

(24) Zhang, D. Y.; Turberfield, A. J.; Yurke, B.; Winfree, E. *Science* **2007**, *318*, 1121.

(25) Yin, P.; Choi, H. M. T.; Calvert, C. R.; Pierce, N. A. *Nature* **2008**, *451*, 318.

(26) Qian, L. L.; Winfree, E. *Science* **2011**, *332*, 1196.

(27) Qian, L. L.; Winfree, E.; Bruck, J. *Nature* **2011**, *475*, 368.

(28) Rentzeperis, D.; Alessi, K.; Marky, L. A. *Nucleic Acids Research* **1993**, *21*, 2683.

Chapter 4 References

(1) Seeman, N. C. *J. Theor. Biol.* 1982, *99*, 237.

(2) Rothemund, P. W. K. *Nature* 2006, *440*, 297.

(3) Winfree, E.; Liu, F.; Wenzler, L. A.; Seeman, N. C. *Nature* 1998, *394*, 539.

(4) Seeman, N. C. *Nature* 2003, *421*, 427.

(5) Gothelf, K. V.; LaBean, T. H. *Org. Biomol. Chem.* 2005, *3*, 4023.

(6) Voigt, N. V.; Torring, T.; Rotaru, A.; Jacobsen, M. F.; Ravnsbaek, J. B.; Subramani, R.; Mamdouh, W.; Kjems, J.; Mokhir, A.; Besenbacher, F.; Gothelf, K. V. *Nat. Nano.* 2010, *5*, 200.

(7) Deng, Z.; Samanta, A.; Nangreave, J.; Yan, H.; Liu, Y. *J. Am. Chem. Soc.* 2012, *134*, 17424.

(8) Barish, R. D.; Schulman, R.; Rothemund, P. W. K.; Winfree, E. *Proc. Natl. Acad. Sci.* 2009, *106*, 6054.

(9) Qian, L. L.; Winfree, E. *Science* 2011, *332*, 1196.

(10) Qian, L. L.; Winfree, E.; Bruck, J. *Nature* 2011, *475*, 368.

(11) Li, W.; Yang, Y.; Yan, H.; Liu, Y. *Nano. Lett.* 2013, *13*, 2980.

(12) Yan, H.; Park, S. H.; Finkelstein, G.; Reif, J. H.; LaBean, T. H. *Science* 2003, *301*, 1882.

(13) He, Y.; Chen, Y.; Liu, H.; Ribbe, A. E.; Mao, C. *J. Am. Chem. Soc.* 2005, *127*, 12202.

(14) Dietz, H.; Douglas, S. M.; Shih, W. M. *Science* 2009, *325*, 725.

(15) Han, D.; Pal, S.; Nangreave, J.; Deng, Z.; Liu, Y.; Yan, H. *Science* 2011, *332*, 342.

(16) Wei, B.; Dai, M.; Yin, P. *Nature* 2012, *485*, 623.

(17) Ke, Y.; Ong, L. L.; Shih, W. M.; Yin, P. *Science* 2012, *338*, 1177.

(18) Zhao, Z.; Liu, Y.; Yan, H. *Nano. Lett.* 2011, *11*, 2997.

(19) Yang, Y.; Han, D.; Nangreave, J.; Liu, Y.; Yan, H. *ACS Nano* 2012, *6*, 8209.

(20) Pound, E.; Ashton, J. R.; Becerril, H. c. A.; Woolley, A. T. *Nano. Lett.* 2009, *9*, 4302.

(21) Zhang, H.; Chao, J.; Pan, D.; Liu, H.; Huang, Q.; Fan, C. *Chem. Commun.* 2012, *48*, 6405.

(22) Sun, X.; Hyeon Ko, S.; Zhang, C.; Ribbe, A. E.; Mao, C. *J. Am. Chem. Soc.* 2009, *131*, 13248.

(23) Lee, J.; Hamada, S.; Hwang, S. U.; Amin, R.; Son, J.; Dugasani, S. R.; Murata, S.; Park, S. H. *Sci. Rep.* 2013, *3*.

(24) Hamada, S.; Murata, S. *Angew. Chem., Int. Ed.* 2009, *48*, 6820.

(25) Schulman, R.; Winfree, E. *Proc. Natl. Acad. Sci.* 2007, *104*, 15236.

(26) Pinheiro, A. V.; Nangreave, J.; Jiang, S.; Yan, H.; Liu, Y. *ACS Nano* 2012, *6*, 5521.

Chapter 5 References

(1) Adleman, L. M. *Science* **1994**, *266*, 1021.

(2) Riehemann, K.; Schneider, S. W.; Luger, T. A.; Godin, B.; Ferrari, M.; Fuchs, H. *Angew. Chem., Int. Ed.* **2009**, *48*, 872.

(3) Simmel, F. C. *Nanomedicine* **2007**, *2*, 817.

(4) Rothemund, P. W. K.; Papadakis, N.; Winfree, E. *PLoS. Biol.* **2004**, *2*, e424.

(5) Barish, R. D.; Schulman, R.; Rothemund, P. W. K.; Winfree, E. *Proc. Natl. Acad. Sci.* **2009**, *106*, 6054.

(6) Qian, L. L.; Winfree, E. *Science* **2011**, *332*, 1196.

(7) Qian, L. L.; Winfree, E.; Bruck, J. *Nature* **2011**, *475*, 368.

(8) Chen, Y.-J.; Dalchau, N.; Srinivas, N.; Phillips, A.; Cardelli, L.; Soloveichik, D.; Seelig, G. *Nat. Nano.* **2013**, *8*, 755.

(9) Wei, B.; Dai, M.; Yin, P. *Nature* **2012**, *485*, 623.

(10) Ke, Y.; Ong, L. L.; Shih, W. M.; Yin, P. *Science* **2012**, *338*, 1177.

APPENDIX A

SUPPLEMENTAL INFORMATION FOR CHAPTER 2

Supporting Information for

3-Input Majority Logic Gate and Multiple Input Logic Circuit Based on DNA Strand Displacement

Wei Li, Yang Yang, Hao Yan, Yan Liu

Department of Chemistry and Biochemistry and The Biodesign Institute

Arizona State University, Tempe, AZ 85287

S2.1 Circularization of the central strands in the Calculators

The circularization is achieved by first hybridizing the two ends of the linear strand (126nt in the single 3-input majority gate, 96 nt in M_X and 159 nt in M_Y) with one 20 nt ssDNA, then ligate the nick on the duplex using T4 DNA ligase (Figure S2.1). 250 pmol linear strand, and 2.5 nmol 20 nt strand are mixed in 1 mL 1×T4 DNA ligase buffer (New England Biolabs). The solution is heated at 90 ^{o}C for 5 minutes, and then cooled with ice. 2000 unit of T4 DNA ligase is added to the cooled solution. The solution then is incubated at 16 ^{o}C overnight.

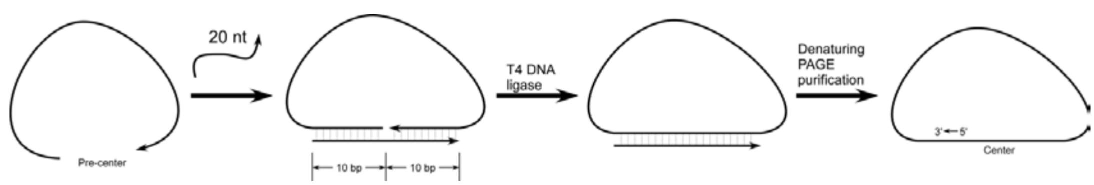

Figure S2.1. The strategy of circularizing the central strand of the Calculators.

After the reaction, the solution is concentrated with Amicon Ultra centrifugal filter (3K Dalton) (Millipore) to about 30 µL. Then the ligated central circular strand is purified with polyacrylamide gel electrophoresis (6% gel, in 1×TBE buffer, 45 mA/gel, and 1.5 hours).

A purifying gel image (EB stained) is shown in Figure S2.2A. This gel shows the result of the circularization of the central strand of the single gate design. The band of the circular strand is cut out from the gel and chopped into small pieces. The shredded gel blocks containing the product is soaked in 500 µL elution buffer (500 mM NH_4OAc, 10 mM $Mg(OAc)_2$, and 2mM EDTA) overnight. The central strand is then extracted from the gel by centrifugation using a Spin X device. The solution is then washed with butanol.

1 mL ethanol is mixed with the 500 µL solution to precipitate the DNA molecules. The solution is kept at -20 °C to make the precipitation fast and complete. Then solid DNA product is separated with centrifuge, and then dried under vacuum in a vacufuge (Eppendorf).

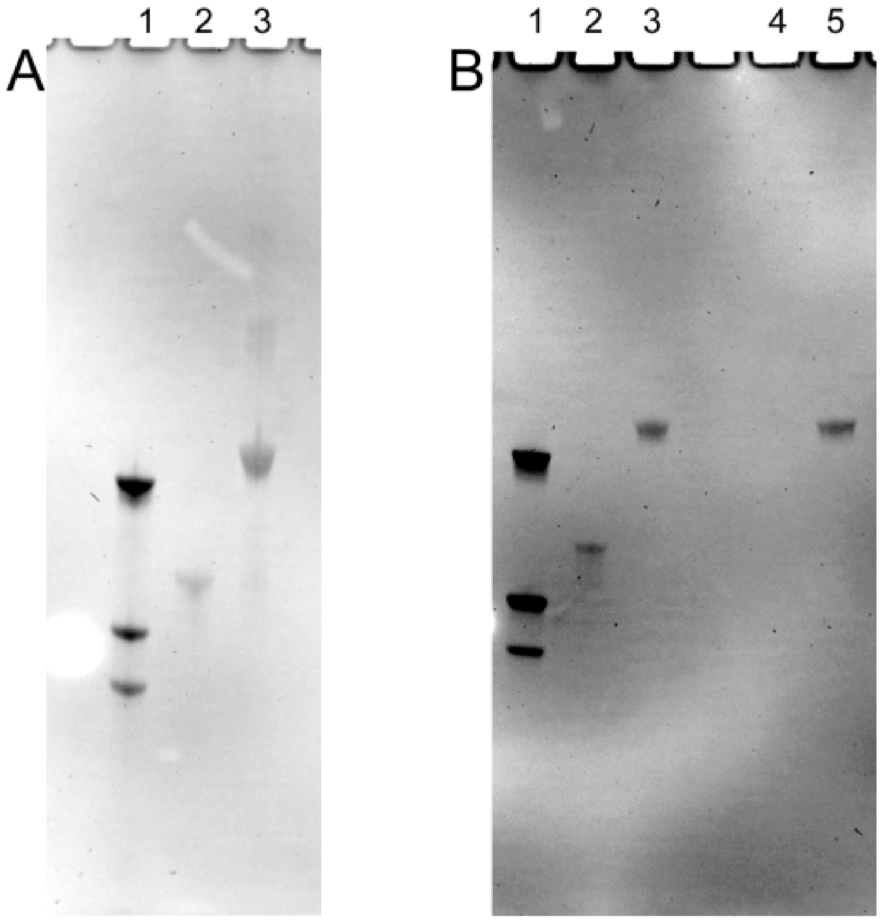

Figure S2.2. Denaturing gel images showing the circularization and characterization of the center strand in the single gate design. (A) The circularization of the center strand. Lane 1: ssDNA ladder, the three bands from top to bottom are, 159 nt, 109 nt, and 96 nt linear ssDNA. Lane 2: the linear pre-center strand (126 nt). Lane 3: the crude product after circularization with T4 DNA ligase. The most intense band with a similar mobility of the 159 nt strand, is identified as the target product, the circular central strand. Above the target product are the bands of concatamers. (B) The circular central strand product pextracted from the left gel is subjected to exonuclease I digestion. Lane 1: ssDNA ladder, same as in (A). Lane 2: the linear center strand with no exonuclease I. Lane 3: circular central strand with no exonuclease I. Lane 4: the linear center strand with exonuclease I. Lane 5: circular central strand with exonuclease I. The gel shows that, under the same exonuclease I conditions, the linear strand in Lane 4 is almost all degraded, while the strand in Lane 5 is not affected. This confirms that the product from Gel (A) is the desired circular strand.

The product from the gel purification is subject to exonuclease I digestion (5 pmol DNA strand in 10 μL 1×NEB buffer 1 (New England Biolabs) with 1 unit exonuclease I (New England Biolabs), incubated at 37 ^{o}C for 1 hour). Exonuclease I cleaves single strand from 3' end to 5' end. If the product recovered from the gel is the circular target product, it should be resistant to digestion by exonuclease I. The result in Figure S2.2B confirms that the recovered DNA strand is the target circular product.

S2.2 Preparation of the Calculators

The purified center circular strand is mixed with the respective side strands A*, B*, and C*, in 1×TAE/Mg^{2+} buffer (1 mM tris acetate, 1 mM EDTA, 12.5 mM magnesium acetate). The final concentration of the center circular strand is 0.5 µM, and the molar ratio of a side strand to the center strand is varied from 1.2:1 to 1:1. For the single gate experiments, more than 1:1 ratio can be used. For multi-gate cascade, 1:1 ratio is used. The solution is incubated in a PCR machine, at 90 ^{o}C for 5 min, 88 ^{o}C for 5 min. Then the temperature is dropped 4 ^{o}C every 5 min until it reaches 25 ^{o}C. The prepared Calculator solution is stored at 4 ^{o}C before use.

S2.3 Preparation of the Detectors

The fluorescence dye modified ssDNA and dark quencher modified ssDNA are mix in 1 × TAE/Mg^{2+} buffer, at the concentration of 0.5 µM each. The solution is incubated in a PCR machine, at 90 ^oC for 5 min, then 88 ^oC for 5 min, with the temperature drops 4 ^oC every 5 min until it reaches 25 ^oC. The Calculator solution is stored at 4 ^oC before use. Figure S2.3 shows a native polyacrylamide gel electrophoresis image characterizing the formation of the Detector of the single gate design.

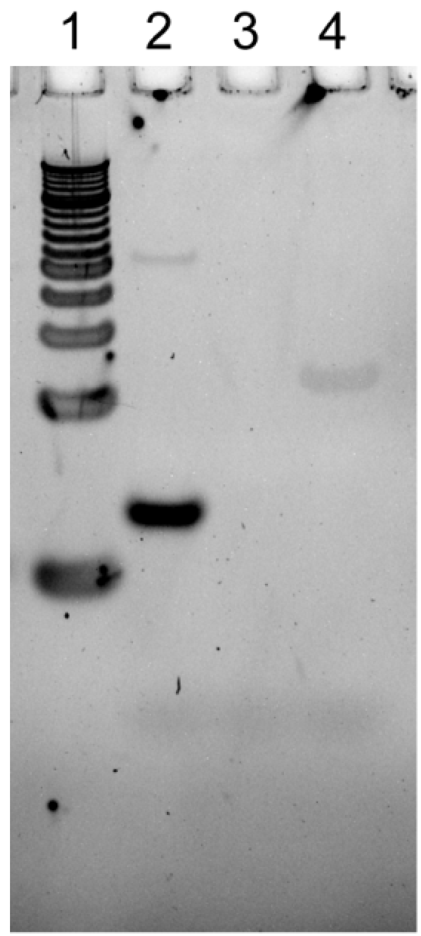

Figure S2.3. Native polyacrylamide gel showing the formation of the Detector of the single gate design. The gel electrophoresis is conducted in 1 × TAE/Mg^{2+} buffer under 200 Volts. The gel is stained with SBRY Gold. Lane 1: 10 bp DNA ladder. Lane 2: 6-

carboxyfluorescein (FAM) modified RS2 ssDNA. The thin slower band is the self-dimer of the RS2 ssDNA. The lower intense band is the monomer form. Lane 3: Iowa Black dark quencher modified RS2*-RS1* ssDNA. No band is visible in this lane, because the Iowa Black dark quencher quenches the fluorescence of SBRY Gold staining. Lane 4: The Detector duplex. The intensity of the band is much lower than that of lane 2, due to the quenching effect of the Iowa Black dark quencher on the fluorescence of SBRY Gold staining and the fluorescence of the FAM on its complementary strand.

S2.4 Fluorescence Kinetics Measurements

Fluorescence kinetics of the single gate design is monitored with a Nanolog fluorometer (Horiba Jobin Yvon). This fluorometer is capable to measure the fluorescence intensity of one sample at one time. The excitation wavelength is set at 495 nm for 6-FAM. The detection wavelength is set at 520 nm for the emission of 6-FAM. The Calculator, input strands, and Detector are mixed in a quartz fluorescence cuvette. The final volume is 120 µL. The reaction buffer is 1×TAE/Mg^{2+} buffer. The sample is controlled at 25 ^{o}C. The Calculator concentration at the beginning of the reaction is 15 nM. The ratio of the Input strand to the Calculator is 1.5:1. The Detector concentration is of the same concentration or 4 folds of the Calculator. Upon the mixing of the reactants, the fluorescence intensity of the sample is measured at every 30 second.

Fluorescence kinetics of the multi-function circuit based on 2 majority gates, and the fluorescence kinetics of each of the two gates, are monitored with a Stratagene MX3005P realtime PCR (Agilent). This realtime PCR is set at a constant temperature of 30 ^{o}C. The fluorescence intensities of the samples are measured every cycle of 1 minute. The realtime PCR can measure the fluorescence intensity of up to 96 samples at one time. The filter is set at 488 nm for excitation and 520 for emission. The Calculators, input strands, and Detector are mixed in an optical PCR tube. The final volume is 30 µL. The reaction buffer is 1×TAE/Mg^{2+} buffer. The M_X Calculator concentration at the beginning of the reaction is 67 nM. M_Y Calculator concentration 135 nM. The concentration of the Input X1 and X2 is 67 nM each. The concentration of the Input Y1, Y2, and Y3 is 135 nM each. The Detector concentration is 33 nM. Upon the mixing of the reactants, the fluorescence intensity of the sample is measured every minute.

The experiment in Figure 2.7C (Y1 = 0, X1 = 1, Y2· Y3 + X2) is conducted in 2 steps. Calculator M_Y is mixed with all the input strands and incubated at 30 ^oC overnight. Then Calculator M_X and the Detector are added, and the fluorescence intensity change is monitored.

The fluorescence intensity increase of each reaction is calculated by subtracting the initial intensity from the final intensity. The reactions under the same computation pattern or single gate are normalized, by setting the highest fluorescence increase as 100%.

S2.5 Fluorescence Kinetics Result of the Two Individual Majority Gate in the Multi-Function Circuit

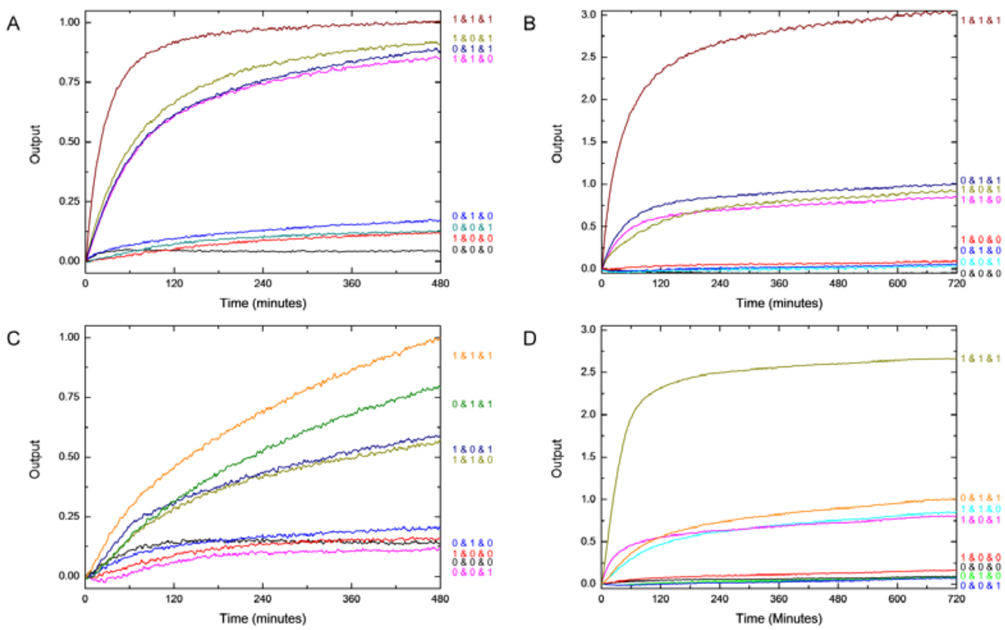

Figure S2.4. Kinetic experiments of the individual majority gates in the multi-function circuit. **(A)** Kinetics of the second generation gate M_X. The ratio between the Detector and the Calculator is 1:1. **(B)** Kinetics of the second generation gate M_x. The ratio between the Detector and the Calculator is 4:1. **(C)** Kinetics of the first generation gate M_Y. The ratio between the Detector and the Calculator is 1:1. **(D)** Kinetics of the first generation gate M_Y. The ratio between the Detector and the Calculator is 4:1. Each curve in these two graphs represents a reaction with the input combination labeled at the end of the curve. The measurement of the fluorescence intensity is started as soon as the Calculator, the Detector, and the inputs of each reaction are mixed at 1-minute intervals. The fluorescence increase is calculated by subtracting the initial intensity from the final intensity. The output is normalized to the highest intensity change to be 1 in A and C , and to the highest intensity change to be 1 for the 2-input cases in B and D.

S2.6 DNA Sequences

The sequences of the strands used in each design are shown with the schematic figures in Figure S2.5.

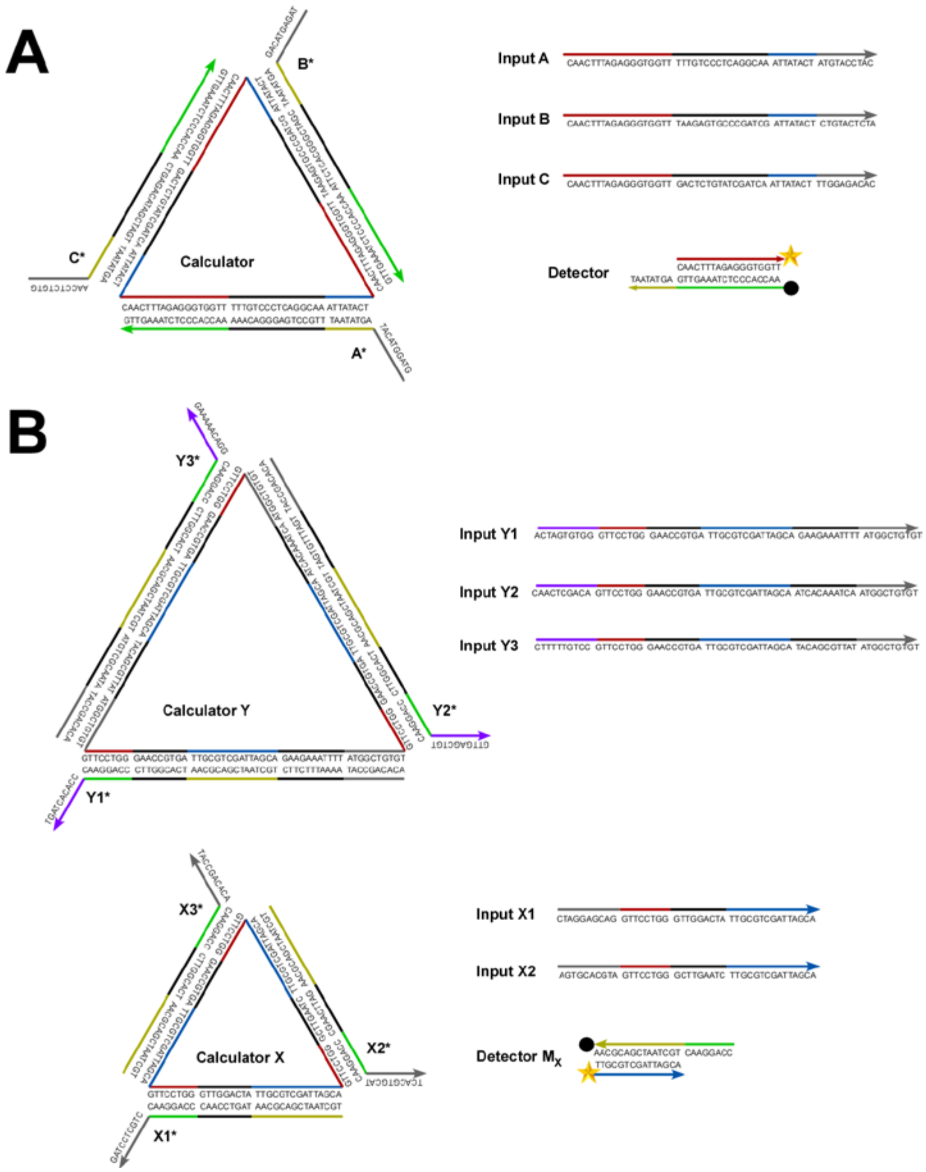

Figure S2.5. Sequences of the DNA strands used in the experiments. **(A)** The sequence of the single gate design. **(B)** The sequence of the multi-function circuit. The stars in (A) and (B) represent 6-FAM (fluorescein) fluorescence dye. The black dots in (A) and (B) represent Iowa Black Dark Quencher.

S2.7 Effect of Secondary Structure of Inputs on Reaction Rates

If the toehold of an input strand is involved in stable secondary structures, the reaction rate would significantly decrease. A set of toehold sequences which is different from the sequences in Figure S2.5A is shown in Figure S2.6A. In this set of sequences, the toehold in Input B has a stable secondary structure (Figure S2.6B). The reaction kinetics is shown in Figure S2.6C. The reactions, of which the true outputs depend on the presence of Input B, are obviously slower than the reactions with Input A and Input C. This result is an example of the effect of the sequences on the reaction rate.

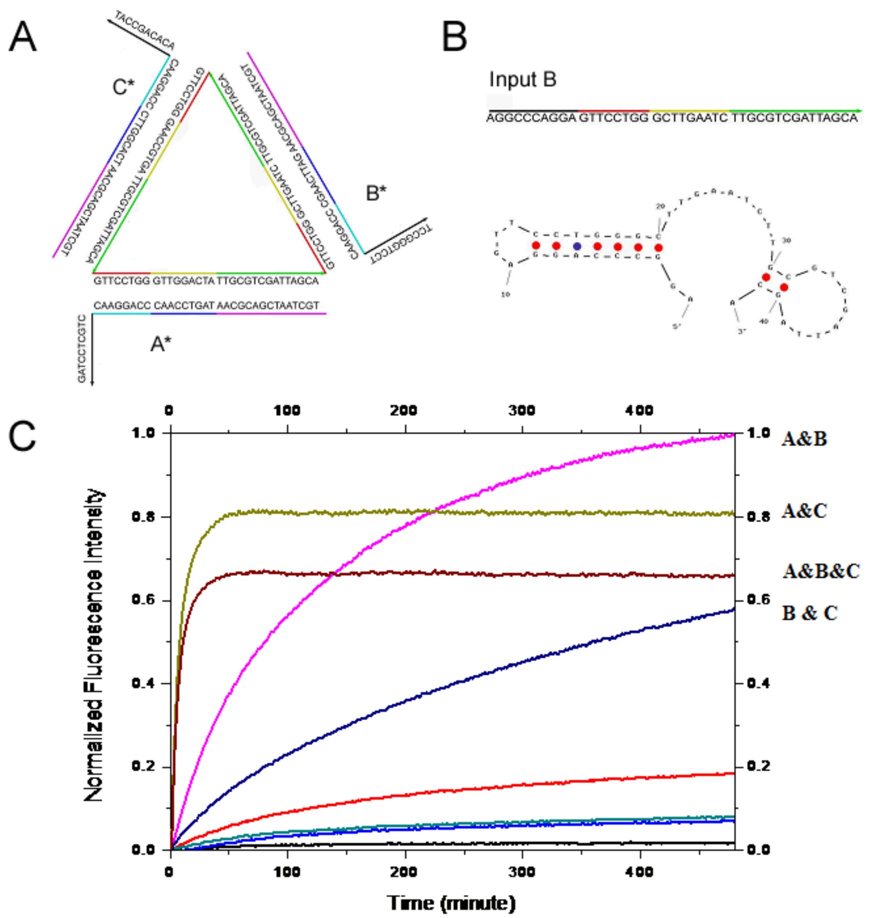

Figure S2.6. Effect of secondary structure of inputs on reaction rates. **(A)** Sequences of logic gate strands. **(B)** The sequence of Input B and the secondary structure of Input B.

The toehold in Input B at 5' end is involved in the secondary structure, thus the exposed part is only 2 nt long. **(C)** The fluorescence kinetics of the logic gate in (A). The true output of reactions A&B and B&C depend on the strand displacement of Input B, so the reaction rate is much lower than those of reactions A&C and A&B&C. The final normalized fluorescence intensities of A&C and A&B&C are lower than 1, because the initial reaction rates are high. Before the starting of the monitoring of the reactions, the fluorescence already increased. After the normalization, the final value is lower than 1.

APPENDIX B

SUPPLEMENTAL INFORMATION FOR CHAPTER 3

Supporting Information for

: 1-Bit Full Adder and Half Adder Based on DNA Strand Displacement

Wei Li, Hao Yan, Yan Liu

Department of Chemistry and Biochemistry and The Biodesign Institute

Arizona State University, Tempe, AZ 85287

S3.1 Experimental Materials and Methods

S3.1.1 Materials. All DNA strands were purchased from Integrated DNA Technologies, Inc. (www.IDTDNA.com) in the format of desalted dry powder. The strands were all purified using denaturing polyacrylamide gel electrophoresis (10% 19:1 acrylamide/bisacrylamide, containing 50% urea) in 1×TBE buffer (pH 8.0, 89 mM tris base, 89 mM boric acid, 2 mM EDTA). The bands corresponding to the full length strands were individually excised from the gel, chopped into small pieces, soaked in 500 μL elution buffer (500 mM NH_4OAc, 10 mM $Mg(OAc)_2$, and 2 mM EDTA) and then shaken overnight to allow the DNA strands to elute from the gel blocks into the solution. After filtering out the gel blocks, the solutions were then mixed with butanol to extract any organic residue. After removing the butanol layer, 1 mL of ethanol was mixed with each solution to precipitate the DNA molecules. The mixtures were kept at -20 ^oC to ensure rapid and complete DNA precipitation. Then the purified DNA strands were spun down using a centrifuge, and then dried under vacuum. The DNA strands were then reconstituted in pure water and their concentrations were measured by absorbance at 260 nm.

S3.1.2 Assembly Procedure. Each DNA duplex was assembled by mixing the component strands in an equal molar ratio (4 mM) in 20 μL 1×TAE/Mg^{2+} buffer. The solution was annealed in a PCR thermocycler with the temperature decreased from 90 ^oC to 25 ^oC at a rate of 4 ^oC every 5 minutes, and then kept at 25 ^oC. For each reaction with a specific combination input, 5 μL of the total solution is used to mix with other strands.

S3.1.3 Fluorescence Kinetics. The fluorescence kinetics experiments were performed on a real-time PCR thermocycler (Stratagene Mx3005P). The thermocycler program is set that the time of each cycle is one minute, so the fluorescence intensity of the solution can be collected once every minute. The temperature of all the cycles is set as 25 ^{o}C. The program contains 1440 cycles, so the fluorescence of the solution is monitored for 24 hours. The filters for FAM and HEX fluorescent dyes are selected in the instrument control.

The final concentration of each DNA strand in the solution is about 0.5 μM after mixing the input strand. The buffer condition is 1×TAE/Mg^{2+} buffer. The fluorescence intensity measurement starts as soon as the input strands are added.

S3.1.4 Fluorescence Data. For each reaction, the first trace is the original data collected by the fluorometer. The second trace is the increase of each reaction at each time point. This is calculated by subtracting the starting fluorescence intensity from the intensity at each time point. The third trace is the data after normalization. All the data in the second trace is divided by the highest fluorescence increase among the reactions of the same logic gate operation. The data in the third trace are shown in Figure 3.6, Figure 3.7, and Figure 3.8.

S3.2 Capping Technique

In the design of the XOR gate and AND gate, we incorporated the "capping technique". Figure S3.1 shows the position of the caps we placed on the strands.

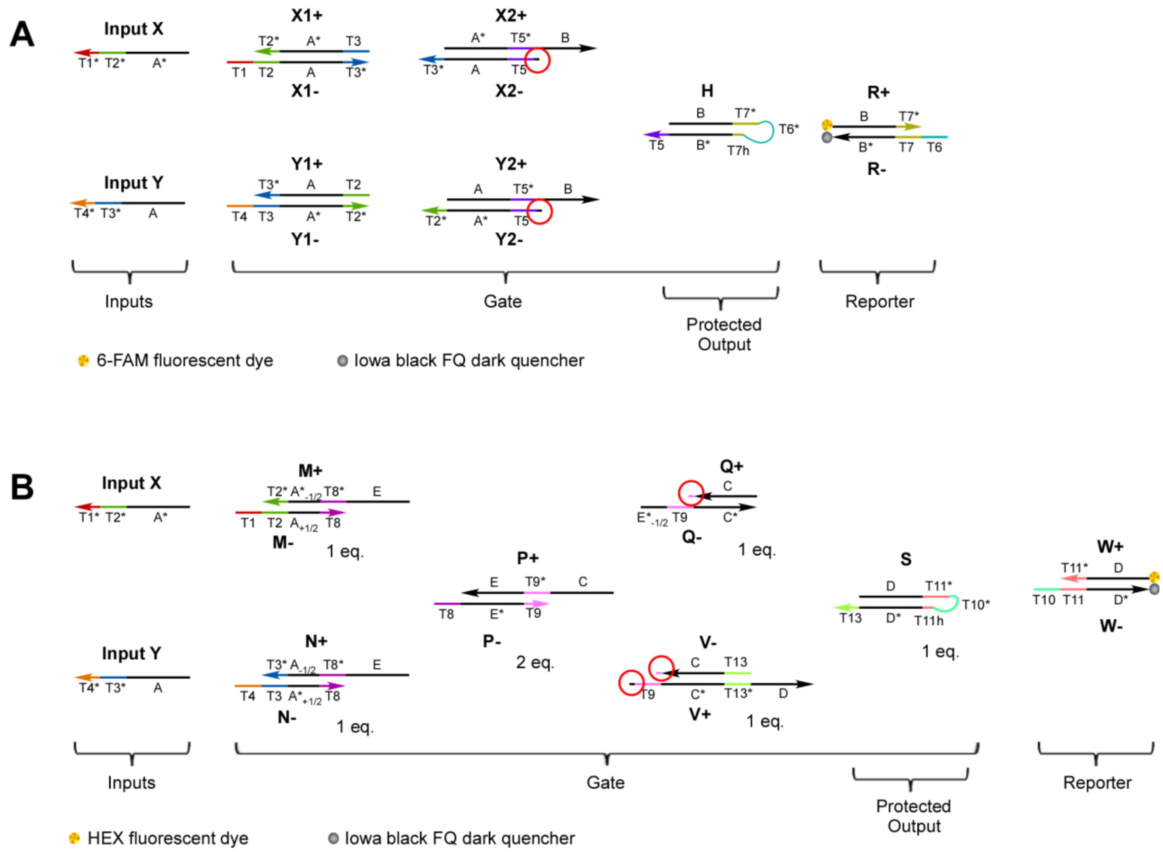

Figure S3.1. The positions of the caps. The caps in the design if marked with red circles. Each cap is a one nucleotide extension from the main strand, and complementary to the corresponding base to the other component strand in the duplex.

The capping technique was introduced by L. L. Qian and E. Winfree (*Science* 2011***, 332,*** 1196). The purpose of the caps is to prevent the non-specific π- π stacking directed DNA strand displacement reaction (Figure S3.2), which may contribute to the leakages of the reactions. Because of the cap, even two DNA double helices stack together, the first “loose” base in the single-stranded migrating domain is different from the first base in the double-stranded domain, and the branch migration cannot occur. It is preferred to add caps wherever is possible in the design.

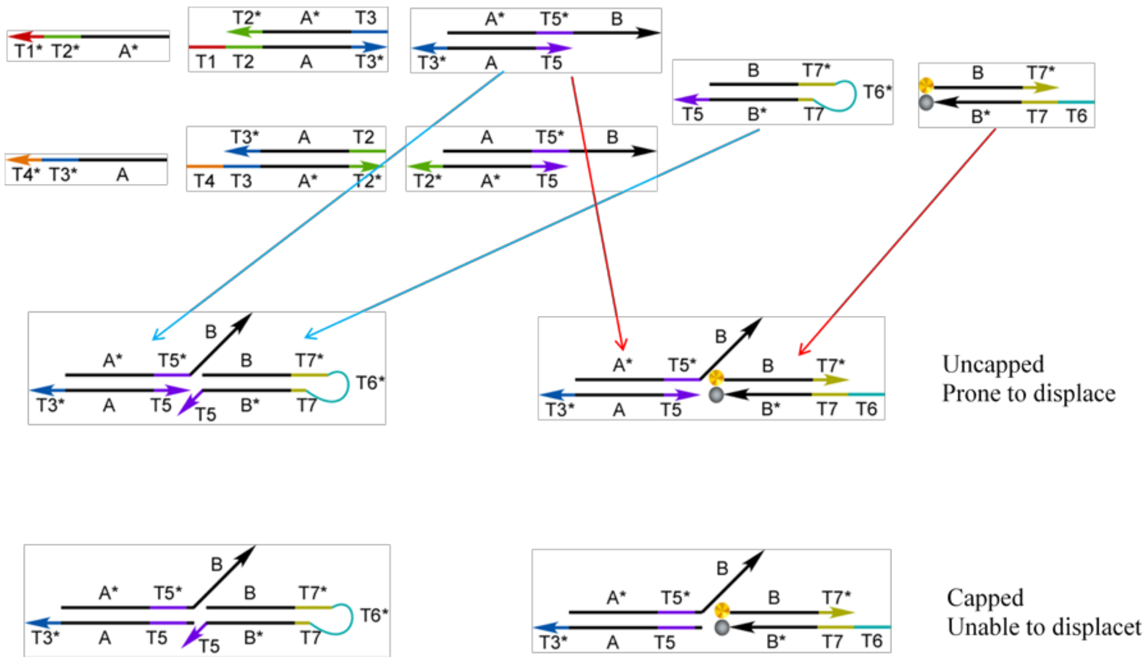

Figure S3.2. The caps can prevent π- π stacking directed DNA strand displacement reactions.

S.3.3 Length of the Toehold Domain in the Hairpins

In the designs of both the XOR gate and AND gate, the outputs are protected in a hairpin structure. With an optimal hairpin loop length, 5 to 8 bases, the hairpin stem is far more stable than a linear DNA double helix of the same length. The yields of the reaction shown in Figure S3.3 is calculated with NuPack.org, and shown in Table S3.1 and Table S3.2, with

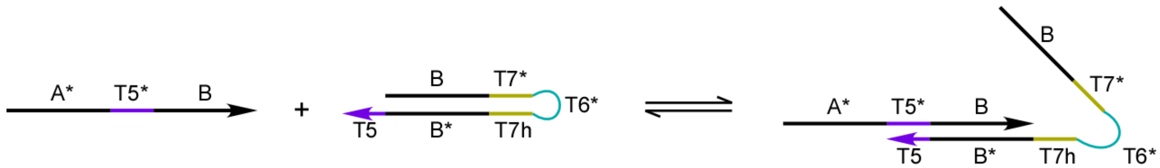

Figure S3.3. The opening reaction of the hairpin structure.

Table S3.1. Relation between Length of T7h and Reaction Yield

Length of T7	5	4	3	2	1	0
Yield (%)	0.12	0.12	0.12	1.9	3.2	57

Lengths: T5 = T5* = T7 = T6* = 5 nt, A* = B = B* = 12 nt

Concentration: 100 nM; Temp. = 25 ^{o}C

Table S3.2. Relation between Temperature, Concentration and Reaction Yield

Yield (%)		Temp. (^{o}C)		
		15	25	35
Conc. (nM)	10	1.1	0.20	0
	100	9.3	1.9	0.56
	1000	40	15	5.1

Lengths: T5 = T5* = T7 = T6* = 5 nt, A* = B = B* = 12 nt, T7 = 2 nt

S3.4 Using Halves of Domain A and A* in the Design of AND Gate

In the design of the AND gate, domains named $A_{+1/2}$, $A_{-1/2}$, $A^*_{+1/2}$, and $A^*_{-1/2}$. These domains correspond to halves of the full length domains A and A*. The subscript +1/2 represents the 5' end six nucleotides of the full length domain, while the subscript -1/2 represents the 3' end six nucleotides of the full length domain.

Domain $A_{+1/2}$ is complementary to Domain $A^*_{-1/2}$, but does not hybridize with $A^*_{+1/2}$. Similarly, Domain $A_{-1/2}$ is complementary to Domain $A^*_{+1/2}$, but does not hybridize with $A^*_{-1/2}$. This strategy can prevent the hybridization of the reactive strands in the AND gate, and avoid the reaction rate being slowed down when both two inputs are added.

APPENDIX C

SUPPLEMENTAL INFORMATION FOR CHAPTER 4

Supporting Information for

Controlled Nucleation and Growth of DNA Tile Arrays within Prescribed DNA Origami Frames and Their Dynamics

Wei Li, Yang Yang, Shuoxing Jiang, Hao Yan, Yan Liu

Department of Chemistry and Biochemistry and The Biodesign Institute

Arizona State University, Tempe, AZ 85287

S4.1 Experimental Materials and Methods

S4.1.1 Materials. All DNA helper strands used in the origami frame were purchased in 96-well plates from Integrated DNA Technologies, Inc. (www.IDTDNA.com), desalted, with concentrations normalized to 200 μM. Single stranded M13mp18 viral DNA and phi X 174 DNA were purchased from New England Biolabs, Inc. (NEB, catalog number: N4040S and N3023S). All DNA strands in the DNA origami frame were used without further purification.

All DNA strands used in the DX tiles were purchased from Integrated DNA Technologies, Inc. (www.IDTDNA.com) in the format of desalted dry powder. The tile strands were all purified using denaturing polyacrylamide gel electrophoresis (10% 19:1 acrylamide/bisacrylamide, containing 50% urea) in 1×TBE buffer (pH 8.0, 89 mM tris base, 89 mM boric acid, 2 mM EDTA). The bands corresponding to the full length strands were individually excised from the gel, chopped into small pieces, soaked in 500 μL elution buffer (500 mM NH_4OAc, 10 mM $Mg(OAc)_2$, and 2 mM EDTA) and then shaken overnight to allow the DNA strands to elute from the gel blocks into the solution. After filtering out the gel blocks, the solutions were then mixed with butanol to extract any organic residue. After removing the butanol layer, 1 mL of ethanol was mixed with each solution to precipitate the DNA molecules. The mixtures were kept at -20 ^{o}C to ensure rapid and complete DNA precipitation. Then the purified DNA strands were spun down using a centrifuge, and then dried under vacuum. The DNA strands were then reconstituted in pure water and their concentrations were measured by absorbance at 260 nm.

S4.1.2 Assembly Procedure. The DNA origami frame structure was assembled by mixing M13mp18 DNA (10 nM) and phi X 174 DNA (10 nM) with the helper strands in a 1:1:30 molar ratio in 1×TAE/Mg^{2+} buffer (pH 8.0, 20 mM Tris base, 20 mM acetic acid, 2 mM EDTA, 12.5 mM $Mg(OAc)_2$). The final volume of the reaction was 100 µL. The solution was annealed in a PCR thermocycler with the temperature decreased from 90 ^{o}C to 70 ^{o}C at a rate of 1 ^{o}C every 5 minutes, from 70 ^{o}C to 40 ^{o}C at a rate of 1 ^{o}C every 15 minutes, then from 40 ^{o}C to 25 ^{o}C at a rate of 1 ^{o}C every 10 minutes, and finally kept at 4 ^{o}C. Following annealing, the origami frame was washed with 1×TAE/Mg^{2+} buffer three times and passed through a 100 kD MWCO Microcon centrifugal filter device (Amicon, catalog number: UFC510096) to remove the excess helper strands.

Each DNA DX tile was assembled by mixing all the strands in the tile in an equal molar ratio (1 mM) in 100 µL 1×TAE/Mg^{2+} buffer. The solution was annealed in a PCR thermocycler with the temperature decreased from 90 ^{o}C to 25 ^{o}C at a rate of 4 ^{o}C every 5 minutes, and then kept at 25 ^{o}C.

The DNA origami frame – DX tile 2D array hybrid was assembled by mixing 1 pmol of purified DNA origami frame (100 µL, 10 nM) with the solutions of the four DX tiles. The amount of each tile was 100 pmol (100 µL, 1 mM). The final 500 µL solution was incubated at 25 ^{o}C overnight. Then the mixture was concentrated to 100 µL using a 100 kD MWCO Amicon centrifugal filter device.

S4.1.3. Agarose Gel Electrophoresis Purification. The assembled frame-array hybrid was loaded onto an agarose gel (0.3% agarose containing 0.5 µg/mL ethidium bromide, 1×TAE/Mg^{2+} buffer) and subjected to gel electrophoresis at 80 volts for one hour on an ice-water bath. The product band was excised from the gel and shredded. The shredded gel blocks were transferred into a Freeze 'N Squeeze DNA Gel Extraction Spin Column (Bio-Rad, catalog number: 732-6165) and centrifuged to recover the buffer containing the purified product. The product was then stored at 4 ^{o}C and characterized by AFM.

S4.1.4 Monomeric Avidin Resin Purification. 100 µL Monomeric Avidin Resin (Thermo Scientific, catalog number: 53146) suspension was transferred into a SigmaPrep^{TM} spin column (Sigma, catalog number: SC1000). The resin was washed with 1×PBS buffer once (Sigma, catalog number: P4417), then washed with 2 mM biotin solution to block the non-reversible binding sites, and finally regenerated with glycine solution. The resin and biotin modified DNA origami frame – 2D array hybrid were mixed and incubated for 30 minutes. The resin bound with the frame-array hybrid was then washed with 1×PBS buffer to remove the free 2D array and DX tiles. The purified frame-array hybrid was then displaced from the resin with 100 µL biotin (2 mM) solution. The solution containing the purified product was then stored at 4 ^{o}C and subjected to AFM characterization.

S4.1.5 AFM Imaging. The AFM imaging was performed using a Dimension FastScan AFM (Bruker). The samples (2 µL to 5 µL) were deposited onto freshly cleaved mica (Ted Pella, Inc.) and left to adsorb for 2 min. Buffer (1×TAE/Mg^{2+}, 100 µL) was added on top of the sample and the sample was imaged in ScanAsyst in Fluid mode, using ScanAssyst Fluid+ probes (Bruker).

S4.1.6 Fluorescence Kinetics. The fluorescence kinetics experiments were performed using a Nanolog fluorometer (Horiba Jobin Yvon). The origami frame was purified with 100 kD MWCO Microcon centrifugal filter devices (Amicon, catalog number: UFC510096) to remove excess helper strands. The concentration of the origami stock solution was 10 nM. The concentration of each tile stock solution was 1 μM. The sample chamber of the fluorometer was preset at 21 ^{o}C. 2.4 μL of Tile C solution (labeled with Fluorescein), and 2.4 μL of Tile D solution were added to a 120 μL quartz fluorescence cuvette. 1×TAE/Mg^{2+} buffer was added to make the final volume 120 μL. To the reaction with tile/origami at a molar ratio of 100:1, 2.4 μL the purified origami solution was added. To the reaction with tile/origami at a molar ratio of 100:2 or 100:3, the volume of the origami stock solution added was doubled or tripled. The sample was placed in the fluorometer and the time dependence of the intensity was monitored. Then 2.4 μL of Tile A solution (labeled with a black quencher) and 2.4 μL of Tile B solution were added to the cuvette and mixed well. The fluorescence intensity was measured once every 30 seconds, with an integration time of 10 seconds. The fluorescence intensities were first corrected for the volume difference, to a total volume of 124.8 μL after the addition of Tile A and B and then the data were corrected for photo bleaching using a control with the same concentration of Tile C and Tile A.

S4.1.7 Fluorescence Data. For each reaction, the first trace is the original data collected by the fluorometer. The second trace is the data after correcting for the volume change. The third trace is the data after correcting for photo bleaching. The fourth trace is the data after normalization, which was used to generate the plots shown in Figure 4.4C and Figure S4.11B.

S4.2 Design of the DX Tiles

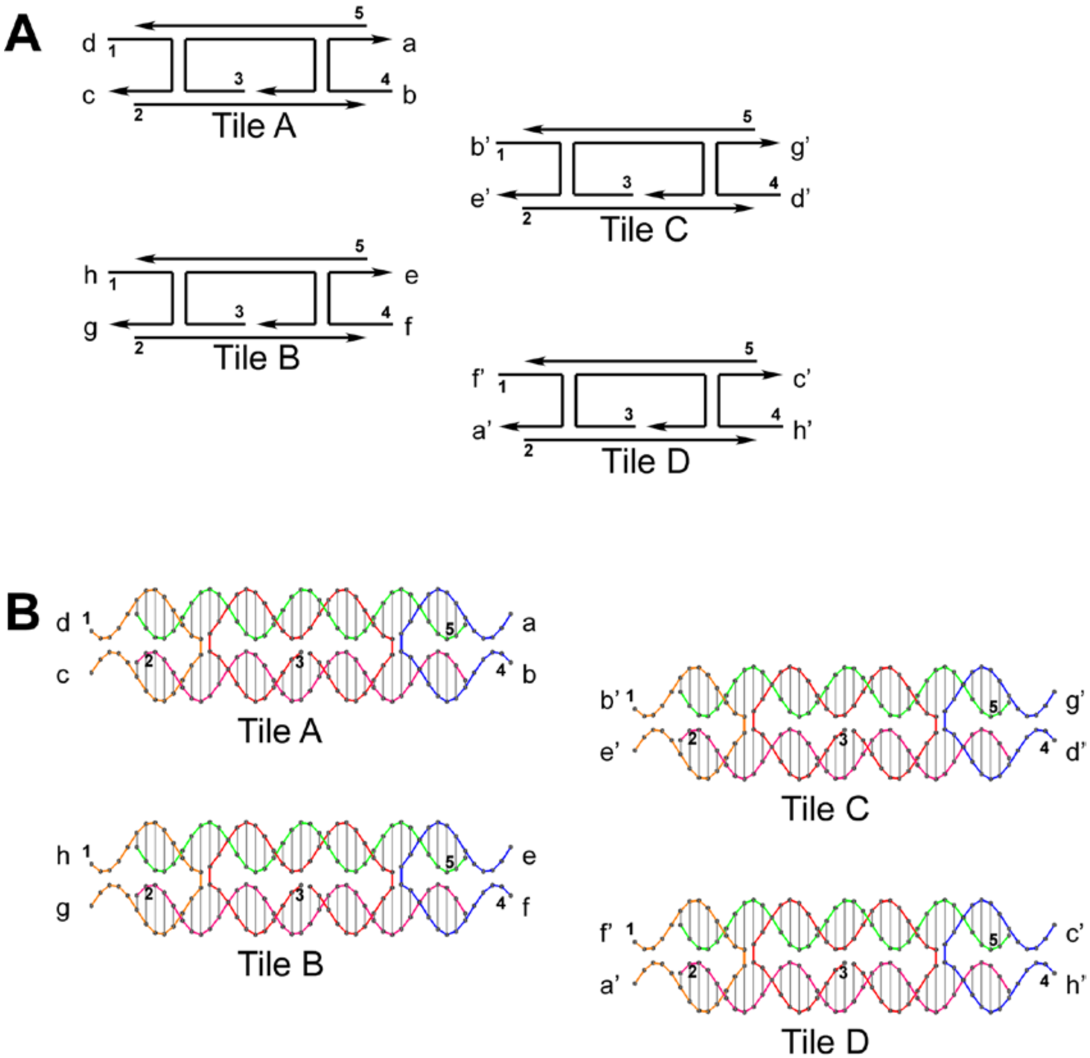

Figure S1. The design of the four DX tiles. **(A)** Schematic design of the four tiles. The four tiles share the same sequences of Strands 2, 3, and 5. Each tile has a specific Strand 1 and 4. The sticky end pairing e.g. a, a' are marked for each tile. **(B)** The detailed design of the four tiles. Each tile is four helical turns long. Strand 3 is 42 nts long. Strands 2 and 5 are both 37 nts long. Strands 1 and 4 are both 26 nts long.

S4.3 PAGE Characterization of DX Tiles

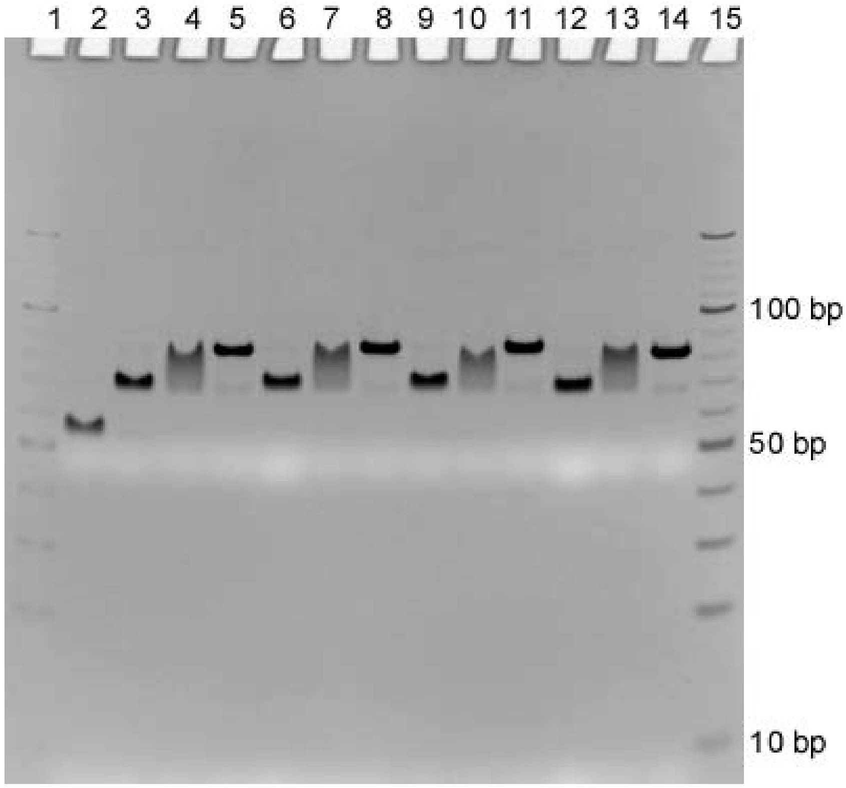

Figure S2. Native polyacrylamide gel electrophoresis characterization of the formation of the four tiles. **Lanes 1 & 15:** 10 bp DNA marker. **Lane 2:** the core structure of the four tiles: Strand A2 + Strand A3 + Strand A5. (For Tile B, C, and D, the core structures all have the same sequences as Tile A). **Lane 3:** core + Strand A1. **Lane 4:** core + Strand A4. **Lane 5:** full Tile A (core + Strand A1 + Strand A4). **Lane 6-8:** the same combinations as Lanes 3-5 for Tile B. **Lane 9-11:** the same combinations as Lanes 3-5 for Tile C. **Lane 12-14:** the same combinations as Lanes 3-5 for Tile D.

S4.4 Design of the DNA Origami Frame

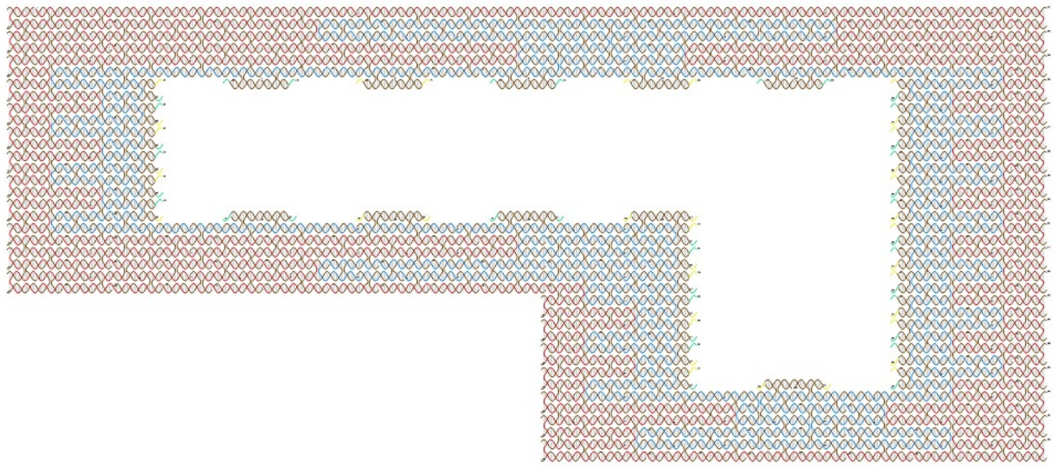

Figure S3. Detailed design of the DNA origami frame. The origami frame is 210 nm wide, 60 nm and 95 nm tall (the two sides). The blue strand represents the phi X 174 scaffold and the red strand corresponds to the M13mp18 scaffold. The interior is decorated with sticky ends complementary to the sticky ends on Tiles A and B. At the outer ends of each helix, two extra thymine bases are added to prevent π-π stacking between origami.

S4.5 AFM Image of Empty Origami Frame

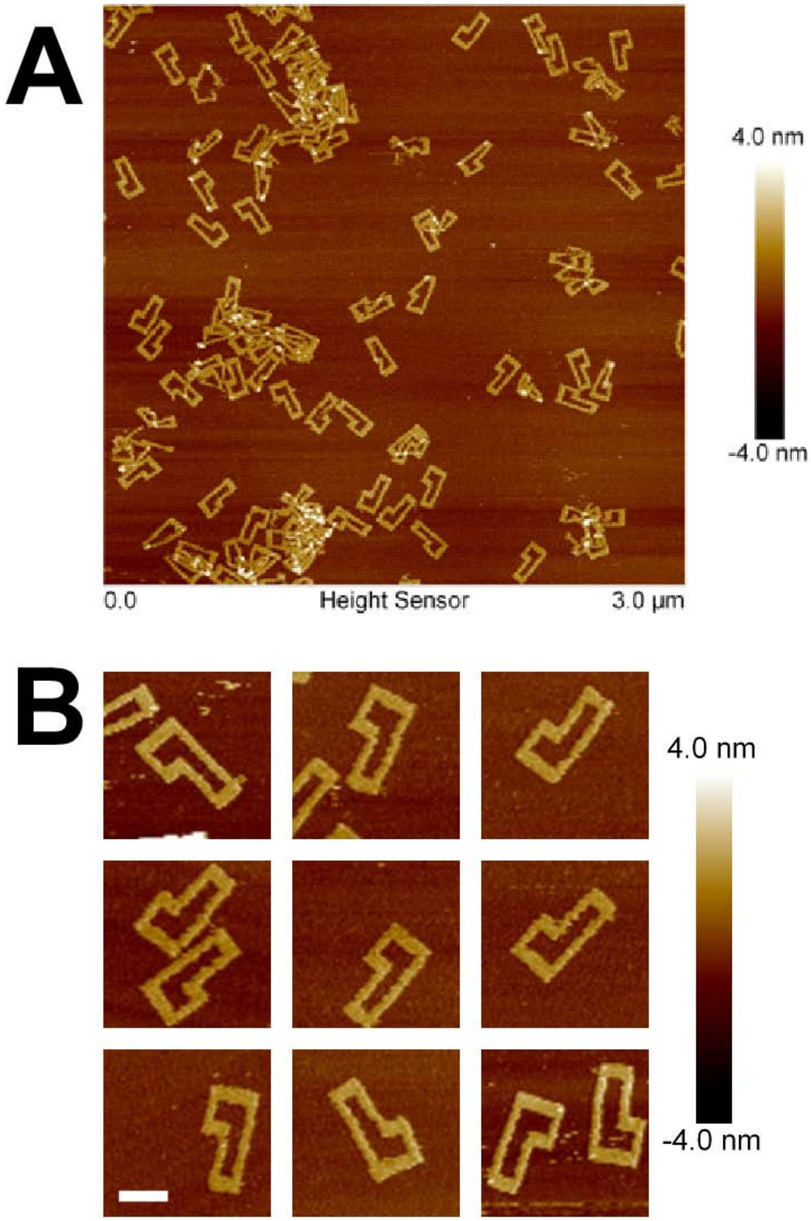

Figure S4. AFM image of the empty origami frame. (A) Zoom-out AFM image of the empty origami frame. Most of the origami frames are well formed. There are several aggregated structures in the image that may be caused by crosslinking of multiple scaffold strands. (B) Zoom-in AFM image of selected well-formed empty origami frame. The scale bar is 100 nm.

S4.6 Examination of the spontaneous formation of the DX tile arrays

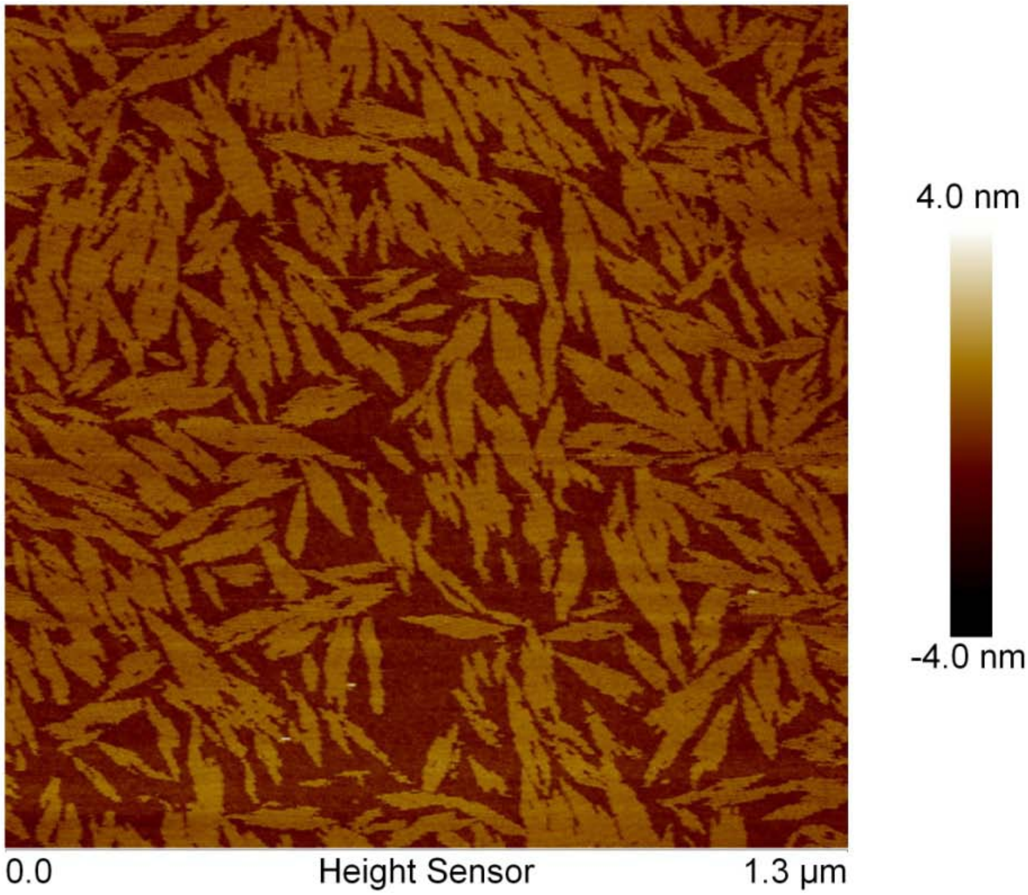

Figure S5. Unregulated growth of 2D arrays of DX tiles. The four DX tiles were mixed together to a final concentration of 250 nM each. The mixture was incubated at 25 ^{o}C overnight and characterized by AFM. The four tiles form 2D arrays as designed.

S4.7 Agarose Gel Image of the Purification of the DNA Origami Frame – 2D Array Hybrid

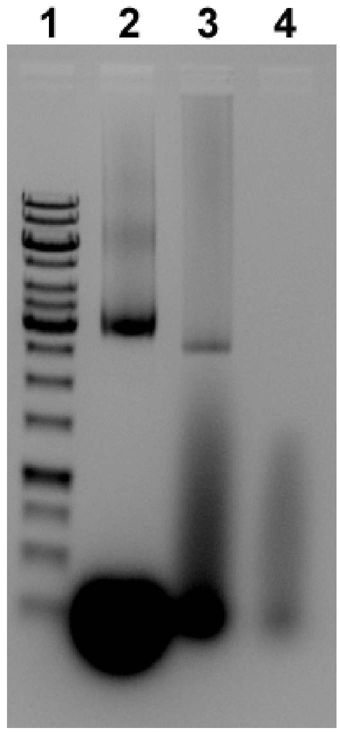

Figure S6. Image of agarose gel electrophoresis showing the purification of the origami-2D array hybrid. **Lane 1:** 1kb DNA ladder. **Lane 2:** Empty origami frame without purification. The fastest intense band corresponds to the extra helper strands. The second fastest band corresponds to the empty origami frame. Upper faint bands are aggregated structures (see Figure S4). **Lane 3:** Origami frame and the four tiles incubated overnight at r.t. The faster band and the smear after it correspond to uncontrolled 2D tile-array of various sizes. The slower band corresponds to the origami-array hybrid, which runs faster than the empty origami frame in Lane 2, because once the frame is fully filled, the structure gets more solid. **Lane 4:** The four tiles incubated overnight at r.t. without the origami frame. The band and smear correspond to uncontrolled 2D tile-array of various sizes.

S4.8 AFM Image of DNA Origami Frame – 2D Array Hybrid Purified by Agarose Gel Electrophoresis

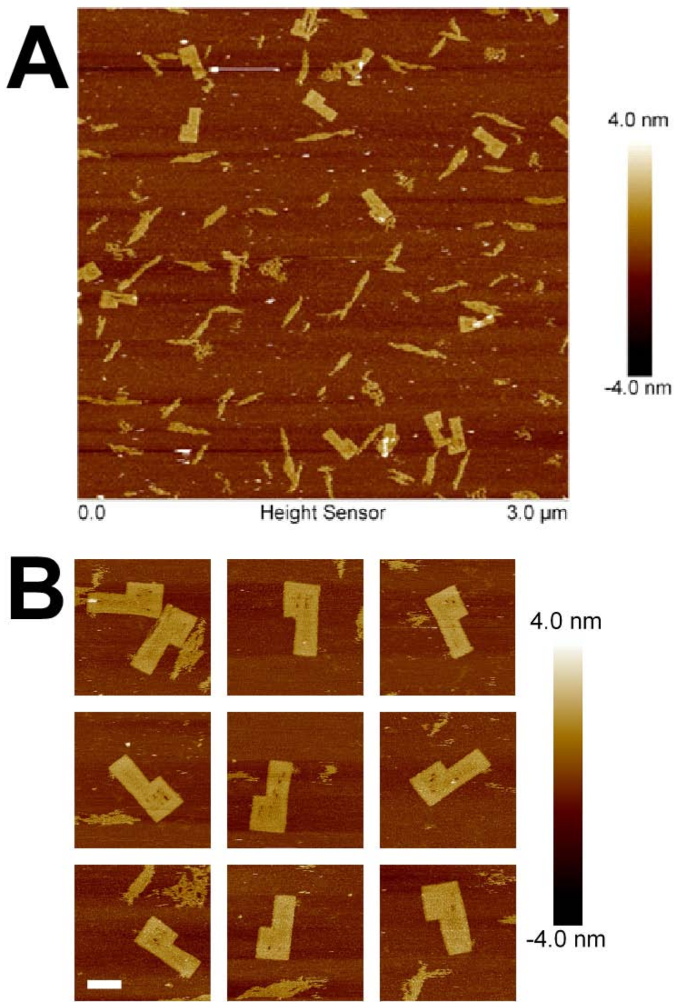

Figure S7. AFM image of Frame-array hybrid purified by agarose gel electrophoresis. (A) Zoom-out AFM image of Frame-array hybrid purified by agarose gel electrophoresis. There were quite a few pieces of free 2D array of DX tiles that were not cleanly removed. Note that these 2D arrays had similar sizes as the frame-array hybrid, which mostly showed a filled interior. (B) Zoom-in AFM image of selected Frame-array hybrid purified by agarose gel electrophoresis. The scale bar is 100 nm.

S4.9 Boitin Modified DNA Origami Frame – 2D Array Hybrid Purified with Monomeric Avidin Resin

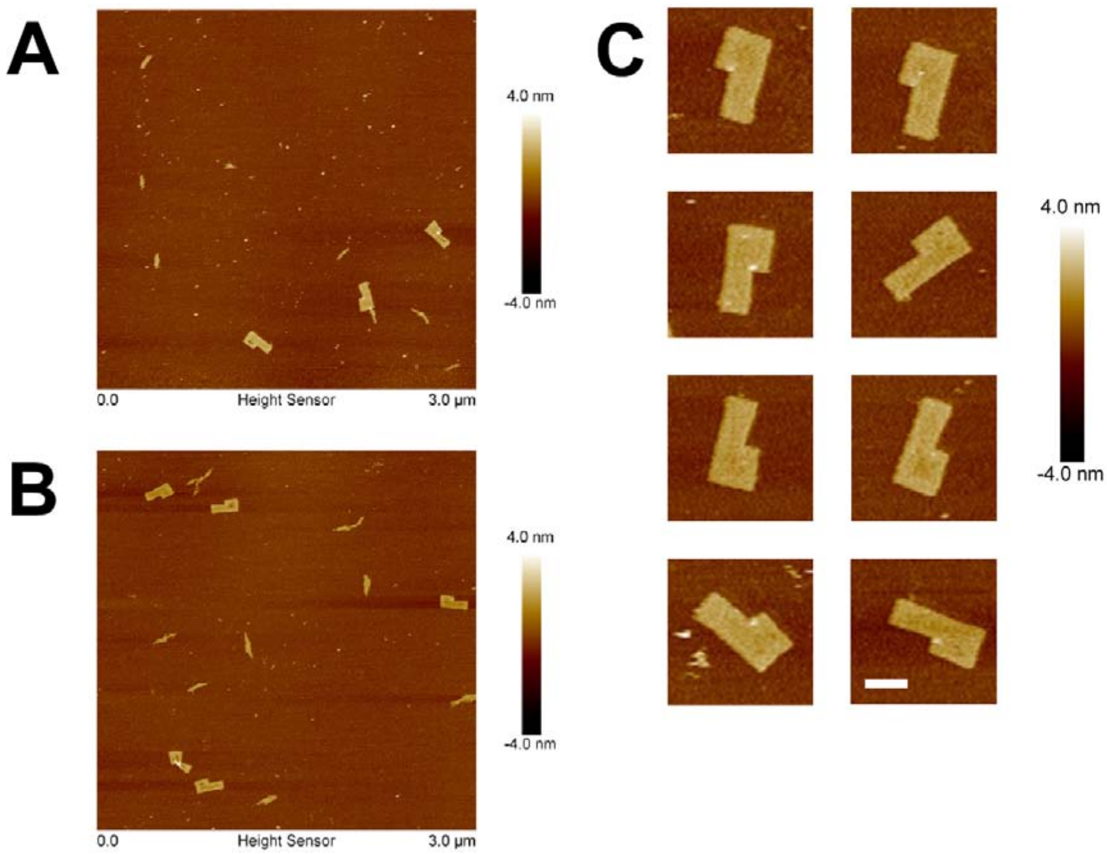

Figure S8. AFM images of Boitin modified frame-array hybrid after purification with monomeric avidin resin. The origami frame was modified with biotin. When purifying with monomeric avidin resin, unmodified tiles and 2D arrays were washed away while the boitin modified frame-array hybrids were bound to the resin. The purified product was then washed off with excess biotin solution. (A) & (B) The AFM images show that using this purification method, fewer free 2D array residues remained. (C) Zoom-in AFM image of selected Frame-array hybrid purified with monomeric avidin resin. The scale bar is 100 nm.

S4.10 DNA Origami Frame – 2D Array Hybrid Before Purification

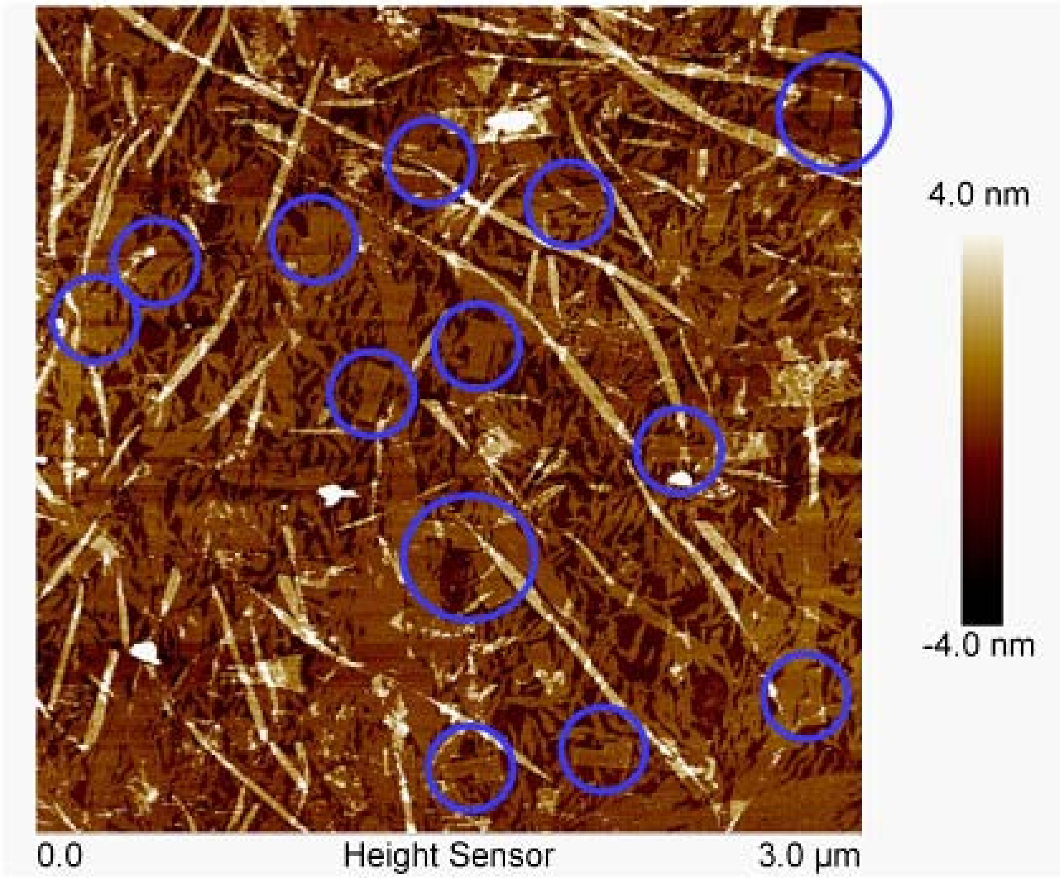

Figure S9. AFM image of unpurified frame-array hybrid. Several, but not all of, distinguishable frame-array hybrid structures are marked in the image.

S4.11 Defects of DNA Origami Frame – 2D Array Hybrid

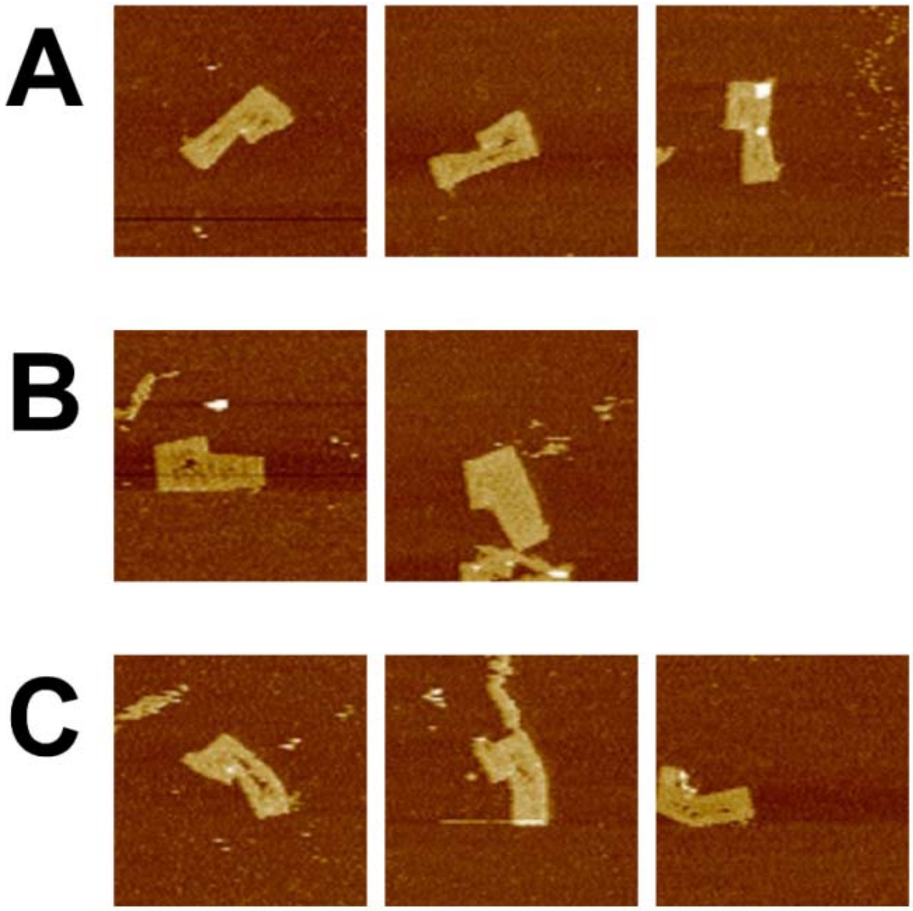

Figure S10. Three major classes of defects in the frame-array hybrids. **(A)** The shrunken frame-array hybrid caused by sticky ends on tiles hybridizing with another row of non-neighboring tiles. **(B)** The widened frame-array hybrid caused by inserting one or two rows of tiles between neighboring rows. **(C)** The bent frame-array hybrid caused by association of sticky ends between non-neighboring columns of tiles. Each image in the figure is 610 nm × 610 nm.

S4.12 Dynamics of the Nucleation of DX Tiles in the Origami Frame

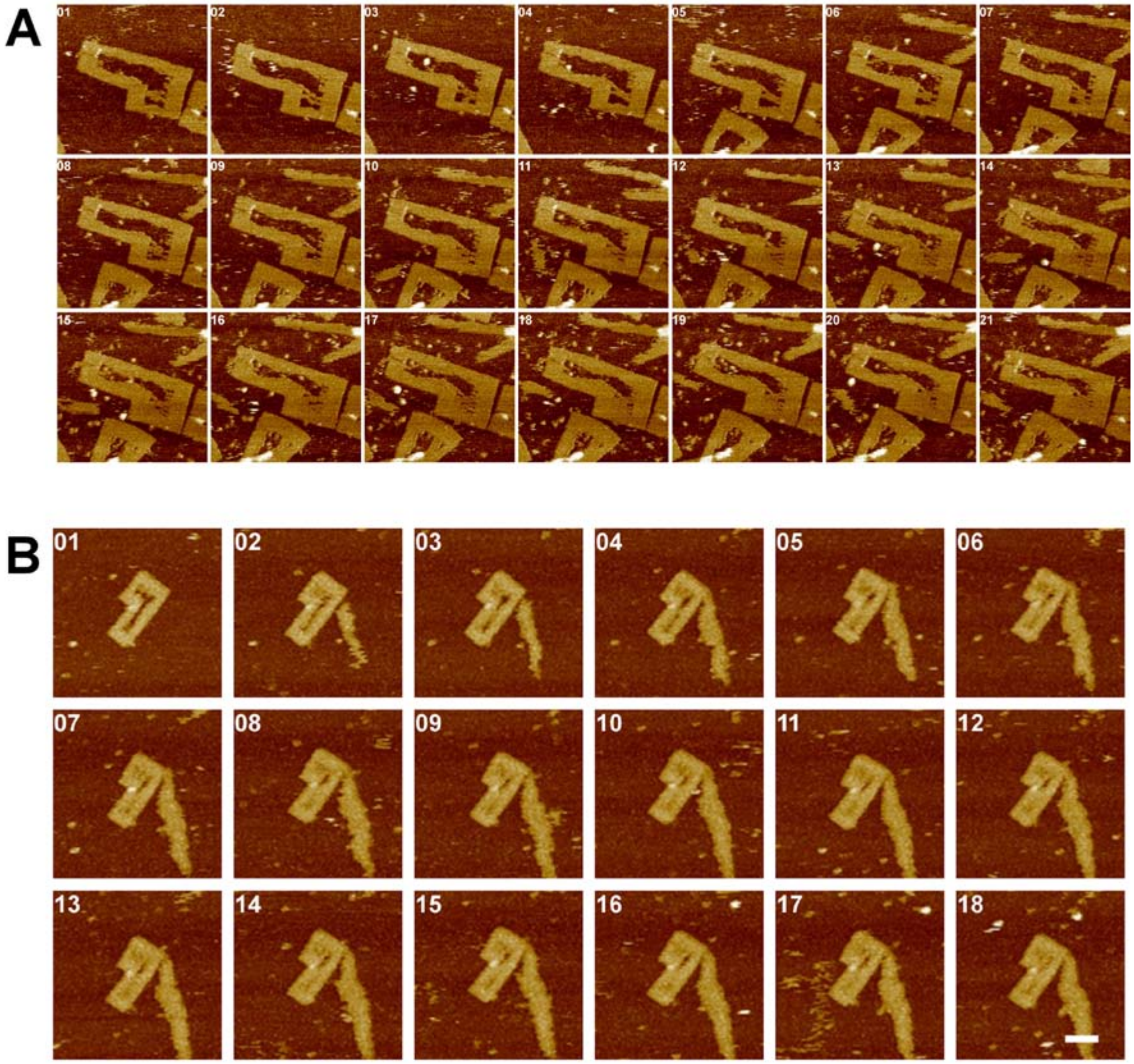

Figure S11. FS-AFM images showing the dynamics of nucleation and growth of DX tiles into the DNA origami frame. (A) This is another example of the experiment shown in Figure 3. Each frame was collected over 87 seconds. Each frame is 287 nm × 287 nm. (B) The full set of images in Figure 3. Each frame was collected over 87 seconds. The scale bar is 100 nm.

S4.13 Kinetics of the Nucleation Process of the Four Tiles

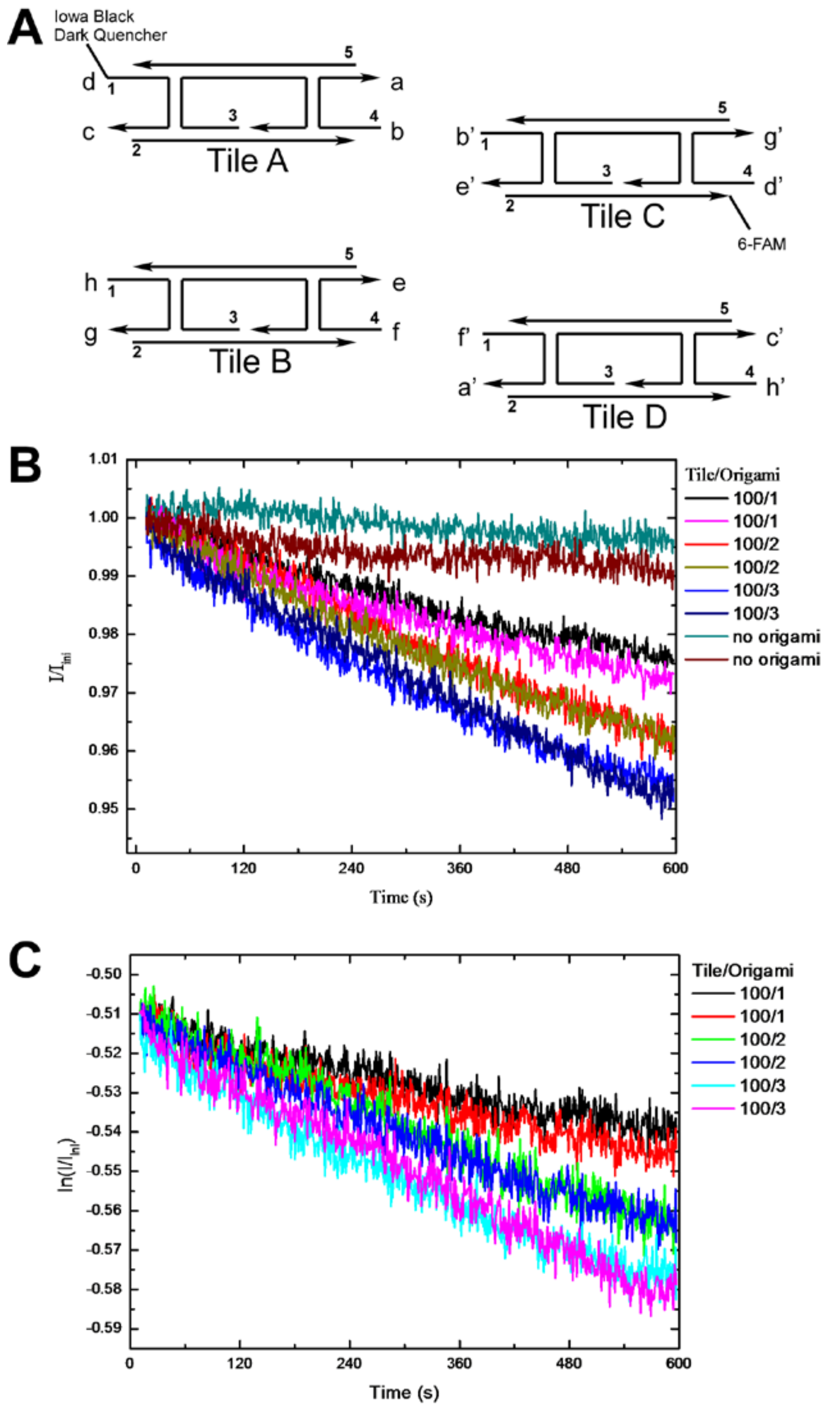

Figure S12. Characterization of the kinetics of the nucleation process. **(A)** The modification of the tiles with a fluorophore and dark quencher. The 5' end of Strand A1 was modified with an Iowa Black Dark Quencher. The 3' end of Strand C2 was modified with 6-FAM. Upon sticky end association in the tile array formation, the fluorophore and the quencher are brought into close proximity and fluorescence quenching is expected. **(B)** Normalized fluorescence decrease. The concentration of each of the tiles was 20 nM in all experiments. The legend indicates the molar ratio between the tiles and the origami frame. Each experiment was conducted in duplicate, the data of which coincided with each other. All curves shown are after correction for photo-bleaching. **(C)** Logarithm of the data in Panel B to the base e. The average of the curves of the reactions without origami seed in Panel B are subtracted from all other curves. Then $\ln(I/I_{ini})$ is plotted against time. The data are then fit by Equation 5 in the main text.

S4.14 DNA Sequences

Sequences of tile strands:

A1: AGGAACCATGAACCCTGCAGCATGTC

A2: GCTGCAGGCGGAATCCGACCCTGTGGCGTTGCACCAT

A3: GTCGGATTCCGCTGGCTTGCCTAGAGTCACCAACGCCACAGG

A4: ACTCAATGGTGCACTAAACCTCTAAG

A5: AGGTTTAGTGGTGACTCTAGGCAAGCCAGGTTCATGG

B1: GTGATCCATGAACCCTGCAGCAGAAC

B2=A2

B3=A3

B4: TAACGATGGTGCACTAAACCTAAGCT

B5=A5

C1: TGAGTCCATGAACCCTGCAGCAGCTT

C2=A2

C3=A3

C4: TTCCTATGGTGCACTAAACCTGTTCT

C5=A5

D1: CGTTACCATGAACCCTGCAGCCTTAG

D2=A2

D3=A3

D4: ATCACATGGTGCACTAAACCTGACAT

D5=A5

Sequences of the helper strands and sticky end strands in the DNA origami frame:

Helper 1

GTATTAACTCACTTGCCTGAGTAGACCGTTGTAGCAATACTTCTTTGATTTT

Helper 2 AGAGTCTGTCCATCACGCAAATTAAAGAACTC

Helper 3 CAGCAGAAGGCCTTGCTGGTAATACGAGTAAA

Helper 4 AAACCGTCTATCAGTGAGGCCACTCCAGAA

Helper 5 ACATCGCCCCGCCAGCCATTGCAAAGGGCGAA

Helper 6 AAAGAACGTGGACTCCAACGTCAACAGGAAAA

Helper 7 TAGTCTTTGGAAATACCTACATTTCCACTATT

Helper 8 TTGTTCCAGTTTGGAACAAGAGTTGACGCT

Helper 9 CGTGGCACTGAAATGGATTATTTAGTTGAGTG

Helper 10 ATCAAAAGAATAGCCCGAGATAGGCATTGGCA

Helper 11 TAGAACCCAGTCACACGACCAGTACCTTATAA

Helper 12

CCTGTTTGATGGTGGTTCCGAAATCGGCAAAATCATAAAAGGGAAAAATTTT

Helper 13 GTCAACCCCGGCGTTATAACCTCAGCGAAAAT

Helper 14 TCCACGCTGGTTTGCCCCAGCAGCACTCAA

Helper 15 CCTAAGCACACGAAGTCATGATTGGCAAGCGG

Helper 16 CCGCCTGGCCCTGAGAGAGTTGCAAATCGCGA

Helper 17 CGAGAAATCAGATTGCGATAAACGGCCCTTCA

Helper 18 AGTGAGACGGGCAACAGCTGATTGTCACAT

Helper 19 CAGCTTATACCTGACTATTCCACTTTTTCACC

Helper 20

GCGGTTTGCGTATTGGGCGCCAGGGTGGTTTTTCGCAACAACTGAACGGACT

Helper 21 TAAAACAGTGGTCATAATCATGGTGGGGAGAG

Helper 22 GCATTAATGAATCGGCCAACGCGCGGCGAATA

Helper 23 TTAGTAATAACAACCGCCTGCATT

Helper 24 AAACTATCGATAAAACAGAGGTGAAAATGAAA

Helper 25 CAATATTAATTAAAAATACCGAACCTCAAA

Helper 26 ACGCTCATAATGCGCGAACTGATAGTCAGTTG

Helper 27 CAATCGTCAGACAATATTTTTGAGAGGAAG

Helper 28 GATTCACCTTCTGACCTGAAAGCGACTAACAA

Helper 29

TACCGCTTCTCAGCGGCAAAAATTCATTCTGGCCATAATACATTTGAGGATT

Helper 30 TCTTTTATGAAAACCTACCGCGCATTCGAC

Helper 31 GTGGTCGGAAAAGTCTGAAACATGAACGTTAT

Helper 32 TAAATTTACAGAAAAAAAGTTTGTATCATT

Helper 33

GGAAACACGTGCCGAAGAAGCTGGAGTAACAGAATGCAATGAAGAAAACCA

C

Helper 34 AGTACGCGTGACGATGTAGCTTTATATCAAAA

Helper 35 AAGATGATGCTGAGAGCCAGCAGCGGCGGTCA

Helper 36 CGAATTATGCATCACCTTGCTGAACGAACCAC

Helper 37 TTGAATACCCTCAATCAATATCTGGCCCTAAA

Helper 38 GGGAGAAAACAGTTGAAAGGAATTATGGCTAT

Helper 39

GTTAACCATTTTACGGAACGTCAGATGAATATAAATATCTTTAGGAGCTAAG

AATA

Helper 40 GAAATTGCTTAGAGCCGTCAATAGAACAGAGA

Helper 41 ACCTACCATTAGACTTTACAAACATTCGCTTG

Helper 42 TGGCAATTAAAGTTTGAGTAACATAATTATGG

Helper 43

GCCAGAGTGCGTATCAAGGAGCGGAATTATCACAAAGAAACCACCAGAGTG

AGAAC

Helper 44 ATAGCCAGGCATTAACCGTCAAACGGTGTCTG

Helper 45 TTACAGTGCCACGAAACAAACATT

Helper 46 AATCTAAATCATTTCAATTACCTGTTAAGTGG

Helper 47 TATCAAACCAAGTTACAAAATCGAACCTGA

Helper 48 GCAAATCACAATAACGGATTCGCCTTAGTAGC

Helper 49 GTTATCTAACAGTAACAGTACCTACCAACA

Helper 50

CTAATAGAGTAGATTTTCAGGTTTGGAAGGACGTCAATAGTCGGACAAGC

Helper 51

TAGAAGTATATCAAAATTATTTGCACGTAAAACAGGTATAATAACCACCATC

Helper 52 TAATTTTACATCAATATAATCCTGGAAGAAGA

Helper 53 TTGCGGAATCATATTCCTGATTAAAATTTA

Helper 54

CATTACCAGGCGTTGACAGATGTATCCATCTGAAGCACCAACAGAAACAACC

TAGAGGAC

Helper 55 TATAACGTCGTTTGGTCAGTTCCAGCGCATGA

Helper 56 CATTTGAAAAAATTAATTACATTTAGCAAAAG

Helper 57 AGCACCAAAAATAATCTCTTTAATCGCAGAGG

Helper 58 GGTAAAGTTAGACCAAACCATGAATTTACATC

Helper 59 ATGGCGACCATTCAAAGGATAAACGGGTTAGA

Helper 60 CTCAAAGCGAACCAAACAGGCAAATCAGATGA

Helper 61 TTTCAAGAAAACTTACCTTTTTTT

Helper 62 CTGGAGACACATAAATCACCTCACTATGTGAG

Helper 63 TTCAGCGAGCAGAAGCAATACCGGCCTCCA

Helper 64 AGATGGCGTTGAGGCAGTCGGGAGGGTAGTCGGGATCGGAGG

Helper 65 CAAGTAAAGGACGGTTGTCAGCGTAAAACTGG

Helper 66 TAGCGATAAGTACATAAATCAATAAACAATTT

Helper 67 TAATTAATCTTGCTTCTGTAAATCCCAGCAAT

Helper 68 TTTAATGGAAACGCTTAGATTATT

Helper 69 TGAATAACTTTCCCTTAGAATCCTAATACCAG

Helper 70 AACAATTTGGCGGCTTTTTGACCTATCGGT

Helper 71 AATCATAGAAGAGTCAATAGTGAATGAAAACA

Helper 72 ATTAGAGCATGCCTACAGTATTGTGTCGCTAT

Helper 73 TTAGACGCTGAGGTCTGAGAGATT

Helper 74 CATCACCCCTTGAATGGCAGATTTTGGGTTAT

Helper 75	AGCAAGCAGCGGCCTCATCAGGGACCAGCT
Helper 76	AAATATATAACCTCCGGCTTAGGTTTTATCAA
Helper 77	TCGCAAGAATGTAAATGCTGATGCTTAGGAAC
Helper 78	TTCTACCTTTTTTTTAGTTAATTT
Helper 79	ATAACTATCAAAGAACGCGAGAAACTTGCCAC
Helper 80	TTAGCCATTTCAAGAAGTCCTTTTATCAGA
Helper 81	ACCGACCGGACCTAAATTTAATGGACTTTTTC
Helper 82	ATCCTTTCACCAAATCAAGCAACTAAATCCAA
Helper 83	TTTTCATCTTCTTGTGATAAATTT
Helper 84	CAAGTCCACTTTATCAGCGGCAGAGAATCATA
Helper 85	AACGGCAGGCAGCAGCAAGATAAAGCACCA
Helper 86	CGCTCAACATAAGAATAAACACCGTTTGAAAT
Helper 87	CGTTATACAAAAAGCCTGTTTAGTTCACGAGT
Helper 88	TTAAGGCGTTAAAGTAGGGCTTTT
Helper 89	ATTACTAGAAATTCTTACCAGTATCTCTTTCT
Helper 90	GCACGCTCAGCAGAGGAAGCATCGCTCTTT
Helper 91	GTAATTTACGCCATATTTAACAACAAAGCCAA
Helper 92	AGTCTCATAGTTGCATTTTAGTAAATCATATG
Helper 93	TTAATTGAGAATGGCAGAGGCATT
Helper 94	GATTGTCCTTTGCATCTCGGCAATAAAGTACC
Helper 95	TTGATTCTTGAATGCCAGCAATCCAGACGA
Helper 96	ACTGAACAAGTAATAAGAGAATATGCCAACAT
Helper 97	AAAACAGGGTAAAGTAATTCTGTCTCTTTTTG

Helper 98 AAATAGCAAACAACATGTTCAGCTGCGTGAAG

Helper 99 ATATACCTGGTCTTTCGTATTCTGAATGCAGA

Helper 100 AGAAACGAGTTTATCAACAATAGATTTTGTGC

Helper 101 AACAGCCAAAAAATAATATCCCATAGACTCGGCGATGCT

Helper 102 CGGATCTGAATACGCAACGCGAGCAGTCCTAATTT

Helper 103

AATCTCGGAAACCTGCTGTTGCTTGGAAAGATTGAATCGGCTGTCTTTCCTT

Helper 104 GCTACAATAAGAACGGGTATTAAATGGCGCAT

Helper 105 TTCGCTCATCTCAGCCGTTTGAGCTTGAGTAACTCCGACGAC

Helper 106 TTTGATTTGGTCATTGGTAAAATACCGTTTTT

Helper 107 AACCTCCCCGTAGGAATCATTACCGTCATTTC

Helper 108 CGGTATTCCAAATCAGATATAGAAAACTACCAGATGCAA

Helper 109 GCATCCTTGGTTCTGCGTTTGCTGATGTATTTCCTAGACAAATTA

Helper 110 AACATACAACCATCAGCTTTACCGAATATGAG

Helper 111 AGAAATATCCTTTGCAGTAGCGCCTCTTTCCA

Helper 112 TTTTTTCGAGCCCCCTGAACAATT

Helper 113 GACAAAAGGAAGCGCATTAGACGGTCAGAGAG

Helper 114 CGACAATAGCCTTTACAGAGAGACCCAATA

Helper 115 ACGCGCCTTTTTTTGTTTAACGTCGCAATAGC

Helper 116 TGAACAAGTATTATTTATCCCAAAAAAGTA

Helper 117 ACGAGCATGCCTAATTTGCCAGTTAGAAGGAA

Helper 118

ATCATTCCTTTATCCTGAATCTTACCAACGCTAAAATACCCAAACAAACTCA

Helper 119 ATTTTCATGACTTGCGGGAGGTTTACTCAACG

Helper 120 ATAGCAAGTAAGAACGCGAGGCGTCTTCCA

Helper 121

GAGCCAATATTGGGAGGGTGTCAATCCTGACGGTGCTTATGGAAGCCAAGCA

Helper 122 GAAATTGTGCCTCCAAGATTTGGATGCCACAA

Helper 123 TCAACCGATAATTGAGCGCTAATAGAGAATTA

Helper 124 GTTTACCACAAGAATTGAGTTAAGATAACATA

Helper 125 ATTTTGTCAAGAAACAATGAAATAAAAAATGA

Helper 126 AAAGAAACCGAAGCCCTTTTTAAGTCCAAATA

Helper 127 GAAAATACGCCGAACAAAGTTACCACAAAATA

Helper 128 ACTCCTTAAACGCAATAATAACGGCGAGCGTC

Helper 129 CCATTAACGTCAGAAGCAGCCTTATGCACCCA

Helper 130 GGGAGCACATATCACCATTATCGATGAAGCCT

Helper 131 GGTGGTCTACGAAAAGACAGAATCTTTTAGCG

Helper 132 TCTAAAAAATGCGGTTATCCATCTGGCTTATC

Helper 133 GCAGCCAGTGAGAAAGAGTAGAAAGGCATGAA

Helper 134 TTAGTCAGAGGGTTGAGGGAGGTT

Helper 135 ATAACCCAGCGCCAAAGACAAAAGCATTAAAG

Helper 136 ATAAGAGCACAATCAATAGAAAAGAGCCAT

Helper 137 TATCTTACGCAAAGACACCACGGAACCAGTAG

Helper 138 AGCAGATAATACATAAAGGTGGCAAACGTC

Helper 139 ACCGAGGATTACGCAGTATGTTAGACCGTAAT

Helper 140

TCACGAACTTCTCAGTAACAGATAAGAACTGGCACTTTAGCGTCAGACTGTA

Helper 141 CAACATACATTGTAGCATTGTGCTCATAGC

Helper 142 CCCTGCATATAGTGTTATTAATATTTCATAAT

Helper 143 AGAGCTTGCCATTTTTCGTCCCCCACCGGA

Helper 144

TTGGGGATCTTGCGGCAAAACTGCGTAACCGTCTCTCAGAACCGCCACCCTC

Helper 145 GCCTCAATCGAATATCCTTAAGAGCTGAATAG

Helper 146 TTGAAGGTAAATATTGACGGAAATTATTGGCGACAT

Helper 147 GTGAATTATCACCGTCACCGACTTTTCATATG

Helper 148 TTGGGAATTAGAGCCAGCAAAATCATAAGTTT

Helper 149 CACCATTACCATTAGCAAGGCCGGAACATATA

Helper 150 ACCAATGAAACCATCGATAGCAGCCAAACGTA

Helper 151 CAGTAGCGACAGAATCAAGTTTGCTGATTAAG

Helper 152 GCGCGTTTTCATCGGCATTTTCGGCAATTCAT

Helper 153 CCCCTTATTAGCGTTTGCCATCTTCAAGTTGG

Helper 154 CAAAATCACCGGAACCAGAGCCACTTCGGGGC

Helper 155 ACCGCCTCCCTCAGAGCCGCCACCTCTCGTTC

Helper 156 CACCACCACACCCTCAGAGCCGCCGGCGTTCA

Helper 157 AGAGCCACGAGCCGCCGCTT

Helper 158 CAAAGCCTTTGCATTCATCAAACGTCAGACGA

Helper 159 AATTTACCAGGAGGTTGAGGCAGGACCAGAAC

Helper 160 TTCAGCATTGACGTTCCAGTAATT

Helper 161 TTGGCCTTCCAGAATGGAAAGCGCCTTGCGAC

Helper 162 ACTGGTAATGGCTTTTGATGATACAGTCTCTG

Helper 163 TTGCGTCATACATAAGTTTTAATT

Helper 164 CCTCGGCACGTGTGAATCATTAGCCCCGTATA

Helper 165 TTCGGGGTCAGTCTCAAGAGAATT

Helper 166 TGAGACTCGCCTTGAGTAACAGTGAGGAGTGT

Helper 167 GCGGATAATAGCGGGGTTTTGCTCTAAGAGGC

Helper 168 AACAGTTATGAAACATGAAAGTATGCTATTTA

Helper 169 TTGGATTAGGATGTGCCGTCGATT

Helper 170 ACTGGCGGGCCACGTATTTTGCAAATAGGTGT

Helper 171 GCGTAACGATAAGTATAGCCCGGAAGTACCAG

Helper 172 TTGAGGGTTGATATCTAAAGTTTT

Helper 173 ATCACCGTTTCCACAGACAGCCCTTGAATTTT

Helper 174 TAAAGGAATCCAGACGTTAGTAAACATAGTTA

Helper 175 TTTTGTCGTCTTTTGCGAATAATT

Helper 176 CTGTATGGGGAGTGAGAATAGAAAAAAAAAAG

Helper 177 TTTAATTTTTTCACGTTGAAAATCTCCAGGAACAAC

Helper 178 GCTCCAAAAGGAGCCTTTAATTGTTTTCAACA

Helper 179 AACAAGCGTTCTTGCAAATCACCATGCCAGCT

Helper 180 CTTTCCAGTCGGGAAACCTGTCGGAAGGCG

Helper 181 GAATCTCTATGAATGGGAAGCCTTACTGCCCG

Helper 182 ACTCACATTAATTGCGTTGCGCTCCAAGAAGG

Helper 183 ATAAGTCAAGGAGAAACATACGAAGTGAGCTA

Helper 184 GTAAAGCCTGGGGTGCCTAATGAGGCGCAT

Helper 185 CATACAAACACTGACCCTCAGCAACATAAAGT

Helper 186 TCCACACAACATACGAGCCGGAAGTCTTAAAC

Helper 187 CTTCATAGCGAATCACCAGAACGGCTCACAAT

Helper 188 TTCCTGTGTGAAATTGTTATCCGCGCCATT

Helper 189 CTGGTGCCAGGCTGCGCAACTGTTATAGCTGT

Helper 190

CCCGGGTACCGAGCTCGAATTCGTAATCATGGTCGGGAAGGGCGATCGGTGC

Helper 191 CCTCAGGATCGCTATTACGCCAGCAGAGGATC

Helper 192 CTTGCATGCCTGCAGGTCGACTCTTGGCGAAA

Helper 193 CTGCCAGTTGCTGCAAGGCGATTAGTGCCAAG

Helper 194 TTGTCACGACGTTGTAAAACGACGGCCAAGTTGGG

Helper 195 GTTCCTGATTAGTCGCAGTAGGCGCCATGC

Helper 196 TGATAAGCAAGCACCTTTAGCGTTGATTGTAT

Helper 197 AACGATACACAGGGTCGCCAGCATTAATAT

Helper 198 TTCTTAGAAAATTTCACGCGGCGGTTGTTAAA

Helper 199 CGCCATTCGGAAACCAGGCAAAGAACGCCA

Helper 200

GGGCCTCTAGATCGCACTCCAGCCAGCTTTCCGGTCCTGTAGCCAGCTTTCA

Helper 201 GGGGGATGTTGAGGGGACGACGACCAACCCGT

Helper 202 TAACGCCAATGGGCGCATCGTAACGGATTG

Helper 203 TTCGTTGGTGTAGGGGTTTTCCCATT

Helper 204 CCTAACGACAAGAGTAAACATAGTGGAAAACG

Helper 205 TCAGAAAAATTTAAATTGTAAACGATATCGGT

Helper 206

TGACCGCTATATAAGCTAAAACTAGCATGTCAAATTCGCATTAAATTTCAAGT

TGC

Helper 207 AAGAGAATTTTTTTAACCAATAGGAAAACATC

Helper 208 TCAGGTCAAATTCGCGTCTGGCCTCACCGCTT

Helper 209 TGCCGGAGAAATGTGAGCGAGTAAAGTATCGG

Helper 210 ATGATATTCCGTGGGAACAAACGGCCGTGCAT

Helper 211 AAGCAAATGCCCCAAAAACAGGAAAACATCAT

Helper 212 TTTGTTAAATCATATGTACCCCGGTTCTTG

Helper 213 TCAGCTCACGATGAACGGTAATCGAGCTTGCA

Helper 214 TCAAAAATTTGCCTGAGAGTCTGTAGAAGT

Helper 215 TCAACATTAGGGTAGCTATTTTTGAGAGATCTACCTCAGGAG

Helper 216 CGGATTCTCAACCGTTCTAGCTGAGCAACGGA

Helper 217 ACCGTAATGAGACAGTCAAATCAATGTGTA

Helper 218 TTGAGAAAGGCCGGGGATAGGTCATT

Helper 219 GGTAACGCTGCATGAAGTAATCACGTTGATAA

Helper 220 CGTCATTTGGCGAGAAAGCTCAGTAAAGGCTA

Helper 221 CGGCGCTTTGTTTTTGAGATGGCATAAATTAA

Helper 222 TTAGGGTTCGAGCATCATCTTGATCCATCAAT

Helper 223 CCTACTGATCGGAGGTTTTACCTCCAAATGAATGGACAGCCA

Helper 224 GACCCATAACCGTGCTCA

Helper 225 AACCATAAAGCCTCGGTACGGTCATACTTTTG

Helper 226	GGTAAAGATGCAATGCCTGAGTAAAGGATA
Helper 227	TTTATATTTTAAATTCAAAAGGGTTT
Helper 228	TTAGGGATTTCAAATAACCCTGAAGGCATCCA
Helper 229	ACCAAAAAGCCTTTATTTCAACGCTAAGCTCA
Helper 230	CGGGAGAACATTATGACCCTGTAAGGCATGGT
Helper 231	AAAATTTTGAGCATAAAGCTAAAAGGCAAA
Helper 232	TTATAAAGCCTCATAGAACCCTCATT
Helper 233	AATCCACTTCGTGCCAAGAAAAGCACAAATGC
Helper 234	GGAGTGGCCCAGTAGTGTTAACAGTCGGTTGT
Helper 235	CAATATAAATTAACACCATCCTTCATTTTCAT
Helper 236	GAATTAGCTAAATCATACAGGCACATCAAT
Helper 237	TTTTAACATCCAAAAAATTAAGCATT
Helper 238	TCTACAGTTGAGGGACATAAAAAGATGAACTT
Helper 239	ATGGTCAACGAGCTGAAAAGGTGGTCGGGAGA
Helper 240	TTGGGGCGTAACCTGTTTAGCTATACGGAGAG
Helper 241	TCTACTAATGACCATTAGATACAAGTTGAT
Helper 242	TTTAGATTTAGTTTAGTAGTAGCATT
Helper 243	ACGACCAAGACGCAATGGAGAAAGTAAAAATG
Helper 244	GCGATAACGCGTCCATCTCGAAGGTTTCGCAA
Helper 245	CGCCAACGCGGAGTAGTTGAAATGTAATTGCT
Helper 246	TCCCAATTTTCATTCCATATAACGTTTTAA
Helper 247	TTTGTCTGGAAGTCTGCGAACGAGTT
Helper 248	CGCTCGGCAGATGGGAAAGGTCATGTAATAAG

Helper 249	CATTTTTGTGCTGTAGCTCAACATAGTCGCCA
Helper 250	GAATATAACGGATGGCTTAGAGCTAAGGGGCC
Helper 251	ATATGCAAAATTGCTCCTTTTGAAGCAAAC
Helper 252	TTAGAGTACCTTTCTAAAGTACGGTT
Helper 253	TTTAGTACTAATTTATCCTCAAGTGCGGCATA
Helper 254	ACATACCATGCAATTAAAATTGTTTAAGAGGT
Helper 255	GAAGCCCCAAGACGAGCGCCTTTAGATTGCAT
Helper 256	TCCAACAGGCGAACCAGACCGGAAAGACTT
Helper 257	TTCGAGCTTCAAAGTCAGGATTAGTT
Helper 258	ATAAAAAATCCAAGTATCGGCAACACGACATT
Helper 259	CTGGCCAATCACAACCACACCAGAAGCAGCATAGCAATCATA
Helper 260	TTACCTTTCCAGGGCGAGCGCCAGCGCTTGCC
Helper 261	ACTATTATTTAAGAGGAAGCCCGAGACCACCT
Helper 262	CAAAAAGAAGTCAGAAGCAAAGCGCGCACGTT
Helper 263	CAAATATCTCAAAAATCAGGTCTTGCTTTA
Helper 264	TTATGACCATAAAGCGTTTTAATTTT
Helper 265	ACTCATCGAGCAGGTTTAAGAGCCAACGAACC
Helper 266	TCAGCGGCCGCACGTAATTTTTGAAACGTTTT
Helper 267	CTGCGCGTCGTCAGTAAGAACGTCTTACCCTG
Helper 268	GCTCAAAGACCTTTCTTTTTGGGTGGAGGC
Helper 269	TTCTTCTGACACGCAAGGTAAACGAGAGGGGG
Helper 270	AACAGTTCTGAATCCCCCTCAAATAGCGTC
Helper 271	TTTAAATATTCATAGAAAACGAGATT

Helper 272	CTGTCGCACTACGCGATTTCATAGGTAATTAT
Helper 273	CAGCGCCTCATTAATAATGTTTTCCGAACAAT
Helper 274	GGCTTTTGAAATGTTTAGACTGGAAGTGTTTC
Helper 275	CTCCAGCAATAAACCAACCATCATAATCGG
Helper 276	TAATAGTACAAAAGAAGTTTTGCCTGAACATA
Helper 277	CAATACTGCGATAAAAACCAAAAAAGAGCA
Helper 278	TTTTACCAGACGACGGAATCGTCATT
Helper 279	TGAGTTTCACCGCCACCCTCAGAAAGCGTCCT
Helper 280	CCACAACCAACCAGAACGTGAAAACCGCCACC
Helper 281	CAAGCCCACACCACCCTCATTTTCTCAACAGG
Helper 282	CATAGAAAGCCACTTCTCCTCATCGTGCCGATCCGTCTG
Helper 283	ACCAGAGTCGGCCAGTCCTTGACGAACCAACGCGT
Helper 284	AGAATCTCTACCATGAACAAAATGATGGCG
Helper 285	GCAAGGATCAAAGTAAGAGCTTCTTCAACAAG
Helper 286	CTCAGAGCATAGGAACCCATGTACGGAAGTAG
Helper 287	CTTTAAGCCCAACAGCCATATAAGTTCCAT
Helper 288	CAGTTTTTACTTTTTGTTAACGTAGCAAGGTC
Helper 289	AAAGGTCGAGGTCGAATTTTCTCCGTAAAC
Helper 290	TAAGGGAACCGAACAAGATAATTTTTCGACT
Helper 291	GTGAGCATTCTGAACAGCTTCTTGCGTAACAC
Helper 292	GGATTAAGTGGTTTTTAGTGAGTTAGGGATAG
Helper 293	GGCGTCGCTCCTAGACCTTTAGCATTTAGCCA
Helper 294	TTTTTGCGCCACTTCGATTTAATTATTTTCCG

Helper 295 GTAACTTTGTAATTCCTGCTTTATCGAGCTGC

Helper 296 CGACAGCTCACTCCGTGGACAGATTTCTTAAA

Helper 297 TCTTTAGCGTCGTAACCCAGCTTGACAATG

Helper 298 CATATCTGTTCTGCTTCAATATCTCCGATATA

Helper 299 AAGCAGTATCCCAGCCTCAATCTGTTAAAG

Helper 300

CATCAGAAAGCGATAAAACTCGCCGCCAAAACGTTCAGCAGCGAAAGACAG

C

Helper 301 TATCAGCTTGCTTTCGAGGTGAATTTGTCATT

Helper 302 CAGCTTGATACCGATAGTTGCGCCGGTAAGTT

Helper 303 ACAACAACCATCGCCCACGCATAAGGTTGAAC

Helper 304 TTCGGTCGCTGAGGCTTGCAGGGACATCTCTC

Helper 305 GCCGCTTTTGCGGGATCGTCACCCCGGCTACA

Helper 306 ATCGGAACGAGGGTAGCAACGGCTACTTCTGC

Helper 307 CATTAAAGGATATTCACAAACAAAGCATGAGC

Helper 308 TCGTCAGCATCATAAAACGCCTCCAATATC

Helper 309 GCAGTCGGGCAAGAACCATACGACTAAATCCT

Helper 310 ACGAAAATTCAGGCACACAAAAACGCATGG

Helper 311 TATTATTCATGCCCCCTGCCTATTTACTGATA

Helper 312 ACCATAAGCGATTGCGTACCCGACTCGGAACC

Helper 313 AAATGAAGCCGCATAAAGTGCACGACCAAA

Helper 314 ATTAGGGTCGAACTGCGATGGGCACCGCCA

Helper 315 CTGTAGCAACTCAGGAGGTTTAGTATACTGTA

Helper 316	CCCTCAGAGTCACCAGTACAAACGCGGCTC
Helper 317	GTTTCAGCGATTTTGCTAAACAACTACAACGC
Helper 318	ATTCTGATTTTCATCCCGAAGTTATCGGTT
Helper 319	AGCGTACCTTGAATGTTGACGGGACGTAAATT
Helper 320	GAGCAGGATGACGGCAGCAATAAATAGCGAGA
Helper 321	ATAAGCAAAAGCGAGGGTATCCCAAGAAAGAT
Helper 322	ACACTATCATTACGAGGCATAGTCACATTC
Helper 323	TTCGCCAAAAGGAATAACCCTCGTTT
Helper 324	TAGCAATCAGCGACGAGCACGAGACAAAGTCC
Helper 325	TAACGGAATGAGATTTAGGAATACCTCAACAG
Helper 326	TCATCAGTCAACATTATTACAGGTTCGGTTAA
Helper 327	AACTAATGAAATCTACGTTAATAAACTGGC
Helper 328	TTGTTGGGAAGAACAGATACATAATT
Helper 329	TGTTCAGTAAAATCGAAATCATCTGCGGTCAG
Helper 330	GGACTCAGACCTATTAGTGGTTGAGTACGGAT
Helper 331	ATCCAAAAAAAGCGGTCTGGAAACAAACACCA
Helper 332	TAGAGGCCCGGCAGAAGCCTGAATAAACGAAC
Helper 333	GTGAATAAAGTAAATTGGGCTTGAGAGCTTAA
Helper 334	TCATTATATTATGCGATTTTAAGGATGGTT
Helper 335	TTTGTGAATTACCCCAGTCAGGACTT
Helper 336	GAACGAGTGGCTTGCCCTGACGAGAGGCGCAT
Helper 337	TAATTTCAAACGTAACAAAGCTGTAATCTT
Helper 338	TTTTACCCAAATCACTTTAATCATTT

Helper 339 CGAGGCGCGAACGGTGTACAGACCACAGCATC

Helper 340 TCCGCGACTGACCTTCATCAAGAGCTCATTCA

Helper 341 AGGCTGGCCTGCTCCATGTTACTTAAAACACT

Helper 342 GACAAGAATCGCCTGATAAATTGCCAAGCG

Helper 343 TTGATTTGTATCACCGGATATTCATT

Helper 344 GTCATGGAATATCCGAAAGTGTTAAGCCGGAA

Helper 345 ACGAAAGAACCCCCAGCGATTATATGTCGAAA

Helper 346 CATCTTTGGGCAAAAGAATACACTACAGAGGC

Helper 347

CGAAACAACACTACGAAGGCACCGAGGAAGTTTCCATTAAACGGGTAAATT

Helper 348 TTATACGTAATGCAGTACAACGGATT

Helper 349 TTTGAGGACTAAAGACTTTTTCATAACCTAAA

Helper 350 CTTTGAAAGAGGACAGATAGACGGTCAATCA

Sticky End Left 1

ATCACGGCCGCTGCACCAGCAAGAAACCAATCCGCGGCATTGATTGCT

Sticky End Left 2

TTCCTACTGACGGATGCCACCGGAAGACATGGCGCCTGTATGGGTTCT

Sticky End Left 3

ATCACTGGTACCTCAAAACTAGGGCATCACCTTGAAGTCACTGGACAT

Sticky End Left 4

TTCCTCCATGAACTGCAACGTACCAGCACCAGAAACGTATCGCGTTCT

Sticky End Left 5

ATCACGGTGGTCAGCTCAGGAAATAAGTGCCAGCCGCCGTCCAGACAT

Sticky End Left 6

TTCCTTCCTTGACTCAACCATACCCCAAGCATTAAAGCACGACGTTCT

Sticky End Left 7 TCGCCGACCAAATCCGGCGCAGGCCAGGACAT

Sticky End Left 8 ATCACAGGTACACGAATCCGGGACAT

Sticky End Left 9

TTCCTCGCTCCGTAGCGTGACATTATGAAAAATATACTTATACGTTCT

Sticky End Left 10

ATCACCACACGCTTCATCCTTAATTCAAAATAATCGCCGTCCAGACAT

Sticky End Left 11

TTCCTTCTAGATCTGTCAAAAACGATCTTGAACACTCTCTTAAGTTCT

Sticky End Left 12

ATCACGGTTCGCAGCATTGGGATTCAACGTGAGAGCGGAAGTCGACAT

Sticky End Left 13

TTCCTACAAACGTCTGTACCATACAGTCACGCAAACTTCCTTCGTTCT

Sticky End Left 14

ATCACCAGCGTATGTAGGAAGTGTACGGCCATTAGAAGCTTCAGACAT

Sticky End Left 15 GCGTGTAGCAACGCTACCTTGCGCCTAGTTCT

Sticky End Right 1

GAAGCGGAGCAGTCCAAATAAAATAGTTCCAGGAGCCTTAG

Sticky End Right 2

TGAGTTCGCTGATGTTATAGATATTTATTGGTATATGCCGCAGCTT

Sticky End Right 3

CGTTATCGGCCAATCAGGGTTAAGTTCACCATATGTTATGTCTTAG

Sticky End Right 4

TGAGTCTTGCGGCAACGTGACGAAGAGTCAATATGTCAAGCAGCTT

Sticky End Right 5

CGTTAATCTACGTGCAAGGCCACTCTGACCAGCAGCCGAGACTTAG

Sticky End Right 6

TGAGTCCACCTATAAGGAAGCCAGCCAGTTTGATGAGCACTAGCTT

Sticky End Right 7

CGTTAGTTCGGATATATTAGACACTCGCAACGGCTAATGGCCTTAG

Sticky End Right 8

TGAGTGGCCGAGACTGCGGACGAAGACATTACAGGTAGTCCAGCTT

Sticky End Right 9

CGTTAGGACAGCGTCACTCCTTCTTTAACCGGAGGTGGCCGCTTAG

Sticky End Right 10

TGAGTCTGAACACCGCTCGACGCTCCATGATGACAGGAACAAGCTT

Sticky End Right 11

CGTTACACGCGGAGACAGGCCGTATAAACGCAATTATAGGCCTTAG

Sticky End Right 12

TGAGTGTGCTCGCGCCTCAACGCCAAACTTTGTCAGTCCTCAGCTT

Sticky End Right 13

CGTTACACTCTTCTACTCGTCAGAACTTGACTCATCGCCGACTTAG

Sticky End Right 14

TGAGTATAGACGCATGATTTCTTATAGTAATCCACGCTCTTTTAAAATGCTGA

CCAA

Sticky End Up 1 TAAACGTTATTGCCCGGCGCCAGGTCCAGCTT

Sticky End Up 2 TTCCTCCGAAGAGTCACACAGTCCTTGACGAAATAAA

Sticky End Up 3 AACTCGTATTCTGAATAATGGAAATCATGGAGCTGGCTTAG

Sticky End Up 4

ATCACCCAGTGCCGAACCATTGTTTGGATTATACTTAAATCCTTTGCCCGATT

AAACT

Sticky End Up 5 GGGTCGGCATCAAAAGCAATCGGCCGCAGCTT

Sticky End Up 6

TTCCTCGAGCCAGCCTGATTAGCATGCCCAGAGATTAGATCAACATC

Sticky End Up 7 TCAGGAACGTTGAACACGACCAGCATAAAGCCTCTTCTTAG

Sticky End Up 8

ATCACTGCTACAGGAAATGAATGTTTATAGGTCTAAAGAAACGCGGCACAAA

GGTACT

Sticky End Up 9 GTCAGTATGCAAATTAGCAACCAGTGGAGCTT

Sticky End Up 10 TTCCTAGAGCTCCATGTCAATAGATGTGGGAGCAAAC

Sticky End Down 1

TGAGTGCGGACGCCCTTCTGTTGATAAGCAAGCATCTCATAAGTCC

Sticky End Down 2

TTTCCAGAGTAGAAACCAATCAATGTGTTTTCCATAATAGAATTAGGCGTTCT

Sticky End Down 3

CGTTAAGTAAGGTGCATTCCAAGTACCGCACTCGATTAGTTGCTATTTTGGCC

GT

Sticky End Down 4

TAAATCAAATCGAGAACAAGCAAGCTGACGGAAATGCGACAT

Sticky End Down 5

TGAGTGCCGGCCTAGTCAACCTCAGCACTAACCTTGCGAGCGCCCA

Sticky End Down 6 AAGAGCCATACCGCTGATCAAGAACTGTTCT

Sticky End Down 7

CGTTACGTGTTGGCAGTGAGCTTTATCAATACCCAGAAGGGTAATAAGTCGA

TAC

Sticky End Down 8

CGTTATTCAGTCGAAGCATATTAAGGCTCACCTTTAGCACTGGTAG

Sticky End Down 9

CCAGCAGTGACAGAATCGTTAGTTGTGACTCATATCTAAATGGCCAGGGACA

T

Sticky End-Scaffold Linker Left 1 CCATACAGCAGCGGCC

Sticky End-Scaffold Linker Left 2 CAGTGACTCCGTCAGT

Sticky End-Scaffold Linker Left 3 GCGATACGAGGTACCA

Sticky End-Scaffold Linker Left 4 TGGACGGCGTTCATGG

Sticky End-Scaffold Linker Left 5 GTCGTGCTTGACCACC

Sticky End-Scaffold Linker Left 6 CTGGCCTGGTCAAGGA

Sticky End-Scaffold Linker Left 7 GTATAAGTGTGTACCT

Sticky End-Scaffold Linker Left 8 TGGACGGCACGGAGCG

Sticky End-Scaffold Linker Left 9 TTAAGAGAAGCGTGTG

Sticky End-Scaffold Linker Left 10 GACTTCCGGATCTAGA

Sticky End-Scaffold Linker Left 11 GAAGGAAGTGCGAACC

Sticky End-Scaffold Linker Left 12 TGAAGCTTACGTTTGT

Sticky End-Scaffold Linker Left 13 TAGGCGCAATACGCTG

Sticky End-Scaffold Linker Up 1

GGACCTGGAAATGGTTAACGCTTGTCCGACTCTTCGG

Sticky End-Scaffold Linker Up 2

CCAGCTCCCAACGCCATCTCCTCCGATCCGGCACTGG

Sticky End-Scaffold Linker Up 3

GCGGCCGACGCACTCTGGCGTCCTCTAGGCTGGCTCG

Sticky End-Scaffold Linker Up 4

AAGAGGCTCGATCAGTAGGTGGCTGTCCACTGTAGCA

Sticky End-Scaffold Linker Up 5

CCACTGGTTATAGCGGTCATGAGCACGGTGGAGCTCT

Sticky End-Scaffold Linker Right 1 GCTCCTGGATCAGCGA

Sticky End-Scaffold Linker Right 2 GCGGCATATTGGCCGA

Sticky End-Scaffold Linker Right 3 ACATAACAGCCGCAAG

Sticky End-Scaffold Linker Right 4 GCTTGACAACGTAGAT

Sticky End-Scaffold Linker Right 5 TCTCGGCTATAGGTGG

Sticky End-Scaffold Linker Right 6 AGTGCTCAATCCGAAC

Sticky End-Scaffold Linker Right 7 GCCATTAGTCTCGGCC

Sticky End-Scaffold Linker Right 8 GGACTACCCGCTGTCC

Sticky End-Scaffold Linker Right 9 CGGCCACCGTGTTCAG

Sticky End-Scaffold Linker Right 10 TGTTCCTGTCCGCGTG

Sticky End-Scaffold Linker Right 11 GCCTATAAGCGAGCAC

Sticky End-Scaffold Linker Right 12 GAGGACTGGAAGAGTG

Sticky End-Scaffold Linker Right 13 TCGGCGATGCGTCTAT

Sticky End-Scaffold Linker Down 1

GCCTAATTATTCAGATCCGAGCATCGCCGGCGTCCGC

Sticky End-Scaffold Linker Down 2

GCATTTCCAGATGAGCGAAGTCGTCGGAGACCTTACT

Sticky End-Scaffold Linker Down 3

AGTTCTTGACCAAGGATGCTTGCATCTGGAGGCCGGC

Sticky End-Scaffold Linker Down 4

CCGGATTCTGATTGGCCAGTATGATTGCTCCAACACG

Sticky End-Scaffold Linker Down 5

CCTGGCCACCGACTCTGGTCAGACGGATCCGACTGAA

Helpers modified with biotin:

Biotin Helper 158

CAAAGCCTTTGCATTCATCAAACGTCAGACGATTTTTTTTTTTTTTTTTTTT

Biotin Helper 159

AATTTACCAGGAGGTTGAGGCAGGACCAGAACTTTTTTTTTTTTTTTTTTTT

Biotin Helper 161

TTGGCCTTCCAGAATGGAAAGCGCCTTGCGACTTTTTTTTTTTTTTTTTTTT

Biotin Helper 162

ACTGGTAATGGCTTTTGATGATACAGTCTCTGTTTTTTTTTTTTTTTTTTTT

Biotin 20A [5’ biotin]AAAAAAAAAAAAAAAAAAAA

APPENDIX D

PERMISSIONS TO USE COPYRIGHTED MATERIALS

Nature Publishing Group

NATURE PUBLISHING GROUP LICENSE TERMS AND CONDITIONS

Mar 20, 2014

This is a License Agreement between Wei Li ("You") and Nature Publishing Group ("Nature Publishing Group") provided by Copyright Clearance Center ("CCC"). The license consists of your order details, the terms and conditions provided by Nature Publishing Group, and the payment terms and conditions.

All payments must be made in full to CCC. For payment instructions, please see information listed at the bottom of this form.

License Number	3344050457902
License date	Mar 08, 2014
Licensed content publisher	Nature Publishing Group
Licensed content publication	Nature
Licensed content title	Self-assembly of a nanoscale DNA box with a controllable lid
Licensed content author	Ebbe S. Andersen, Mingdong Dong, Morten M. Nielsen, Kasper Jahn, Ramesh Subramani, Wael Mamdouh, Monika M. Golas, Bjoern Sander, Holger Stark, Cristiano L. P. Oliveira, Jan Skov Pedersen, Victoria Birkedal, Flemming Besenbacher, Kurt V. Gothelf, Jørgen Kjems
Licensed content date	May 7, 2009
Volume number	459
Issue number	7243
Type of Use	reuse in a dissertation / thesis
Requestor type	academic/educational
Format	print and electronic
Portion	figures/tables/illustrations
Number of figures/tables/illustrations	2
High-res required	n/a
Figures	Figure 1, Figure 3
Author of this NPG article	no
Your reference number	None
Title of your thesis / dissertation	Programmed DNA Self-Assembly and Logic Circuits
Expected completion date	Apr 2014
Estimated size (number of pages)	200
Total	**0.00 USD**

NATURE PUBLISHING GROUP LICENSE TERMS AND CONDITIONS

Mar 20, 2014

NATURE PUBLISHING GROUP LICENSE TERMS AND CONDITIONS

Mar 20, 2014

This is a License Agreement between Wei Li ("You") and Nature Publishing Group ("Nature Publishing Group") provided by Copyright Clearance Center ("CCC"). The license consists of your order details, the terms and conditions provided by Nature Publishing Group, and the payment terms and conditions.

All payments must be made in full to CCC. For payment instructions, please see information listed at the bottom of this form.

License Number	3344050154052
License date	Mar 08, 2014
Licensed content publisher	Nature Publishing Group
Licensed content publication	Nature
Licensed content title	Hierarchical self-assembly of DNA into symmetric supramolecular polyhedra
Licensed content author	Yu He, Tao Ye, Min Su, Chuan Zhang, Alexander E. Ribbe, Wen Jiang, Chengde Mao
Licensed content date	Mar 13, 2008
Volume number	452
Issue number	7184
Type of Use	reuse in a dissertation / thesis
Requestor type	academic/educational
Format	print and electronic
Portion	figures/tables/illustrations
Number of figures/tables/illustrations	3
High-res required	n/a
Figures	Figure 2, Figure 3, Figure 4
Author of this NPG article	no
Your reference number	None
Title of your thesis / dissertation	Programmed DNA Self-Assembly and Logic Circuits
Expected completion date	Apr 2014
Estimated size (number of pages)	200
Total	**0.00 USD**

NATURE PUBLISHING GROUP LICENSE TERMS AND CONDITIONS

Mar 20, 2014

This is a License Agreement between Wei Li ("You") and Nature Publishing Group ("Nature Publishing Group") provided by Copyright Clearance Center ("CCC"). The license consists of your order details, the terms and conditions provided by Nature Publishing Group, and the payment terms and conditions.

All payments must be made in full to CCC. For payment instructions, please see information listed at the bottom of this form.

License Number	3344050057510
License date	Mar 08, 2014
Licensed content publisher	Nature Publishing Group
Licensed content publication	Nature
Licensed content title	Synthesis from DNA of a molecule with the connectivity of a cube
Licensed content author	Junghuei Chen, Nadrian C. Seeman
Licensed content date	Apr 18, 1991
Volume number	350
Issue number	6319
Type of Use	reuse in a dissertation / thesis
Requestor type	academic/educational
Format	print and electronic
Portion	figures/tables/illustrations
Number of figures/tables/illustrations	1
Figures	Figure 1
Author of this NPG article	no
Your reference number	None
Title of your thesis / dissertation	Programmed DNA Self-Assembly and Logic Circuits
Expected completion date	Apr 2014
Estimated size (number of pages)	200
Total	**0.00 USD**

NATURE PUBLISHING GROUP LICENSE TERMS AND CONDITIONS

Mar 20, 2014

This is a License Agreement between Wei Li ("You") and Nature Publishing Group ("Nature Publishing Group") provided by Copyright Clearance Center ("CCC"). The license consists of your order details, the terms and conditions provided by Nature Publishing Group, and the payment terms and conditions.

All payments must be made in full to CCC. For payment instructions, please see information listed at the bottom of this form.

License Number	3344041487062
License date	Mar 08, 2014
Licensed content publisher	Nature Publishing Group
Licensed content publication	Nature
Licensed content title	Self-assembly of DNA into nanoscale three-dimensional shapes
Licensed content author	Shawn M. Douglas, Hendrik Dietz, Tim Liedl, Bjorn Hogberg, Franziska Graf et al.
Licensed content date	May 21, 2009
Volume number	459
Issue number	7245
Type of Use	reuse in a dissertation / thesis
Requestor type	academic/educational
Format	print and electronic
Portion	figures/tables/illustrations
Number of figures/tables/illustrations	1
High-res required	no
Figures	Figure 4
Author of this NPG article	no
Your reference number	None
Title of your thesis / dissertation	Programmed DNA Self-Assembly and Logic Circuits
Expected completion date	Apr 2014
Estimated size (number of pages)	200
Total	**0.00 USD**

Terms and Conditions

Terms and Conditions for Permissions

Nature Publishing Group hereby grants you a non-exclusive license to reproduce this material for this purpose, and for no other use,subject to the conditions below:

1. NPG warrants that it has, to the best of its knowledge, the rights to license reuse of this material. However, you should ensure that the material you are requesting is original to Nature Publishing Group and does not carry the copyright of another entity (as credited in the published version). If the credit line on any part of the material you have requested indicates that it was reprinted or adapted by NPG with permission from another source, then you should also seek permission from that source to reuse the material.

2. Permission granted free of charge for material in print is also usually granted for any electronic version of that work, provided that the material is incidental to the work as a whole and that the electronic version is essentially equivalent to, or substitutes for, the print version.Where print permission has been granted for a fee, separate permission must be obtained for any additional, electronic re-use (unless, as in the case of a full paper, this has already been accounted for during your initial request in the calculation of a print run).NB: In all cases, web-based use of full-text articles must be authorized separately through the 'Use on a Web Site' option when requesting permission.

3. Permission granted for a first edition does not apply to second and subsequent editions and for editions in other languages (except for signatories to the STM Permissions Guidelines, or where the first edition permission was granted for free).

4. Nature Publishing Group's permission must be acknowledged next to the figure, table or abstract in print. In electronic form, this acknowledgement must be visible at the same time as the figure/table/abstract, and must be hyperlinked to the journal's homepage.

5. The credit line should read:
   Reprinted by permission from Macmillan Publishers Ltd: [JOURNAL NAME] (reference citation), copyright (year of publication)
   For AOP papers, the credit line should read:
   Reprinted by permission from Macmillan Publishers Ltd: [JOURNAL NAME], advance online publication, day month year (doi: 10.1038/sj.[JOURNAL ACRONYM].XXXXX)

   Note: For republication from the *British Journal of Cancer*, the following credit lines apply.
   Reprinted by permission from Macmillan Publishers Ltd on behalf of Cancer Research UK: [JOURNAL NAME] (reference citation), copyright (year of publication)For AOP papers, the credit line should read:
   Reprinted by permission from Macmillan Publishers Ltd on behalf of Cancer Research UK: [JOURNAL NAME], advance online publication, day month year (doi: 10.1038/sj.[JOURNAL ACRONYM].XXXXX)

6. Adaptations of single figures do not require NPG approval. However, the adaptation should be credited as follows:

   Adapted by permission from Macmillan Publishers Ltd: [JOURNAL NAME] (reference citation), copyright (year of publication)

Note: For adaptation from the *British Journal of Cancer*, the following credit line applies.
Adapted by permission from Macmillan Publishers Ltd on behalf of Cancer Research UK: [JOURNAL NAME] (reference citation), copyright (year of publication)

7. Translations of 401 words up to a whole article require NPG approval. Please visit http://www.macmillanmedicalcommunications.com for more information.Translations of up to a 400 words do not require NPG approval. The translation should be credited as follows:

   Translated by permission from Macmillan Publishers Ltd: [JOURNAL NAME] (reference citation), copyright (year of publication).

   Note: For translation from the *British Journal of Cancer*, the following credit line applies.
   Translated by permission from Macmillan Publishers Ltd on behalf of Cancer Research UK: [JOURNAL NAME] (reference citation), copyright (year of publication)

We are certain that all parties will benefit from this agreement and wish you the best in the use of this material. Thank you.
Special Terms:
v1.1

If you would like to pay for this license now, please remit this license along with your payment made payable to "COPYRIGHT CLEARANCE CENTER" otherwise you will be invoiced within 48 hours of the license date. Payment should be in the form of a check or money order referencing your account number and this invoice number RLNK501245408. Once you receive your invoice for this order, you may pay your invoice by credit card. Please follow instructions provided at that time.

Make Payment To:
Copyright Clearance Center
Dept 001
P.O. Box 843006
Boston, MA 02284-3006

For suggestions or comments regarding this order, contact RightsLink Customer Support: customercare@copyright.com or +1-877-622-5543 (toll free in the US) or +1-978-646-2777.

Gratis licenses (referencing $0 in the Total field) are free. Please retain this printable license for your reference. No payment is required.

AAAS

THE AMERICAN ASSOCIATION FOR THE ADVANCEMENT OF SCIENCE LICENSE TERMS AND CONDITIONS

Mar 20, 2014

This is a License Agreement between Wei Li ("You") and The American Association for the Advancement of Science ("The American Association for the Advancement of Science") provided by Copyright Clearance Center ("CCC"). The license consists of your order details, the terms and conditions provided by The American Association for the Advancement of Science, and the payment terms and conditions.

All payments must be made in full to CCC. For payment instructions, please see information listed at the bottom of this form.

License Number	3344041208261
License date	Mar 08, 2014
Licensed content publisher	The American Association for the Advancement of Science
Licensed content publication	Science
Licensed content title	DNA Origami with Complex Curvatures in Three-Dimensional Space
Licensed content author	Dongran Han, Suchetan Pal, Jeanette Nangreave, Zhengtao Deng, Yan Liu, Hao Yan
Licensed content date	Apr 15, 2011
Volume number	332
Issue number	6027
Type of Use	Thesis / Dissertation
Requestor type	Scientist/individual at a research institution
Format	Print and electronic
Portion	Figure
Number of figures/tables	1
Order reference number	None
Title of your thesis / dissertation	Programmed DNA Self-Assembly and Logic Circuits
Expected completion date	Apr 2014
Estimated size(pages)	200
Total	**0.00 USD**

THE AMERICAN ASSOCIATION FOR THE ADVANCEMENT OF SCIENCE LICENSE TERMS AND CONDITIONS

Mar 20, 2014

This is a License Agreement between Wei Li ("You") and The American Association for the Advancement of Science ("The American Association for the Advancement of Science") provided by Copyright Clearance Center ("CCC"). The license consists of your order details, the terms and conditions provided by The American Association for the Advancement of Science, and the payment terms and conditions.

All payments must be made in full to CCC. For payment instructions, please see information listed at the bottom of this form.

License Number	3344041158912
License date	Mar 08, 2014
Licensed content publisher	The American Association for the Advancement of Science
Licensed content publication	Science
Licensed content title	Folding DNA into Twisted and Curved Nanoscale Shapes
Licensed content author	Hendrik Dietz, Shawn M. Douglas, William M. Shih
Licensed content date	Aug 7, 2009
Volume number	325
Issue number	5941
Type of Use	Thesis / Dissertation
Requestor type	Scientist/individual at a research institution
Format	Print and electronic
Portion	Figure
Number of figures/tables	1
Order reference number	None
Title of your thesis / dissertation	Programmed DNA Self-Assembly and Logic Circuits
Expected completion date	Apr 2014
Estimated size(pages)	200
Total	**0.00 USD**

THE AMERICAN ASSOCIATION FOR THE ADVANCEMENT OF SCIENCE LICENSE TERMS AND CONDITIONS

Mar 20, 2014

This is a License Agreement between Wei Li ("You") and The American Association for the Advancement of Science ("The American Association for the Advancement of Science") provided by Copyright Clearance Center ("CCC"). The license consists of your order details, the terms and conditions provided by The American Association for the Advancement of Science, and the payment terms and conditions.

All payments must be made in full to CCC. For payment instructions, please see information listed at the bottom of this form.

License Number	3344041108352
License date	Mar 08, 2014
Licensed content publisher	The American Association for the Advancement of Science
Licensed content publication	Science
Licensed content title	Rapid Chiral Assembly of Rigid DNA Building Blocks for Molecular Nanofabrication
Licensed content author	R. P. Goodman, I. A. T. Schaap, C. F. Tardin, C. M. Erben, R. M. Berry, C. F. Schmidt, A. J. Turberfield
Licensed content date	Dec 9, 2005
Volume number	310
Issue number	5754
Type of Use	Thesis / Dissertation
Requestor type	Scientist/individual at a research institution
Format	Print and electronic
Portion	Figure
Number of figures/tables	1
Order reference number	None
Title of your thesis / dissertation	Programmed DNA Self-Assembly and Logic Circuits
Expected completion date	Apr 2014
Estimated size(pages)	200
Total	**0.00 USD**

THE AMERICAN ASSOCIATION FOR THE ADVANCEMENT OF SCIENCE LICENSE TERMS AND CONDITIONS

Mar 20, 2014

This is a License Agreement between Wei Li ("You") and The American Association for the Advancement of Science ("The American Association for the Advancement of Science") provided by Copyright Clearance Center ("CCC"). The license consists of your order details, the terms and conditions provided by The American Association for the Advancement of Science, and the payment terms and conditions.

All payments must be made in full to CCC. For payment instructions, please see information listed at the bottom of this form.

License Number	3344041032803
License date	Mar 08, 2014
Licensed content publisher	The American Association for the Advancement of Science
Licensed content publication	Science
Licensed content title	DNA-Templated Self-Assembly of Protein Arrays and Highly Conductive Nanowires
Licensed content author	Hao Yan, Sung Ha Park, Gleb Finkelstein, John H. Reif, Thomas H. LaBean
Licensed content date	Sep 26, 2003
Volume number	301
Issue number	5641
Type of Use	Thesis / Dissertation
Requestor type	Scientist/individual at a research institution
Format	Print and electronic
Portion	Figure
Number of figures/tables	1
Order reference number	None
Title of your thesis / dissertation	Programmed DNA Self-Assembly and Logic Circuits
Expected completion date	Apr 2014
Estimated size(pages)	200
Total	**0.00 USD**

THE AMERICAN ASSOCIATION FOR THE ADVANCEMENT OF SCIENCE LICENSE TERMS AND CONDITIONS

Mar 20, 2014

License Number	3342870995980
License date	Mar 06, 2014
Licensed content publisher	The American Association for the Advancement of Science
Licensed content publication	Science
Licensed content title	Scaling Up Digital Circuit Computation with DNA Strand Displacement Cascades
Licensed content author	Lulu Qian, Erik Winfree
Licensed content date	Jun 3, 2011
Volume number	332
Issue number	6034
Type of Use	Thesis / Dissertation
Requestor type	Scientist/individual at a research institution
Format	Print and electronic
Portion	Figure
Number of figures/tables	3
Order reference number	None
Title of your thesis / dissertation	Programmed DNA Self-Assembly and Logic Circuits
Expected completion date	Apr 2014
Estimated size(pages)	200
Total	**0.00 USD**

Terms and Conditions

American Association for the Advancement of Science TERMS AND CONDITIONS

Regarding your request, we are pleased to grant you non-exclusive, non-transferable permission, to republish the AAAS material identified above in your work identified above, subject to the terms and conditions herein. We must be contacted for permission for any uses other than those specifically identified in your request above.

The following credit line must be printed along with the AAAS material: "From [Full Reference Citation]. Reprinted with permission from AAAS."

All required credit lines and notices must be visible any time a user accesses any part of the AAAS material and must appear on any printed copies and authorized user might make.

This permission does not apply to figures / photos / artwork or any other content or materials included in your work that are credited to non-AAAS sources. If the requested material is sourced to or references non-AAAS sources, you must obtain authorization from that source as well before using that material. You agree to hold harmless and indemnify AAAS against any claims arising from your use of any content in your work that is credited to non-AAAS sources.

If the AAAS material covered by this permission was published in Science during the years 1974 - 1994, you must also obtain permission from the author, who may grant or withhold permission, and who may or may not charge a fee if permission is granted. See original article for author's address. This condition does not apply to news articles.

The AAAS material may not be modified or altered except that figures and tables may be modified with permission from the author. Author permission for any such changes must be secured prior to your use.

Whenever possible, we ask that electronic uses of the AAAS material permitted herein include a hyperlink to the original work on AAAS's website (hyperlink may be embedded in the reference citation).

AAAS material reproduced in your work identified herein must not account for more than 30% of the total contents of that work.

AAAS must publish the full paper prior to use of any text.

AAAS material must not imply any endorsement by the American Association for the Advancement of Science.

This permission is not valid for the use of the AAAS and/or Science logos.

AAAS makes no representations or warranties as to the accuracy of any information contained in the AAAS material covered by this permission, including any warranties of
merchantability or fitness for a particular purpose.

If permission fees for this use are waived, please note that AAAS reserves the right to charge for reproduction of this material in the future.

Permission is not valid unless payment is received within sixty (60) days of the issuance of this permission. If payment is not received within this time period then all rights granted herein shall be revoked and this permission will be considered null and void.

In the event of breach of any of the terms and conditions herein or any of CCC's Billing and Payment terms and conditions, all rights granted herein shall be revoked and this permission will be considered null and void.

AAAS reserves the right to terminate this permission and all rights granted herein at its discretion, for any purpose, at any time. In the event that AAAS elects to terminate this permission, you will have no further right to publish, publicly perform, publicly display, distribute or otherwise use any matter in which the AAAS content had been included, and all fees paid hereunder shall be fully refunded to you. Notification of termination will be sent to the contact information as supplied by you during the request process and termination shall be immediate upon sending the notice. Neither AAAS nor CCC shall be liable for any costs, expenses, or damages you may incur as a result of the termination of this permission, beyond the refund noted above.

This Permission may not be amended except by written document signed by both parties.

The terms above are applicable to all permissions granted for the use of AAAS material. Below you will find additional conditions that apply to your particular type of use.

FOR A THESIS OR DISSERTATION

If you are using figure(s)/table(s), permission is granted for use in print and electronic versions of your dissertation or

thesis. A full text article may be used in print versions only of a dissertation or thesis.
Permission covers the distribution of your dissertation or thesis on demand by ProQuest / UMI, provided the AAAS material covered by this permission remains in situ.
If you are an Original Author on the AAAS article being reproduced, please refer to your License to Publish for rules on reproducing your paper in a dissertation or thesis.

FOR JOURNALS:

Permission covers both print and electronic versions of your journal article, however the AAAS material may not be used in any manner other than within the context of your article.

FOR BOOKS/TEXTBOOKS:

If this license is to reuse figures/tables, then permission is granted for non-exclusive world rights in all languages in both print and electronic formats (electronic formats are defined below).
If this license is to reuse a text excerpt or a full text article, then permission is granted for non-exclusive world rights in English only. You have the option of securing either print or electronic rights or both, but electronic rights are not automatically granted and do garner additional fees. Permission for translations of text excerpts or full text articles into other languages must be obtained separately.
Licenses granted for use of AAAS material in electronic format books/textbooks are valid only in cases where the electronic version is equivalent to or substitutes for the print version of the book/textbook. The AAAS material reproduced as permitted herein must remain in situ and must not be exploited separately (for example, if permission covers the use of a full text article, the article may not be offered for access or for purchase as a stand-alone unit), except in the case of permitted textbook companions as noted below.
You must include the following notice in any electronic versions, either adjacent to the reprinted AAAS material or in the terms and conditions for use of your electronic products: "Readers may view, browse, and/or download material for temporary copying purposes only, provided these uses are for noncommercial personal purposes. Except as provided by law, this material may not be further reproduced, distributed, transmitted, modified, adapted, performed, displayed, published, or sold in whole or in part, without prior written permission from the publisher."
If your book is an academic textbook, permission covers the following companions to your textbook, provided such companions are distributed only in conjunction with your textbook at no additional cost to the user:

- Password-protected website
- Instructor's image CD/DVD and/or PowerPoint resource
- Student CD/DVD

All companions must contain instructions to users that the AAAS material may be used for non-commercial, classroom purposes only. Any other uses require the prior written permission from AAAS.
If your license is for the use of AAAS Figures/Tables, then the electronic rights granted herein permit use of the Licensed Material in any Custom Databases that you distribute the electronic versions of your textbook through, so long as the Licensed Material remains within the context of a chapter of the title identified in your request and cannot be downloaded by a user as an independent image file.
Rights also extend to copies/files of your Work (as described above) that you are required to provide for use by the visually and/or print disabled in compliance with state and federal laws.
This permission only covers a single edition of your work as identified in your request.

FOR NEWSLETTERS:

Permission covers print and/or electronic versions, provided the AAAS material reproduced as permitted herein remains in situ and is not exploited separately (for example, if permission covers the use of a full text article, the article may not be offered for access or for purchase as a stand-alone unit)

FOR ANNUAL REPORTS:

Permission covers print and electronic versions provided the AAAS material reproduced as permitted herein remains in situ and is not exploited separately (for example, if permission covers the use of a full text article, the article may not be offered for access or for purchase as a stand-alone unit)

FOR PROMOTIONAL/MARKETING USES:

Permission covers the use of AAAS material in promotional or marketing pieces such as information packets, media kits, product slide kits, brochures, or flyers limited to a single print run. The AAAS Material may not be used in any manner which implies endorsement or promotion by the American Association for the Advancement of Science (AAAS) or Science of any product or service. AAAS does not permit the reproduction of its name, logo or text on promotional literature.

If permission to use a full text article is permitted, The Science article covered by this permission must not be altered in any way. No additional printing may be set onto an article copy other than the copyright credit line required above. Any alterations must be approved in advance and in writing by AAAS. This includes, but is not limited to, the placement of sponsorship identifiers, trademarks, logos, rubber stamping or self-adhesive stickers onto the article copies.

Additionally, article copies must be a freestanding part of any information package (i.e. media kit) into which they are inserted. They may not be physically attached to anything, such as an advertising insert, or have anything attached to them, such as a sample product. Article copies must be easily removable from any kits or informational packages in which they are used. The only exception is that article copies may be inserted into three-ring binders.

FOR CORPORATE INTERNAL USE:

The AAAS material covered by this permission may not be altered in any way. No additional printing may be set onto an article copy other than the required credit line. Any alterations must be approved in advance and in writing by AAAS. This includes, but is not limited to the placement of sponsorship identifiers, trademarks, logos, rubber stamping or self-adhesive stickers onto article copies.

If you are making article copies, copies are restricted to the number indicated in your request and must be distributed only to internal employees for internal use.

If you are using AAAS Material in Presentation Slides, the required credit line must be visible on the slide where the AAAS material will be reprinted

If you are using AAAS Material on a CD, DVD, Flash Drive, or the World Wide Web, you must include the following notice in any electronic versions, either adjacent to the reprinted AAAS material or in the terms and conditions for use of your electronic products: "Readers may view, browse, and/or download material for temporary copying purposes only, provided these uses are for noncommercial personal purposes. Except as provided by law, this material may not be further reproduced, distributed, transmitted, modified, adapted, performed, displayed, published, or sold in whole or in part, without prior written permission from the publisher." Access to any such CD, DVD, Flash Drive or Web page must be restricted to your organization's employees only.

FOR CME COURSE and SCIENTIFIC SOCIETY MEETINGS:

Permission is restricted to the particular Course, Seminar, Conference, or Meeting indicated in your request. If this license covers a text excerpt or a Full Text Article, access to the reprinted AAAS material must be restricted to attendees of your event only (if you have been granted electronic rights for use of a full text article on your website, your website must be password protected, or access restricted so that only attendees can access the content on your site).

If you are using AAAS Material on a CD, DVD, Flash Drive, or the World Wide Web, you must include the following notice in any electronic versions, either adjacent to the reprinted AAAS material or in the terms and conditions for use of your electronic products: "Readers may view, browse, and/or download material for temporary copying purposes only, provided these uses are for noncommercial personal purposes. Except as provided by law, this material may not be further reproduced, distributed, transmitted, modified, adapted, performed, displayed, published, or sold in whole or in part, without prior written permission from the publisher."

FOR POLICY REPORTS:

These rights are granted only to non-profit organizations and/or government agencies. Permission covers print and electronic versions of a report, provided the required credit line appears in both versions and provided the AAAS material reproduced as permitted herein remains in situ and is not exploited separately.

FOR CLASSROOM PHOTOCOPIES:

Permission covers distribution in print copy format only. Article copies must be freestanding and not part of a course pack. They may not be physically attached to anything or have anything attached to them.

FOR COURSEPACKS OR COURSE WEBSITES:

These rights cover use of the AAAS material in one class at one institution. Permission is valid only for a single semester after which the AAAS material must be removed from the Electronic Course website, unless new permission is obtained for an additional semester. If the material is to be distributed online, access must be restricted to students and instructors enrolled in that particular course by some means of password or access control.

FOR WEBSITES:

You must include the following notice in any electronic versions, either adjacent to the reprinted AAAS material or in the terms and conditions for use of your electronic products: "Readers may view, browse, and/or download material for temporary copying purposes only, provided these uses are for noncommercial personal purposes. Except as provided by law, this material may not be further reproduced, distributed, transmitted, modified, adapted, performed, displayed, published, or sold in whole or in part, without prior written permission from the publisher."

Permissions for the use of Full Text articles on third party websites are granted on a case by case basis and only in cases where access to the AAAS Material is restricted by some means of password or access control. Alternately, an E-Print may be purchased through our reprints department (brocheleau@rockwaterinc.com).

REGARDING FULL TEXT ARTICLE USE ON THE WORLD WIDE WEB IF YOU ARE AN 'ORIGINAL AUTHOR' OF A SCIENCE PAPER

If you chose "Original Author" as the Requestor Type, you are warranting that you are one of authors listed on the License Agreement as a "Licensed content author" or that you are acting on that author's behalf to use the Licensed content in a new work that one of the authors listed on the License Agreement as a "Licensed content author" has written.

Original Authors may post the 'Accepted Version' of their full text article on their personal or on their University website and not on any other website. The 'Accepted Version' is the version of the paper accepted for publication by AAAS including changes resulting from peer review but prior to AAAS's copy editing and production (in other words not the AAAS published version).

FOR MOVIES / FILM / TELEVISION:

Permission is granted to use, record, film, photograph, and/or tape the AAAS material in connection with your program/film and in any medium your program/film may be shown or heard, including but not limited to broadcast and cable television, radio, print, world wide web, and videocassette.

The required credit line should run in the program/film's end credits.

FOR MUSEUM EXHIBITIONS:

Permission is granted to use the AAAS material as part of a single exhibition for the duration of that exhibit. Permission for use of the material in promotional materials for the exhibit must be cleared separately with AAAS (please contact us at permissions@aaas.org).

FOR TRANSLATIONS:

Translation rights apply only to the language identified in your request summary above.

The following disclaimer must appear with your translation, on the first page of the article, after the credit line: "This translation is not an official translation by AAAS staff, nor is it endorsed by AAAS as accurate. In crucial matters, please refer to the official English-language version originally published by AAAS."

FOR USE ON A COVER:

Permission is granted to use the AAAS material on the cover of a journal issue, newsletter issue, book, textbook, or annual report in print and electronic formats provided the AAAS material reproduced as permitted herein remains in situ and is not exploited separately

By using the AAAS Material identified in your request, you agree to abide by all the terms and conditions herein.

Questions about these terms can be directed to the AAAS Permissions department permissions@aaas.org.

Other Terms and Conditions:

v 2

If you would like to pay for this license now, please remit this license along with your payment made payable to "COPYRIGHT CLEARANCE CENTER" otherwise you will be invoiced within 48 hours of the license date. Payment should be in the form of a check or money order referencing your account number and this invoice number RLNK501243222. Once you receive your invoice for this order, you may pay your invoice by credit card. Please follow instructions provided at that time.

Make Payment To:
Copyright Clearance Center
Dept 001
P.O. Box 843006
Boston, MA 02284-3006

For suggestions or comments regarding this order, contact RightsLink Customer Support: customercare@copyright.com or +1-877-622-5543 (toll free in the US) or +1-978-646-2777.

Gratis licenses (referencing $0 in the Total field) are free. Please retain this printable license for your reference. No payment is required.

American Chemical Society

Copyright Clearance Center RightsLink®

Home | Account Info | Help

ACS Publications High quality. High impact.

Title: Spatially-Interactive Biomolecular Networks Organized by Nucleic Acid Nanostructures

Author: Jinglin Fu, Minghui Liu, Yan Liu, and Hao Yan

Publication: Accounts of Chemical Research

Publisher: American Chemical Society

Date: Aug 1, 2012

Copyright © 2012, American Chemical Society

Logged in as:
Wei Li
Account #:
3000759124

LOGOUT

PERMISSION/LICENSE IS GRANTED FOR YOUR ORDER AT NO CHARGE

This type of permission/license, instead of the standard Terms & Conditions, is sent to you because no fee is being charged for your order. Please note the following:

- Permission is granted for your request in both print and electronic formats, and translations.
- If figures and/or tables were requested, they may be adapted or used in part.
- Please print this page for your records and send a copy of it to your publisher/graduate school.
- Appropriate credit for the requested material should be given as follows: "Reprinted (adapted) with permission from (COMPLETE REFERENCE CITATION). Copyright (YEAR) American Chemical Society." Insert appropriate information in place of the capitalized words.
- One-time permission is granted only for the use specified in your request. No additional uses are granted (such as derivative works or other editions). For any other uses, please submit a new request.

If credit is given to another source for the material you requested, permission must be obtained from that source.

BACK | CLOSE WINDOW

Copyright Clearance Center RightsLink®

Home | Account Info | Help

ACS Publications
High quality. High impact.

Title: Three-Helix Bundle DNA Tiles Self-Assemble into 2D Lattice or 1D Templates for Silver Nanowires

Author: Sung Ha Park et al.

Publication: Nano Letters

Publisher: American Chemical Society

Date: Apr 1, 2005

Logged in as:
Wei Li
Account #:
3000759124

LOGOUT

PERMISSION/LICENSE IS GRANTED FOR YOUR ORDER AT NO CHARGE

This type of permission/license, instead of the standard Terms & Conditions, is sent to you because no fee is being charged for your order. Please note the following:

- Permission is granted for your request in both print and electronic formats, and translations.
- If figures and/or tables were requested, they may be adapted or used in part.
- Please print this page for your records and send a copy of it to your publisher/graduate school.
- Appropriate credit for the requested material should be given as follows: "Reprinted (adapted) with permission from (COMPLETE REFERENCE CITATION). Copyright (YEAR) American Chemical Society." Insert appropriate information in place of the capitalized words.
- One-time permission is granted only for the use specified in your request. No additional uses are granted (such as derivative works or other editions). For any other uses, please submit a new request.

If credit is given to another source for the material you requested, permission must be obtained from that source.

BACK | CLOSE WINDOW

Copyright Clearance Center RightsLink®

Home | Account Info | Help

ACS Publications
High quality. High impact.

Title: Six-Helix Bundles Designed from DNA
Author: Frederick Mathieu et al.
Publication: Nano Letters
Publisher: American Chemical Society
Date: Apr 1, 2005

Logged in as:
Wei Li
Account #:
3000759124

LOGOUT

PERMISSION/LICENSE IS GRANTED FOR YOUR ORDER AT NO CHARGE

This type of permission/license, instead of the standard Terms & Conditions, is sent to you because no fee is being charged for your order. Please note the following:

- Permission is granted for your request in both print and electronic formats, and translations.
- If figures and/or tables were requested, they may be adapted or used in part.
- Please print this page for your records and send a copy of it to your publisher/graduate school.
- Appropriate credit for the requested material should be given as follows: "Reprinted (adapted) with permission from (COMPLETE REFERENCE CITATION). Copyright (YEAR) American Chemical Society." Insert appropriate information in place of the capitalized words.
- One-time permission is granted only for the use specified in your request. No additional uses are granted (such as derivative works or other editions). For any other uses, please submit a new request.

If credit is given to another source for the material you requested, permission must be obtained from that source.

BACK | CLOSE WINDOW

Copyright Clearance Center RightsLink®

Home | Account Info | Help

ACS Publications
High quality. High impact.

Title: Designed Two-Dimensional DNA Holliday Junction Arrays Visualized by Atomic Force Microscopy

Author: Chengde Mao,Weiqiong Sun, and, and Nadrian C. Seeman*

Publication: Journal of the American Chemical Society

Publisher: American Chemical Society

Date: Jun 1, 1999

Logged in as:
Wei Li
Account #:
3000759124

LOGOUT

PERMISSION/LICENSE IS GRANTED FOR YOUR ORDER AT NO CHARGE

This type of permission/license, instead of the standard Terms & Conditions, is sent to you because no fee is being charged for your order. Please note the following:

- Permission is granted for your request in both print and electronic formats, and translations.
- If figures and/or tables were requested, they may be adapted or used in part.
- Please print this page for your records and send a copy of it to your publisher/graduate school.
- Appropriate credit for the requested material should be given as follows: "Reprinted (adapted) with permission from (COMPLETE REFERENCE CITATION). Copyright (YEAR) American Chemical Society." Insert appropriate information in place of the capitalized words.
- One-time permission is granted only for the use specified in your request. No additional uses are granted (such as derivative works or other editions). For any other uses, please submit a new request.

If credit is given to another source for the material you requested, permission must be obtained from that source.

BACK | CLOSE WINDOW

Copyright Clearance Center RightsLink®

Home | Account Info | Help

ACS Publications
High quality. High impact.

Title: Controlled Nucleation and Growth of DNA Tile Arrays within Prescribed DNA Origami Frames and Their Dynamics

Author: Wei Li, Yang Yang, Shuoxing Jiang, Hao Yan, and Yan Liu

Publication: Journal of the American Chemical Society

Publisher: American Chemical Society

Date: Mar 1, 2014

Logged in as:
Wei Li
Account #:
3000759124

LOGOUT

PERMISSION/LICENSE IS GRANTED FOR YOUR ORDER AT NO CHARGE

This type of permission/license, instead of the standard Terms & Conditions, is sent to you because no fee is being charged for your order. Please note the following:

- Permission is granted for your request in both print and electronic formats, and translations.
- If figures and/or tables were requested, they may be adapted or used in part.
- Please print this page for your records and send a copy of it to your publisher/graduate school.
- Appropriate credit for the requested material should be given as follows: "Reprinted (adapted) with permission from (COMPLETE REFERENCE CITATION). Copyright (YEAR) American Chemical Society." Insert appropriate information in place of the capitalized words.
- One-time permission is granted only for the use specified in your request. No additional uses are granted (such as derivative works or other editions). For any other uses, please submit a new request.

BACK | CLOSE WINDOW

Copyright Clearance Center RightsLink®

Home | Account Info | Help

ACS Publications High quality. High impact.

Title: Three-Input Majority Logic Gate and Multiple Input Logic Circuit Based on DNA Strand Displacement

Author: Wei Li, Yang Yang, Hao Yan, and Yan Liu

Publication: Nano Letters

Publisher: American Chemical Society

Date: Jun 1, 2013

Logged in as:
Wei Li
Account #:
3000759124

LOGOUT

PERMISSION/LICENSE IS GRANTED FOR YOUR ORDER AT NO CHARGE

This type of permission/license, instead of the standard Terms & Conditions, is sent to you because no fee is being charged for your order. Please note the following:

- Permission is granted for your request in both print and electronic formats, and translations.
- If figures and/or tables were requested, they may be adapted or used in part.
- Please print this page for your records and send a copy of it to your publisher/graduate school.
- Appropriate credit for the requested material should be given as follows: "Reprinted (adapted) with permission from (COMPLETE REFERENCE CITATION). Copyright (YEAR) American Chemical Society." Insert appropriate information in place of the capitalized words.
- One-time permission is granted only for the use specified in your request. No additional uses are granted (such as derivative works or other editions). For any other uses, please submit a new request.

BACK | CLOSE WINDOW

Other Sources

For Figure 1.10.

Rothemund, P. W. K.; Papadakis, N.; Winfree, E. *PLoS Biol* **2004**, *2*, e424.

APPENDIX E

CO-AUTHOR APPROVAL

I verify that the following co-authors have approved of my use of our publications in my dissertation.

Yan Liu (Arizona State University)

Hao Yan (Arizona State University)

Yang Yang (Arizona State University[1])

Shuoxing Jiang (Arizona State University)

[1]Note: The author's address is listed as when the research was performed.